International
Progress Report

IPR-06-21

Äspö Hard Rock Laboratory

Äspö Task Force on modelling of groundwater flow and transport of solutes

Modelling of Task 6D, 6E, 6F and 6F2. Flow, transport and retention in a sparsely fractured granite

Urban Svensson
Computer-aided Fluid Engineering AB

September 2006

Svensk Kärnbränslehantering AB
Swedish Nuclear Fuel
and Waste Management Co
Box 5864
SE-102 40 Stockholm Sweden
Tel 08-459 84 00
+46 8 459 84 00
Fax 08-661 57 19
+46 8 661 57 19

Äspö Hard Rock Laboratory

Report no.
IPR-06-21
No.
F65K
Author
Urban Svensson
Date
September 2006
Checked by
Jan-Olof Selroos
Date
February 2007
Approved
Anders Sjöland
Date
2007-02-22

Äspö Hard Rock Laboratory

Äspö Task Force on modelling of groundwater flow and transport of solutes

Modelling of Task 6D, 6E, 6F and 6F2. Flow, transport and retention in a sparsely fractured granite

Urban Svensson
Computer-aided Fluid Engineering AB

September 2006

Keywords: Numerical simulation, Flow, Transport, Dispersion, Retention

Abstract

Task 6 deals with flow, transport and retention in fracture networks, considering both short and long (i.e. *PA*) time scales. A number of modelling tasks have been defined, based on the TRUE Block Scale experiment at Äspö HRL.

This report describes the results obtained using the code DarcyTools, which has been developed in parallel with Task 6. The dispersion and retention module in DarcyTools is called FRAME, which utilizes the multi-rate diffusion concept. A significant part of the work carried out in Task 6 has been directed towards evaluating the FRAME input parameters.

The main results of the work are, for this reason, related to how well DarcyTools/FRAME has performed in Task 6. It is argued that FRAME is an efficient tool for simulation of dispersion and retention and it can also be shown that the input parameters can be interpreted and constrained.

Sammanfattning

Task 6 behandlar flöde, transport och retention i spricknätverk, med speciell hänsyn till två tidsskalor (experimentell och *PA).* Ett antal modelleringsupppgifter har formulerats utgående från förhållandena i TRUE Block volymen, Äspölaboratoriet.

Rapporten redogör för resultat som erhållits med beräkningsprogrammet DarcyTools, som utvecklats parallellt med arbetet i Task 6. Modulen som hanterar dispersion och retention kallas FRAME, som bygger på ”the multi-rate diffusion concept”. En stor del av arbetet i Task 6 har ägnats åt de parametrar som ingår i FRAME.

Det är därför inte förvånande att slutsatserna av arbetet till stor del handlar om hur väl DarcyTools/FRAME har fungerat. Det generella intrycket från Task 6 arbetet är att realistiska simuleringar har erhållits genomgående. Det har vidare visats att de parametrar som ingår i FRAME kan tolkas fysikaliskt och riktlinjer för lämpliga värden kan ges.

Executive summary

A full account of the Task 6 objectives and supporting arguments is given in the Task 6C report (Dershowitz et al., 2003). Let us quote the following sentences regarding the general objectives.

Äspö Task Force Task 6 consists of a set of numerical experiments that use a common set of hydrostructural models to test performance assessment codes and site characterisation codes. The comparison of the results of these simulations serves several objectives (Benabderrahmane et al., 2000):

1. *Assessment of simplifications used in PA models.*
2. *Determination of how the experimental tracer and flow experiments can constrain the range of parameters used in PA models.*
3. *Support of the design of site characterisation programs to assure that the results have optimal value for performance assessment calculations.*
4. *Better understanding of site-specific flow and transport behaviour at different scales using site characterisation models.*

The present report deals with Tasks 6D, 6E, 6F and 6F2. These tasks utilize the information presented in the Task 6C report and focus on transport and retention processes in a 3D fracture network (6D, 6E and 6F2) or in a single fracture (6F).

The main objective of this report is to compile the work carried out in the subtasks 6D, 6E, 6F and 6F2 into a single report. A secondary objective is to summarize the developments (concepts and methods) undertaken in the subtasks and formulate some conclusions regarding these.

Task 6 was initiated about five years ago. The development of the simulation model DarcyTools was started at about the same time. Hence, the work undertaken in Task 6 has to a large extent formed the transport model in DarcyTools. The dispersion and retention module in DarcyTools is called FRAME, which rests on a number of concepts and assumptions of which the most essential are:

- *Fractures smaller than the grid size are assumed to be filled with stagnant water (immobile volumes) and exchange matter with the flowing water (mobile volumes) by diffusion only.*
- *Subgrid fractures are assumed to follow a power-law (same as for resolved fractures).*
- *All immobile volumes can be represented by a set of boxes(or storage volumes), each with its own length scale, volume and effective diffusion coefficient.*

Results from simulations have mainly been presented in form of breakthrough-curves. Some of these have been compared with field data. However, in most cases inter comparison between different models have been the only feasible way to establish confidence in the results (in particular so for *PA* time scale simulations).

The main conclusions of the work will be formulated as evaluations of the methods and concepts embodied in DarcyTools/FRAME.

- The present conceptual view of a conductive structure is that a range (in terms of length and time scales) of immobile water volumes is in contact with the mobile water. The subgrid model FRAME is based on the multi-rate diffusion model, which is designed to handle such cases. We may hence conclude that the basic concept in FRAME is well suited for the present task.

- During the course of the work, the FRAME parameters have been evaluated and a set of parameters has been established. It should be noted that FRAME departs from traditional models in several ways (long-tailed breakthrough-curves, no dispersion coefficients, mass-centre does not move with the water velocity). These features have contributed to the prediction of realistic breakthrough-curves.

- The fact that FRAME is fully integrated in a 3D flow code has simplified simulations in the fracture network tasks. The split-up of a tracer cloud at fracture intersections and inclusion of heterogeneity in a fracture plane are hence accounted for.

These experiences from the application of DarcyTools/FRAME in Task 6, lead to the conclusion that FRAME is well suited to handle tracer transport along single flow channels or in complex fracture networks. Also the different time scales considered in Task 6 can be handled without problem, as the multirate model accommodates such effects by definition.

Contents

List of Tables

List of Figures

1 Introduction

1.1 Background

A full account of the Task 6 objectives and supporting arguments is given in the Task 6C report (Dershowits et al., 2003). Let us quote the following sentences regarding the general objectives.

Äspö Task Force Task 6 consists of a set of numerical experiments that use a common set of hydrostructural models to test performance assessment codes and site characterisation codes. The comparison of the results of these simulations serves several objectives (Benabderrahmane et al., 2000):

1. *Assessment of simplifications used in PA models.*
2. *Determination of how the experimental tracer and flow experiments can constrain the range of parameters used in PA models.*
3. *Support of the design of site characterisation programs to assure that the results have optimal value for performance assessment calculations.*
4. *Better understanding of site-specific flow and transport behaviour at different scales using site characterisation models.*

The present report deals with Tasks 6D, 6E, 6F and 6F2. These tasks utilize the information presented in the Task 6C report and focus on transport and retention processes in a 3D fracture network (6D, 6E and 6F2) or in a single fracture (6F).

1.2 Objectives

The main objective of this report is to compile the work carried out in the subtasks 6D, 6E, 6F and 6F2 into a single report. A secondary objective is to summarize the developments (concepts and methods) undertaken in the subtasks and formulate some conclusions regarding these.

1.3 Outline of report

After this brief introduction, the modelling tasks are described (Chapter 2). A fairly detailed account of the code DarcyTools is the subject of Chapter 3. The dispersion and retardation module in DarcyTools is called FRAME. The parameter values in FRAME are evaluated and discussed in Chapter 4. The four tasks Task D, E, F and F2 then follow in Chapter 5 to 8. A discussion of results and some conclusions of the work can be found in Chapter 9. Appendix A provides some additional studies of the dispersion characteristics of FRAME.

2 Modelling Tasks

2.1 Introduction

A 200 x 200 x 200 m^3 domain, which is part of the TRUE Block Scale experiment, is considered. The hydrostructural model is developed within Task 6C (Dershowitz et al., 2003). In addition to 11 deterministic structures and 25 synthetic 100 m scale structures, 5 660 synthetic background fractures are generated. In Figure 2-1, the deterministic and synthetic structures are illustrated. Head boundary conditions are provided for the domain as well as injection and pumping data for the tracer experiment.

Each structure has been classified with respect to "Geological Structure Type", where type 1 represents fractures with typical shear indicators (fault), while type 2 is representing non-faults. A further classification is introduced by the "Complexity Factor", which indicates how many parallel flow channels a structure has. Further details concerning these two classifications can be found in the Task 6C report.

A conceptual picture of a typical structure in the TRUE Block Scale experiment is given by Figure 2-2. It is interesting to note that a fracture network, which is connected to the water carrying channel, is present on both scales shown. However, it is clear from this figure that further conceptual simplifications are needed before transport simulations can be attempted. One such simplification is given in Table 2-1, where the extent and porosity of different zones are given for the two Geological Structure Types. This information will be utilised in the modelling approach used in this report.

Below a brief account of each modelling task will be given, in order to introduce the reader to the cases considered.

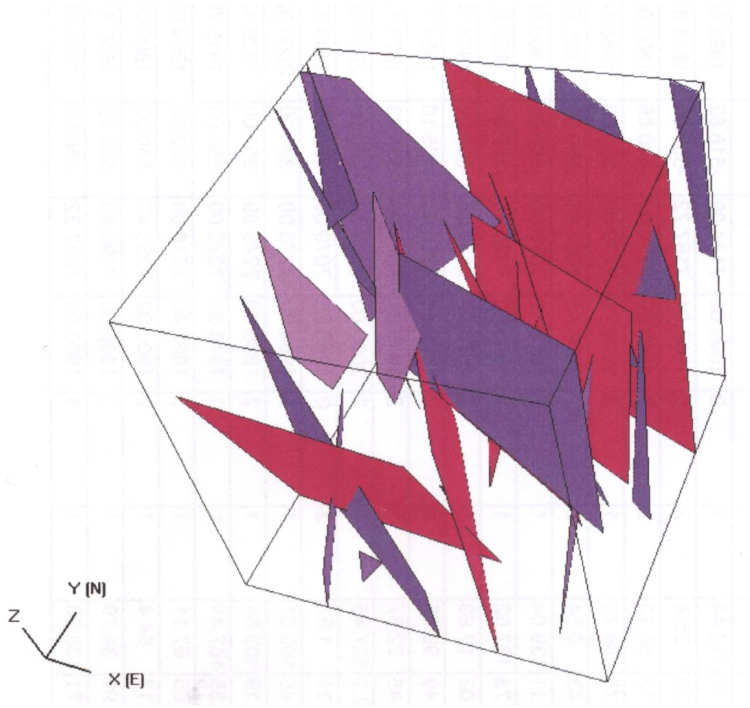

Figure 2-1. *Synthetic 100-m Structures (Blue) with Deterministic 100-m Structures (Red) in 200-m Scale Model.*

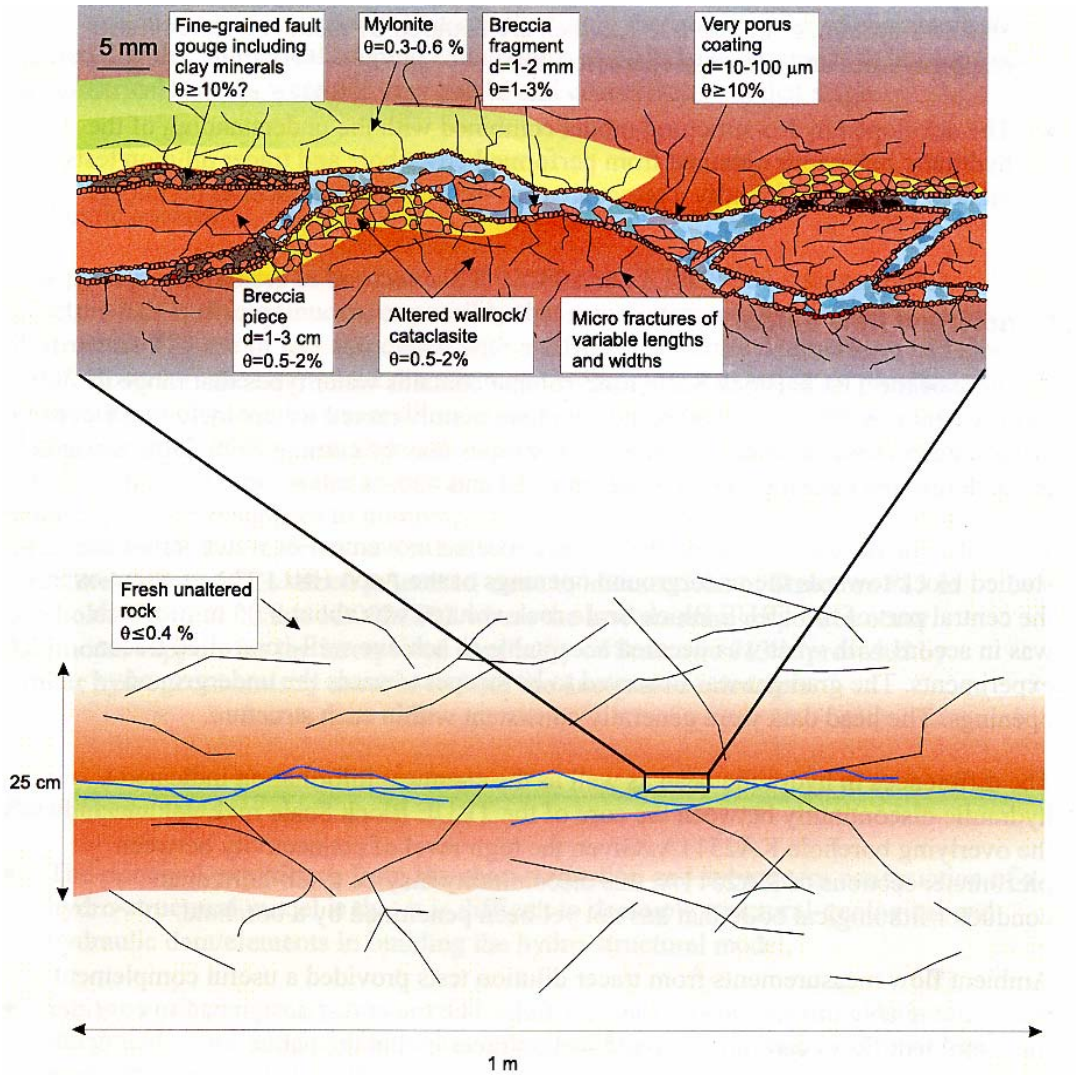

Figure 2-2. *Generalised conceptual model of a typical conductive structure involved in the tracer experiment (from Winberg et al., 2003).*

Table 2-1. Property data for the two structure types (from the Task 6C report). Properties of 100-m Scale Geological Structure Type 1 (Fault).

Rock type	Extent (cm)	Porosity %	Formation factor (-)
Intact wall rock	-	0.3	7.E-5
Altered zone	20	0.6	2.E-4
Cataclasite d_{cat}	2	1	5.E-4
Fault gouge d_g	0.5	20	5.E-2
Fracture coating d_c	0.05	5	6.E-3

Properties of 100 m Scale Geological Structure Type 2 (Non-fault).

Rock type	Extent (cm)	Porosity %	Formation factor (-)
Intact wall rock	-	0.3	7.E-5
Altered zone	10	0.6	2.E-4
Fracture coating d_c	0.05	5	6.E-3

2.2 Task 6C – Semi-synthetic hydro-structural model

The hydro-structural model introduced by Figure 2-1 and Table 2-1 is given a full account in Task 6C. The micro-structural elements as well as the procedures used to assign hydraulic, transport and other properties are described. A hydro-structural model on the 2000 metre scale is also presented in the report.

2.3 Task 6D – Block scale transport on a tracer test time scale

Task 6D is concerned with tracer transport and retention in three dimensional fracture networks. A novel feature of the task is that new information, i.e. new for transport models, is to be used; all structures and fractures are classified as fault/non-fault (the Geological Structure Type) and with respect to the number of parallel flow channels (the Complexity Factor). The challenge is to take this information into account in the simulation model. If the classification scheme correctly indicates the "resistance" to transport, it is easy to see the value of the task. Using a uniform resistance would be analogous to using the same transmissivity for all structures in a flow simulation.

The task considers experimental time scales and is actually based on a TRUE Block Scale tracer experiment (Test C2).

2.4 Task 6E – Block scale transport on a PA time scale

The same hydro-structural model as used in Task 6D is also used in Task 6E, but the forcing is intended to simulate PA time scales. This is achieved by specifying a head difference of 1 metre from the east to west boundary of the domain.

2.5 Task 6F – Test bench

In Task 6F a simplified geometry, "a test bench", is used in order to more clearly capture the effect of the Geological Structure Type specification. A 20 metres long section of a fracture, with fixed head boundary conditions, defines the test bench. Three sets of hydraulic gradients are used in order to cover both experimental and PA time scales.

2.6 Task 6F2 – Sensitivity study

This task has the general objective to provide sensitivity studies, but the modelling groups are quite free to choose what should be studied. The contribution in this report is perhaps not even a proper sensitivity study as the topic chosen is merely a discussion of how a fracture network and its properties should be specified. However, the questions of "flow geometry" and "flow wetted surface" have been a major concern throughout Task 6 and the chosen topic can hence be motivated from that point of view.

3 Model description

3.1 Introduction

Task 6 was initiated about five years ago. The development of DarcyTools was started at about the same time. Hence, the work undertaken in Task 6 has to a large extent formed the transport model in DarcyTools. Considering this background, it seems motivated to give an overview of the concepts embodied in DarcyTools, with special emphasis on transport related issues. The rest of this section is therefore devoted to an account of the geometrical, flow and transport models in DarcyTools.

3.2 Geometrical description

The situation considered is outlined in Figure 3-1; essentially it is a fracture network contained in some domain with a length scale, L.

A key assumption of DarcyTools is that "*the number of fractures in a certain length interval follows a power law*". This seems to be an undisputable assumption as it basically only states that there are more small fractures than big ones.

Numerical models normally discretize space in some way. DarcyTools is a finite-volume code and the domain in Figure 3-1 is meshed to consist of a large number of cells. Typically a grid of 100 x 100 x 100 cells is used. The next assumption introduced is related to this grid and can be stated as follows: "*in a sparsely fractured granite, flow is assumed to be distributed on relatively few flow channels, that are due to large scale fractures and zones. It is assumed that all essential flow channels are due to fractures and zones that are larger than the grid size*". If the grid size, Δ, is 0.01L this is thus the lower limit for water-carrying fractures.

Fractures smaller than the grid size, Δ, are, as discussed above, assumed to have a negligible contribution to the flow rate, but are assumed to be essential for dispersion and retention, when dealing with transport.

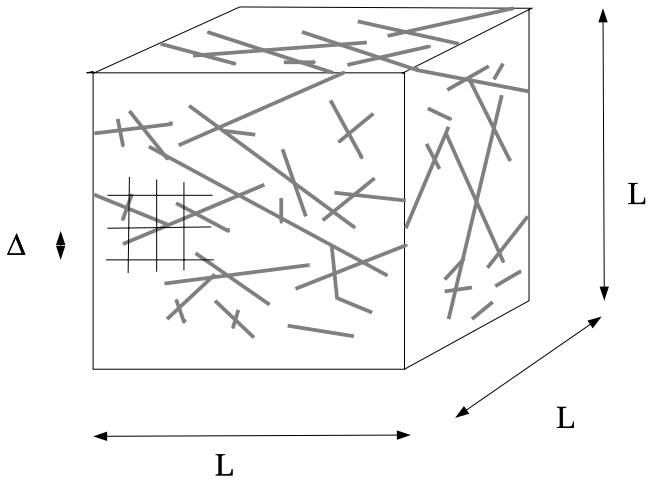

Figure 3-1. *Situation considered. A fracture network in a domain of length scale L. A grid with a cell size equal to* Δ *is also indicated.*

A subgrid model, FRAME (FRActal scaling laws and Multirate Equations), has been developed to handle these processes.

The concepts introduced form the basis of DarcyTools. In fact, the concept that fractures larger than Δ carry the water and fractures smaller than Δ are responsible for dispersion and retention is called the SOS-concept (Separation Of Scales). Figure 3-2 summarises the SOS-concept.

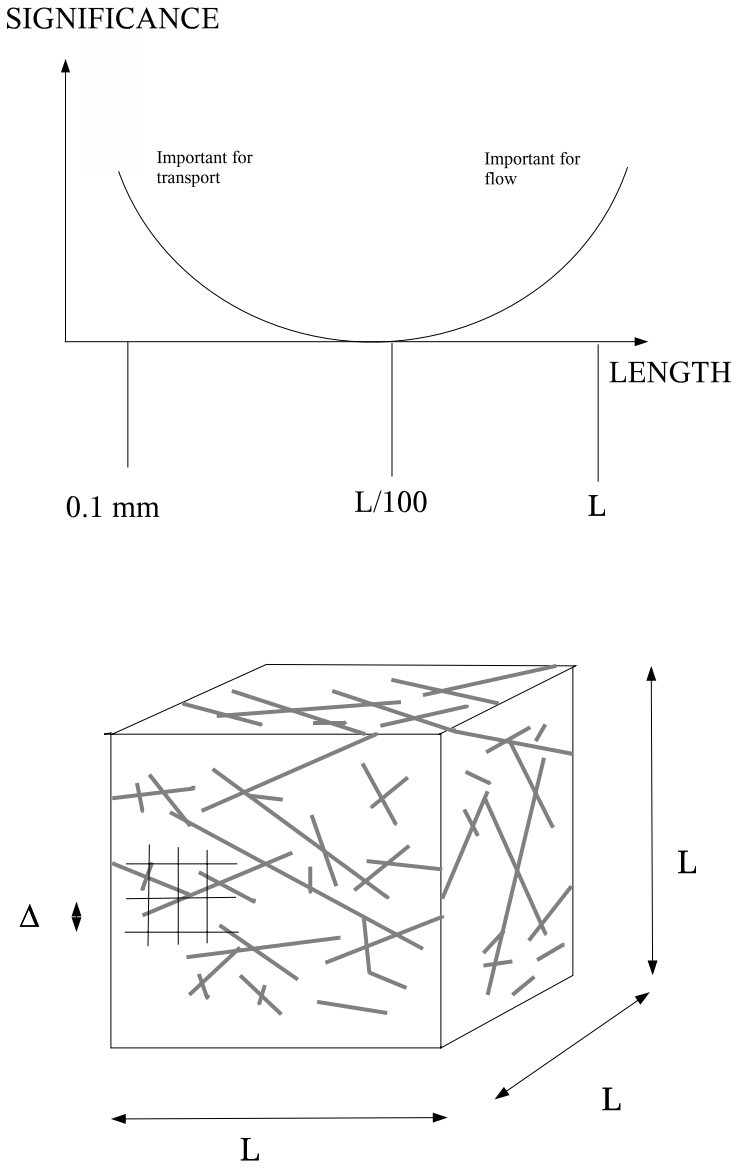

- Fractures larger than L/100 important for flow.
- Fractures smaller than L/100 important for transport (dispersion, retention).
- $\Rightarrow$ choose $\Delta \approx$ L/100 and treat small fractures in a subgrid model.

Figure 3-2. *The SOS-concept (Separation Of Scales).*

3.3 Flow model

Most numerical models of groundwater flow subdivide the studied domain into smaller volumes. If a computational grid is defined, we call these smaller volumes grid cells, and we apply the conservation laws and other constitutive relations to these. Also material properties, like hydraulic conductivity and porosity, need to be specified for the grid cells. These properties are often measured on a smaller scale (support scale) and a technique to express these on the scale of the grid cells is thus needed (upscaling). When material properties for all grid cells have been obtained, the flow simulation can be performed. In DarcyTools, we do however not follow this traditional route and the main argument for this can be stated as follows:

- In a sparsely fractured rock it is believed that most of the flow is due to a limited number of major fractures and fracture zones. The main task is thus to identify these and to represent them in the numerical model. If refined modelling is required, the next size class of fractures or fracture zones should be considered. From this point of view it seems more logical to first consider large fractures, and then progressively smaller ones, than to upscale properties from a small scale.

It is not possible to represent all fractures in the grid, simply because there are too many. In DarcyTools the smallest fracture considered will often be of the same size as the grid size. Smaller fractures, $l < l_{\min}$, are however also of importance (for dispersion) and in DarcyTools represented as storage volumes (immobile zones), see Figure 3-3. In fact, storage volumes are defined as *all* immobile zones , with $l < l_{\min}$, that exchange matter with the flowing water by molecular diffusion only.

We have thus subdivided all fractures in contact (isolated fractures are not considered) into what will be called conductive elements and storage volumes. Storage volumes will be treated as subgrid effects and are represented in the subgrid model FRAME, to be described below. Conductive elements generate all grid properties by the GEHYCO-method which can now be formulated as:

- A conductive element contributes to the grid value of a variable by an amount which is equal to the intersecting volume times the value of the variable in question. Contributions from all elements that intersect the control volume are added and the sum is divided by the volume of the cell.

This basic principle will now be explained and illustrated, using Figure 3-4. A conductive element of thickness b is crossing a computational grid, which has a cell size of Δ. A staggered grid is to be used, which means that scalar quantities, like pressure and salinity, are stored at cell centres while velocity vectors are stored at cell wall centres, see Figure 3-4. This grid arrangement was first introduced by Harlow and Welch (1965) and is described in text books, see for example Patankar (1980). Each variable is assumed to be representative for a certain control volume, which is the volume the discretized equations are formulated for. For a velocity cell it is clear that the driving pressure force can be easily formulated. As we are going to apply the Darcy law to the velocity cell we also need a relevant cell conductivity to obtain the cell wall velocity. How to calculate this conductivity, and other properties, is the main subject of the GEHYCO-method.

To obtain the porosity, as an example, of the scalar cell marked in Figure 3-4 the following steps are performed.

- Calculate the intersecting volume between the conductive element and the cell; this volume is marked in the figure.
- If the porosity of the conducting element is θ_e, the contribution to the free volume is $\theta_e V_i$, where V_i is the intersecting volume.
- Calculate the contributions from all conductive elements that cross the cell.
- Obtain the cell porosity as the sum of all contributions divided by the cell volume.

In Figure 3-4 a control volume for a velocity cell is also marked. The procedure to obtain the conductivity for this control volume is analogue to the steps above.

By this procedure the porosity, flow wetted surface and storativity are determined for all scalar cells and the conductivities and diffusivities for all cell walls.

An assumption in the statement above is that "contributions from all elements that intersect a cell are added". If two, or more, fractures intersect a velocity cell, the cell conductivity should represent a fracture intersection (neglecting the case of parallel fractures of various orientations). Neretnieks (1993) discusses various concepts about channelling at intersections, but concludes that no firm information is available. He cites however a number of observations that support the idea that "fracture intersections form easy pathways". In lack of any firm information, it will therefore be assumed that contributions can be added. Fracture intersections will hence form "easy pathways".

The basic principle of the method is obviously very simple but, as has been demonstrated (see the DarcyTools documentation, Svensson et al., 2006) still general enough to handle even complex fracture networks. A few properties of the method can already at this stage be identified:

- All cell wall conductivities will be different, as we generate three conductivity values (in a 3D case) for each scalar cell. A conductivity field that is anisotropic on the cell scale is hence always generated.
- A fracture smaller than the cell size can not generally contribute to the anisotropy or correlation of the conductivity field.

Some simple calculations that illustrate the GEHYCO method, and also demonstrate the accuracy that can be expected, can be found in Svensson et al. (2006).

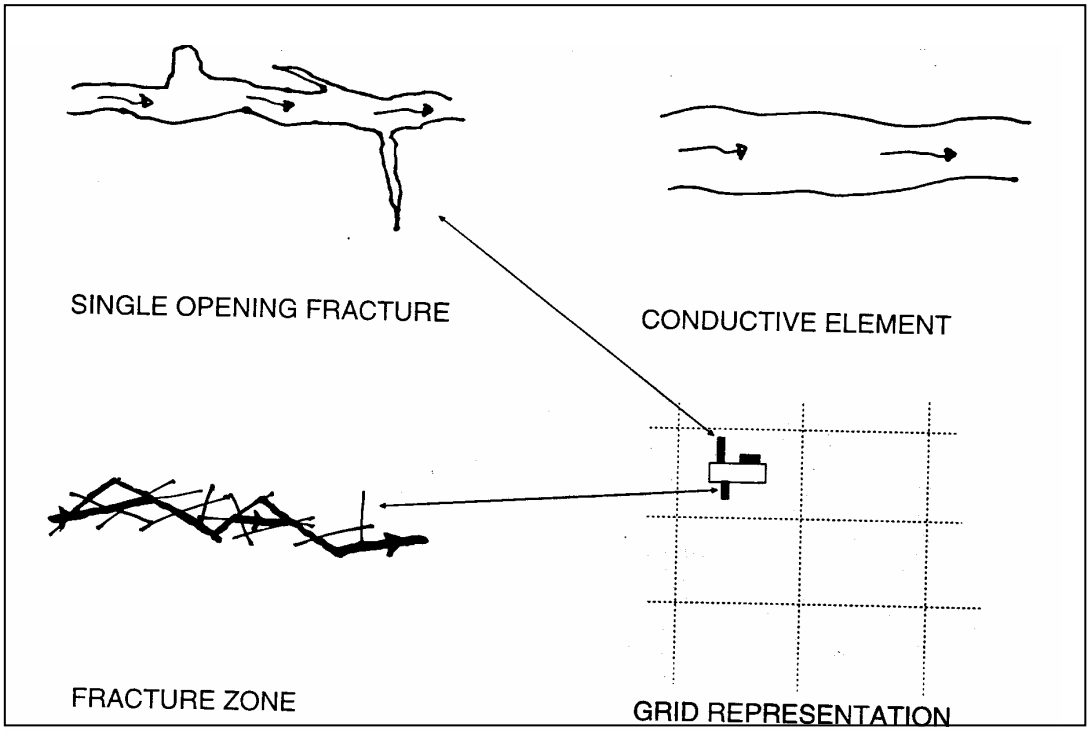

Figure 3-3. *Representation of kinematic (or mobile) and storage (or immobile) volumes in the grid. The open rectangle in the grid represents a kinematic volume (generated by the conductive element), while filled rectangles represent storage volumes.*

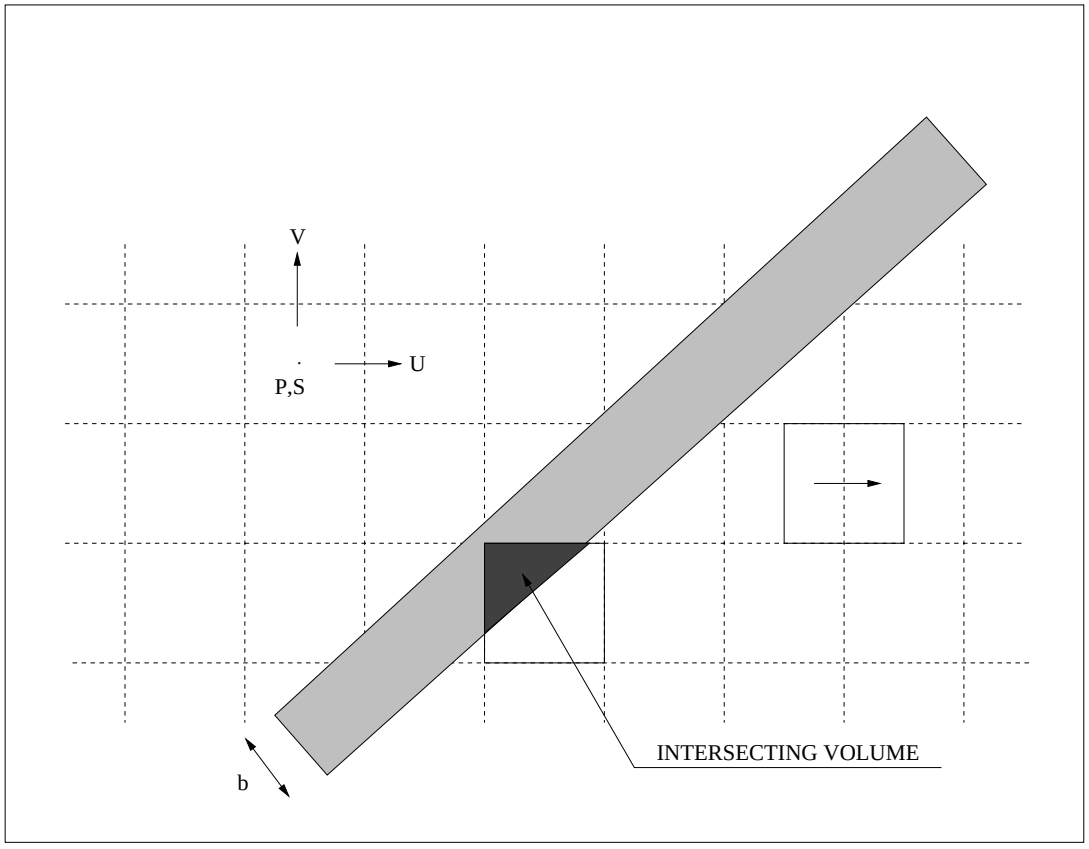

Figure 3-4. *Illustration of concepts and methods for calculating grid properties.*

3.4 Transport model

When discussing transport and dispersion of solutes it is useful to distinguish between two different problems with respect to the time scale. The first kind of problem is the field experiment with a time scale from weeks to perhaps a year. A longer time scale, which may be thousands of years, needs to be considered when, for example, the water types present in the fracture network is to be analysed. At Äspö HRL, water from the last glaciation (about 11 000 years ago) has been found already at a depth of a few hundred metres. The relevant processes for the two problems will now be described, in turn.

Let us think of a typical field tracer experiment where a tracer is injected in one borehole and the arrival in another, pumped, borehole is studied. The curve describing the time distribution of the concentration in the pumped borehole is called the breakthrough curve (BTC). Obviously the tracer is transported by advection between the two boreholes, and the flow field is hence an important element in the analysis. A number of dispersion processes will however affect the tracer as it travels through the fracture network. The most important of these are:

- **Intersections.** At a fracture intersection a tracer cloud may split up and enter pathways with different lengths and fluid velocities. This type of dispersion is often called macro-dispersion.
- **Channelling.** Spreading occurs within each fracture plane as the different streamlines have different path lengths and velocities. The flow channels may also merge or split up.
- **Taylor dispersion.** A velocity profile exists between the two bounding walls of the fracture. The resulting dispersion effect is called shear- or Taylor dispersion.
- **Matrix diffusion and sorption.** Interaction with the rock, stagnant pools and microfissures causes a number of processes that in effect lead to a delay and dispersion of a tracer pulse. These include: sorption on the fracture walls, diffusion into the rock matrix with sorption on inner surfaces and interaction with gouge.

As mentioned earlier, the diffusion into dead-end fractures of various sizes is by molecular diffusion. In order to illustrate the typical penetration depth for this process one may think of a substance with a certain molecular diffusion constant $\left(D_{mol} = 10^{-10}\ \mathrm{m}^2/s\right)$ and an experimental time scale of, say, one month $\left(t \approx 2.6 \times 10^6\ \mathrm{s}\right)$. The penetration length can then be estimated as $\sqrt{D_{mol} \times t} = 0.016$ metres. As the immobile zone is mainly made up of small fractures one can conclude that small scale dispersion is mainly governed by processes on the mm to cm scale.

For the transport problem on long time scales we may use the salinity field to illustrate some key features. First we can note the time scale for exchange in larger (> metres) dead-end fracture systems. If we put $D_{mol} = 10^{-10}$ m^2/s and $L = 10$ metres, we find that the time scale is 10^{12} seconds, or 30 000 years $\left(t = L^2 / D_{mol}\right)$. It is thus not surprising to find water from the last glaciation, or the Litorina Sea (≈ 7 000 years BP), in the fracture system at Äspö HRL. Gravitational forces may further enhance the entrapment of water in dead-end zones. If, for example, Litorina water (which has higher salinity

than the present Baltic water) is located in a dead-end fracture extending downwards from the mobile zone gravitational forces will enhance the entrapment. The same principle applies to glaciation water (which has a lower density than present Baltic water) in a dead-end fracture extending upwards from the mobile zone. If we further note that the volume of all immobile zones is larger than the volume of the mobile zone, one can draw the conclusion that the salinity field is "stiff" and requires very long time scales to reach a steady state. On a shorter time scale all processes listed above is of course also active for the dispersion of salt.

DarcyTools has two built-in options for transport simulation; a particle tracking algorithm, PARTRACK, and advection/dispersion equations. The reasons why two methods are needed are based on the following assumptions:

- Salinity. The salinity field strongly influences the flow field through the density field. It is difficult to describe the salinity field by a set of particles and an advection/dispersion equation is therefore the best choice.

- Temperature. The main heat flux component is conduction and an advection/dispersion equation is hence the obvious choice for this variable. It will further be assumed that the water and rock is always in thermal equilibrium and only one temperature is thus solved for.

- Tracers. Simulation of tracer transport is best performed with a particle approach as this method is free from numerical dispersion effects. It is also possible to treat sorbing tracers (like radionuclides) with this technique.

These are the main scalars that need to be considered in applications. If additional scalar simulations are requested a decision about the most appropriate method has to be taken.

Transport of salt and tracers are assumed to be restricted to the water phase. Dispersion is hence due to mixing at fracture intersections (macro dispersion) and exchange with immobile zones (micro dispersion, as embodied in FRAME). FRAME is hence developed for both the advection/dispersion equation (as used for salt) and PARTRACK (as used for tracers).

FRAME rests on a number of concepts and assumptions of which the most essential are:

- *Fractures smaller than Δ are assumed to be filled with stagnant water (immobile volumes) and exchange matter with the flowing water (mobile volumes) by diffusion only.*

- *Subgrid fractures are assumed to follow a power-law (same as for resolved fractures).*

- *All immobile volumes can be represented by a set of boxes (or storage volumes), each with its own length scale, volume and effective diffusion coefficient.*

In Figure 3-5 some subgrid processes and concepts are illustrated. Let us consider a computational cell with a through flow, i.e. a cell with a flow channel. The flow "sees" a certain surface area, the flow wetted surface (FWS), as it passes the cell. The FWS may bring the flowing water in contact with other fractures, gouge material, stagnant pools, etc. Most of these volumes can be expected to have stagnant water and mass exchange is hence due to molecular diffusion. For a stagnant pool the relevant diffusion

coefficient may be that for pure water, while diffusion into crossing fractures and the rock matrix may proceed with a diffusion rate that is several orders of magnitude smaller. As above, we will call the volume with flowing water the mobile zone and the volumes with no advection the immobile zone. Fractures and volumes which are not in contact with the mobile zone are of course of no relevance and can be excluded from the discussion. The situation outlined in Figure 3-5 is quite complicated and does not lend itself to direct descriptions of individual processes. The idealised problem is illustrated in Figure 3-6. The box with the smallest length-scale (dimension perpendicular to the mobile zone) will have the largest diffusion coefficient and normally also the largest contact area with the mobile zone. This volume will hence have a fast response. The multi rate diffusion technique (Haggerty and Gorelick, 1995) provides an efficient way to handle this problem computationally.

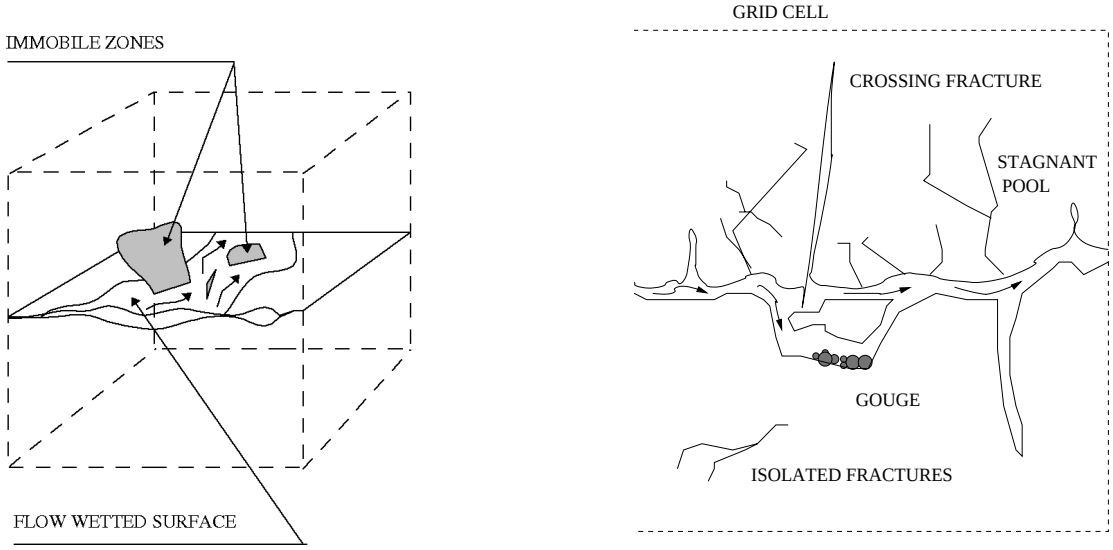

Figure 3-5*. Illustration of subgrid processes and concepts.*

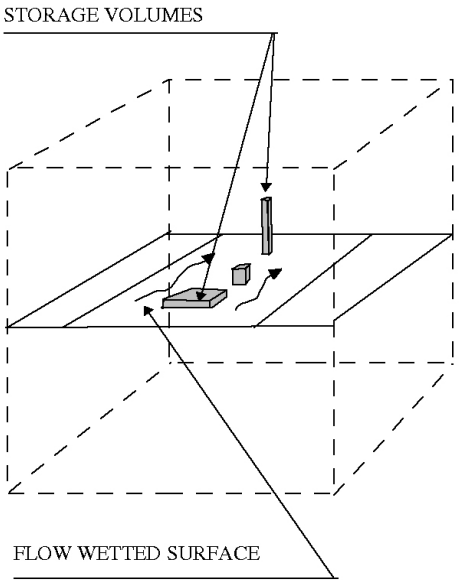

Figure 3-6. *The assumed structure of subgrid volumes and areas.*

After this general introduction to FRAME, we will end this chapter by a brief introduction to the FRAME parameters. In Figure 3-7 the parameters to be discussed are introduced. Connected to the mobile zone, a range of "first order diffusion boxes" are found. Each box has a certain volume and an exchange rate attached to it. The volume distribution is governed by the total immobile volume, Vol_{im}, and the slope of the distribution which can be related to k, the late time slope of the breakthrough curve (BTC). The maximum and minimum exchange rates are denoted $\alpha_{\min}$ and $\alpha_{\max}$ respectively. The ratio Vol_{im}/Vol_m is denoted β_c where index *c* stands for cell. We will also need $\beta_G = \sum Vol_{im} / \sum Vol_m$, where *G* stands for global and is hence the volume ratio for the whole computational domain.

The parameter β_c will vary from cell to cell, while β_G is a constant in a particular simulation. The β_c distribution is based on the concept that "the immobile volume in each cell is proportional to the *FWS* in the cell ". This results in the following relation:

$$\beta_c = \beta_G \left(\frac{FWS}{Vol_m} \right)_{cell} / \frac{\sum FWS}{\sum Vol_m} \tag{3-1}$$

It is interesting to note that β_c is then proportional to a_w, the *FWS* per unit mobile volume, that is part of the relation $F = a_w \times t$, where *F* is the so called *F*-factor and *t* a residence time. The *F*- factor is well established as the main controlling factor in retention processes and it is hence of importance to note the close link between β_c and a_w.

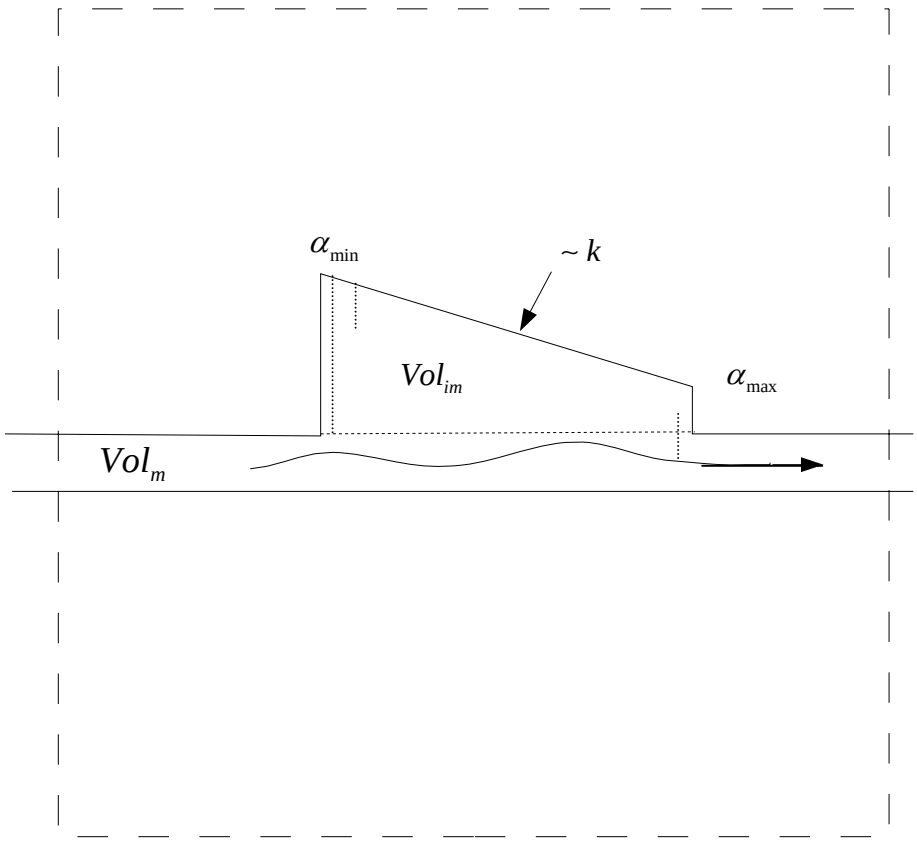

Figure 3-7. *The FRAME parameters.*

Now let us consider the effects the Geological Structure Type (*GST*) and Complexity Factor (*CF*) will have on retention.

GST: According to Table 2-1 the main difference between type 1 and 2 is that type 1 has more and thicker porous layers adjacent to the flow channel.

CF: Increasing the number of parallel flow channels increases the flow wetted surface and hence the access to the matrix.

The approach that will be tested in this report can now be formulated as follows:

> *GST = 1 has more retention capacity than GST = 2 and an increase in CF increases the retention capacity, as compared to CF equal to 1. These effects can qualitatively be accounted for by distributing more immobile volumes to cells which contain these high retention structures.*
>
> Thus: $vol_{im} \sim FWS \times \left(1 + C_{GST}\left(2 - GST\right)\right) \times \left(1 + C_{CF}\left(CF - 1\right)\right)$ (3-2)
>
> where C_{GST} and C_{CF} are constants.

It is clear that *GST* = 2 and *CF* = 1 will reduce the expression to the "standard" formulation outlined above. It should further be noted that specifying *GST* = 1 and *CF* > 1 will increase vol_{im} for a cell that is crossed by such a fracture, but it will also decrease vol_{im} where *GST* = 2 and *CF* = 1, as the global ratio vol_{im} / vol_m is constant. The right hand side of (3-2) is thus a weighting factor that is ascribed to each structure and fracture and then calculated for each computational cell by the "intersecting volume concept" (see Svensson et al., 2006).

4 Results – general

4.1 Introduction

As FRAME constitutes a novel approach to transport and retention modelling it is needed to demonstrate that its parameters can be determined and understood. This is the objective of this section. The main departures from the traditional approach are:

- No dispersion coefficient is specified; instead the dispersion is a result of exchange with immobile volumes.
- The shape of the cloud is not Gaussian, as in the traditional theory, but "long-tailed".
- The centre of the cloud does not travel with the water velocity, but is delayed.

Unfortunately there is no theory (or analytical solution) available that determines the dispersion and delay of the cloud as a function of $\alpha_{\min}$, $\alpha_{\max}$, k and β_c. It is the objective of this chapter to relate the dispersion and delay to the basic parameters of FRAME.

When simulating a BTC all FRAME parameters (see Figure 3-7) affect the shape of the BTC. Presently the following values are recommended:

- $\alpha_{\min} = 10^{-10}\left[s^{-1}\right]$. This value will give diffusion boxes that are slow enough considering the time scale of most field experiments.
- $\alpha_{\max} = 10^{-3}\left[s^{-1}\right]$. Can be interpreted as the rate based on a molecular diffusion coefficient of 10^{-9} m^2/s and a length scale of 10^{-3} m. $\left(\alpha_{\max} = D_{mol} / l^2\right)$. The smallest length scale is hence assumed to be comparable to a typical aperture.
- *k*, the late time slope of the BTC. In the earlier Task 6 work it was found that $k = 2.0$ fits data quite well and we will adopt this value.
- β_G. A value of 10.0 was estimated in earlier Task 6 work.

In this chapter we will further analyse and establish these parameter values and in particular introduce the geological structure type and complexity factor.

4.2 β_c and β_G

In the TRUE Block Scale project a number of tracer transport experiments have been conducted. Some results, relevant for this study, are given by Figure 4-1 and Table 4-1, taken from the SKB report TR-02-15. The general conclusion from these studies is that the dispersion α_L scales with path length and the regression coefficient is 0.07. It should further be noted that α_L was evaluated by:

$$\alpha_L = \frac{L_p}{8}\frac{\left(t_{84} - t_{16}\right)^2}{t_{50}^2} \tag{4-1}$$

where L_p is path length and t_{16}, t_{50}, t_{84} are times to 16%, 50% and 84% mass recovery.

Here we will select a few of this transport experiments (favouring those with high recovery) and compare with simulations.

The simulations will be performed as follows: Use the water velocity, U_w and β_c as calibration parameters and try to fit T_{50} and α_L for a given experiment. Study a number of experiments and conclude the findings regarding β_c. Note, as we study a one-dimensional path β_c is equal to β_G.

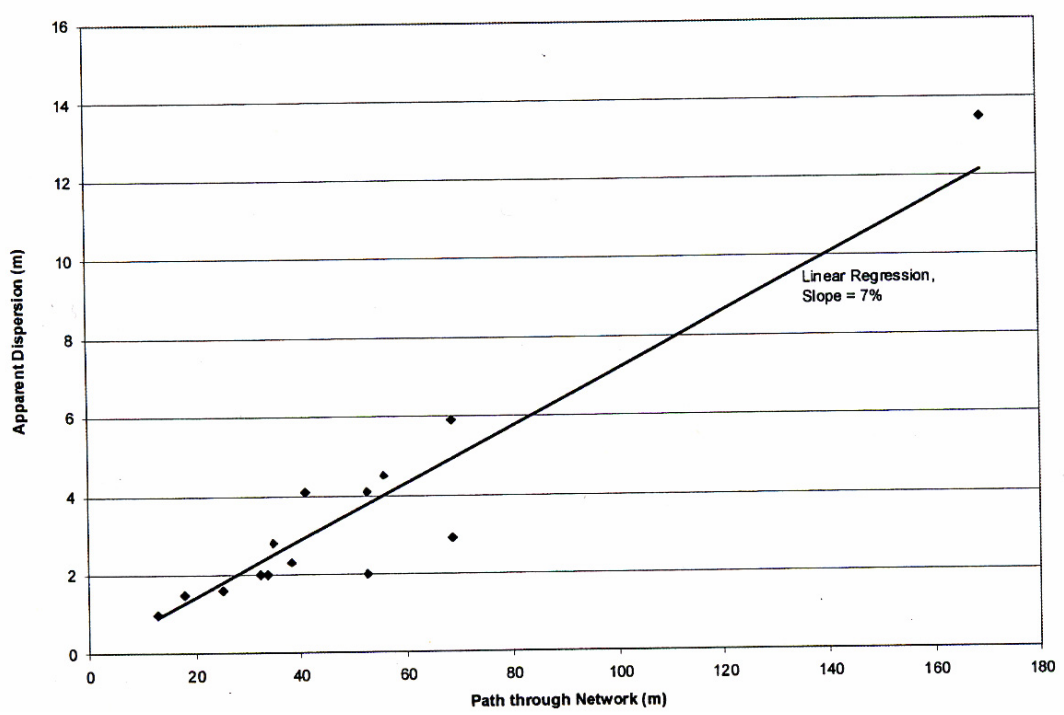

Figure 4-1. *Apparent dispersion for conservative tracers as a function of the path length through the fracture network*

Table 4-1. Tracer tests in TRUE Block Scale Experiment.

Test	Pathway Source → Sink	Path Length[1] (m)	FIZ Crossings[1]	Effective Dispersion[2] (m)	Measured Recovery	Projected Ultimate Recovery[3]
A4a	KI0025F03:P5 → KI0023B:P6	17.9	0	1.5	38%	70%
A4b	KI00F03:P6 → KI0023B:P6	52.7	2	2	51%	90%
A4c	KI0025F03:P7 → KI0023B:P6	68.6	3	2.9	0	0
A5a	KA2563A:S4 → KI0025F03:P5	38.4	0	2.3	64%	72%
A5b	KI0025F02:P3 → KI0025F03:P5	55.9	1	4.5	0	0
A5c	KI0025F02:P5 → KI0025F03:P5	12.9	0	1	130%	100%
A5d	KI0025F02:P6 → KI0025F03:P5	41.1	1	4.1	43%	60%
A5e	KI0025F03:P6 → KI0025F03:P5	35	1	2.8	95%	100%
B1a	KI0025F03:P5 → KI0023B:P6	17.9	0	1.5	99%	100%
B1b	KI0025F03:P6 → KI0023B:P6	52.7	2	4.1	45%	65%
B1c	KI0025F02:P5 → KI0023B:P6	33.8	0	2	36%	38%
B2a	KI0025F03:P6 → KI0023B:P6	52.7	2	4.1	49%	60%
B2b	KI0025F02:P3 → KI0023B:P6	32.5	0	2	82%	85%
B2c	KA2563A:S1 → KI0023B:P6	169.2	2	13.5	3%	10%
B2d	KI00F03:P7 → KI0023B:P6	68.6	3	2.9	76%	80%
B2e	KI0025F03:P3 → KI0023B:P6	25.3	1	1.6	32%	36%
B2g	KI0025F03:P5 → KI0023B:P6	17.9	0	1.5	97%	99%
C1	KI0025F03:P5 → KI0023B:P6	17.9	0	1.5	111%	100%
C2	KI0025F03:P7 → KI0023B:P6	68.6	3	5.9	80%	100%
C3	KI00F02:P3 → KI0023B:P6	32.5	0	2	72%	80%

1. Path length and number of fracture intersection zone (FIZ) crossing calculated through the hydrostructural model.
2. Effective dispersion calculated using formula from /Domenico and Schwartz, 1992/, subtracting the dispersion in the injection curve calculated using the same formula.
3. Projected ultimate recovery (PUR) calculated by graphical projection of measured breakthrough curves to 10,000 hours.

Table 4-2. Measured and simulated α_L in some TRUE Block Scale Experiments.

Test	Measurements			Simulations					
	Path L (m)	α_L (m)	T_{50} (h)	$U_w \times 10^4$ (m/s)	β_c	T_{50} (h)	T_{16} (h)	T_{84} (h)	α_L (m)
C1	17.9	1.5	20	3.8	2.5	18.8	15.8	31.9	1.48
C2	68.6	5.9	260	1.9	4.4	263	207	426	5.94
C3	32.5	2.0	820	0.28	3.6	818	670	1247	2.02
A5e	35.0	2.8	153.6	1.4	3.5	150	119	239	2.80
A5a	38.4	2.3	81.8	2.2	2.3	80.0	65.9	121.0	2.33
A5c	12.9	1.0	7.8	5.9	2.1	7.86	6.40	12.61	1.01
A4b	52.7	2.0	163.5	1.4	1.7	160	137	226	2.04
B2a	52.7	4.1	460.7	0.85	4.2	460	368	733	4.14
B2b	32.5	2.0	472.9	0.42	3.1	477	392	725	1.98

The outcome of the simulations can be studied in Table 4-2. As we have two parameters (U_w and β_c) to fit the experimental data, a good agreement for α_L can be achieved; the small differences found could be eliminated by further tuning of U_w and β_c. However, the main conclusion and result is still that β_c varies between 1.7 → 4.4. This is a fairly narrow range considering the variations in path length (12.9 → 68.6 m) and T_{50} (7.8 → 820 hours) in the experiments.

The experiments discussed involve fractures 20, 21, 22 and 23 in the TRUE Block Scale volume. The fractures have lengths from 24 to 120 metres. Probably also a number of large fractures belonging to the stochastic network affect the experiments. The conclusion from the previous section is thus: fractures/zones with length scales of 20 → 200 metres should have a β_c in the range of 1.0 → 5.0 in order to provide the right dispersion.

Next we will generate the complete fracture network (including deterministic zones) in the TRUE Block Scale volume and study the relation between β_G and β_c for the large zones. The reason for this is that it is β_G that is the input parameter to FRAME. Once again we will rely on the experiences from earlier work, when specifying the properties of the stochastic network. The key feature of the network is the power-law (with coefficient 2.6) distribution of lengths. Stochastic fractures in the length interval 2 → 200 metres were generated, while eleven deterministic zones were specified. Thicknesses and apertures were calculated according to the DarcyTools manuals. The TRUE Block Scale volume is 200 x 200 x 200 m^3.

The main result is given by Figure 4-2, where the cell porosity is plotted versus β_c. It is easily concluded that the largest porosities are due to the largest fractures/zones and we may conclude that the largest zones have a β_c in the range 1-5. As β_c is linearly related to β_G, it is part of the result that β_G was put to 10 in this simulation. In the figure, four horizontal lines appear. These are related to the four stochastic fracture sets that were specified. The lines can be explained as “cells that only have fractures from one set” (details left out).

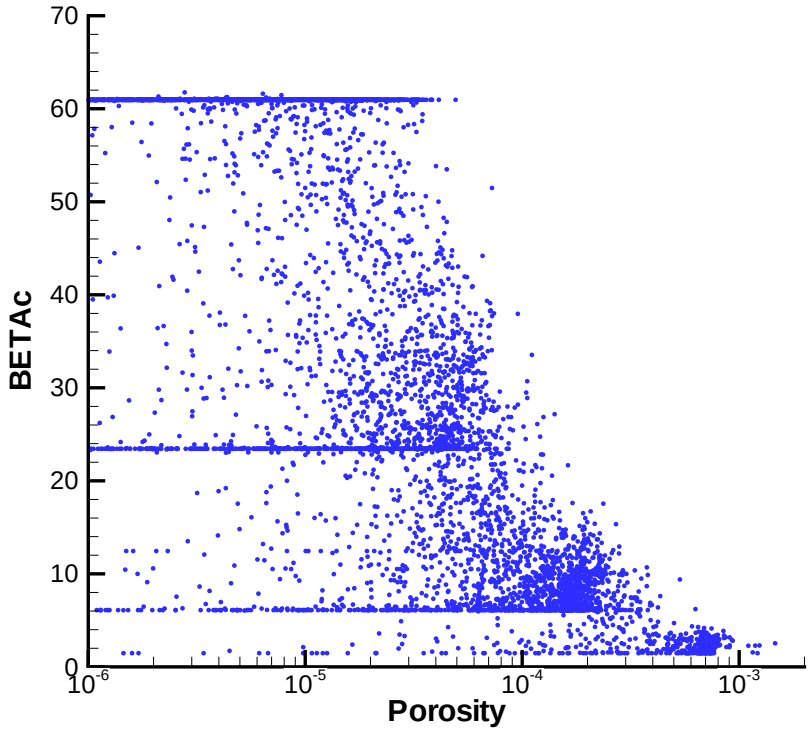

Figure 4-2. *The TRUE Block Scale fracture network. Simulated correlation between* β_c *and porosity.*

A further analysis of the result can be carried out by the earlier mentioned relation between β_c and a_w $\left(FWS/Vol_m\right)$:

$$\beta_c = \beta_G \; a_w / \left(\frac{\sum FWS}{\sum Vol_m} \right) \tag{4-2}$$

$$\Rightarrow a_w = \frac{\beta_c}{\beta_G} \left(\frac{\sum FWS}{\sum Vol_m} \right) \tag{4-3}$$

As $\beta_c = 1-60$, $\beta_G = 10$, $\sum FWS = 5\times10^6$ m^2 and $\sum Vol_m = 475$ m^3 (as calculated from the fracture network) we get the relation

$$a_w \approx \left(1 \rightarrow 60\right)\times10^3 \tag{4-4}$$

In a recent paper (Cvetkovic et al., 2004), a relation between F and t $\left(F = a_w t\right)$ is discussed and it was found that:

$$F = 3241t^{1.59} \tag{4-5}$$

and hence $a_w = 3241t^{0.59}$. Note that Cvetkovic et al. use a notation where $F = \beta$ and $t = \tau$. The transport times obtained by Cvetkovic et al. were in the range $4 \rightarrow 300$ years, which give a_w values in the range $\left(7 \rightarrow 94\right)\times10^3$. It may seem odd to compare the a_w ranges as Cvetkovic et al. obtained their relation from transport simulations, while (4-4) is obtained directly from the fracture network properties. Nevertheless, it is encouraging that the inherent a_w-values are compatible in the two models.

4.3 Late time slope, *k*

Of the FRAME parameters we specify for a non-sorbing tracer $\left(\alpha_{\min},\ \alpha_{\max},\ \overline{\beta}_{\mathrm{t}} \text{ and } k\right)$ the "late time slope of the BTC", *k*, is not directly related to the physical properties of the immobile volumes. From comparisons with measured BTC:s, we know that a value around 2.0 seems to produce good agreement and it is also possible to find some support in the literature for this value (Haggerty et al., 2000).

It is however possible to relate *k* to measurable parameters, like porosity and diffusion coefficients. This is the objective of this section

The ratio between the immobile and mobile volumes, β_G, is regarded as an input parameter in this analysis.

In Svensson et al. (2006), Appendix B, it is shown that *k* can be related to three properties of the immobile zones:

- D_f, the power-law coefficient of the fracture network that makes up the immobile volumes.
- $e_T \sim l^{\gamma}$, the aperture, which is assumed to be related to the length scale, *l*, of the immobile volume.
- $D_e \sim l^{\psi}$, the effective diffusion coefficient is assumed to be related to *l*.

The following relation is derived:

$$k = \frac{D_f - \gamma - 2\psi + 1}{2 - \psi} \tag{4-6}$$

For a computational cell, with a given β_c, we will now explicitly generate the number of fractures that can be in contact with the mobile zone, using a certain D_f. We then specify a γ and can estimate the volumes in different size classes. A small computer program was written for this analysis. It can further be shown that $D_f - \gamma$ governs the porosity distribution perpendicular to the mobile zone. Similarly it can be shown that ψ governs how the effective diffusion coefficient for a certain "sample length" in this direction decreases.

It should be noted that β_c only provides a linear scaling in this analysis, a value of 10.0 was used in the following.

In Figure 4-3, the porosity distributions for three values on $D_f - \gamma$ are shown together with a curve that is estimated from measurements, see Figure 4-4. Some support for $D_f - \gamma = 3.0$ (best slope as compared to measurements, see Figure 4-3) can be found; however data does not allow any firm statements. An often cited value on D_f is 2.6 (also the standard value used in DarcyTools) which gives γ equal to -0.4.

Archie's law will be used to estimate ψ.

In the Task 6C report the following form of the Archie's law is given

$$F = 0.71 \times \varepsilon^{1.58} \tag{4-7}$$

where *F* is the formation factor $\left(D_e = F \times D_w\right)$ and ε the porosity for a sample. We now study different sample lengths by averaging the properties over different distances in a direction perpendicular to the mobile zone. Once the porosity is estimated we can determine the *F*-value from equation (4-7). We can also calculate D_e for all size intervals in the sample and average (volume averaging). The result is shown in Figure 4-5, where curves for three different ψ are shown. Once again, it is difficult draw any firm conclusions but $\psi = -1.0$ is anyway regarded as acceptable. From Figure 4-5 we find that the diffusion coefficient changes by a factor of five when the sample length changes from 1 mm to 1 cm. This is in fair agreement with the data shown in Figure 4-6.

The values found; $D_f = 2.6$, $\gamma = -0.4$ and $\psi = -1.0$ give a $k = 2.0$, according to equation (4-6). One way to summarise the results of this section is thus to state that "a set of values for D_f, γ, and ψ which gives a realistic *k* and imply a realistic distribution of porosity and diffusivity in the matrix, have been found". The comparisons with data and Archie's law are however not conclusive, but do at least not contradict these sources of information. A further comparison with the porosity distribution in structures at Äspö is given by Figure 4-7. For the C_{GST} and C_{CF} values adopted (details in Section 4.4) we find that $\beta_{cell} = 12.4$ for structure 20, see Table 4-3. The calculated distribution in Figure 4-7 is based on this value.

The main conclusion from this section is, in the author's view, that the FRAME parameter *k* can be related to the porosity and diffusivity distributions in the matrix. It is further of value to demonstrate that plausible values on D_f, γ, and ψ give a *k* equal to 2.0, which also has been found to give realistic BTC:s in tracer simulations.

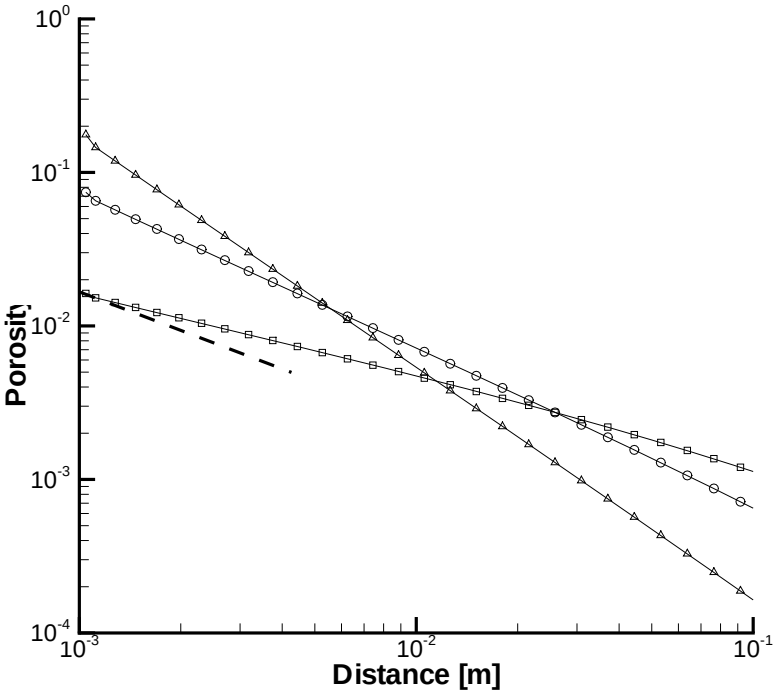

Figure 4-3. *Porosity distributions for three values of* $D_f - \gamma$ *and measured distribution (* ------- *).*

$D_f - \lambda = 2.5$

$D_f - \lambda = 3.0$

$D_f - \lambda = 3.5$

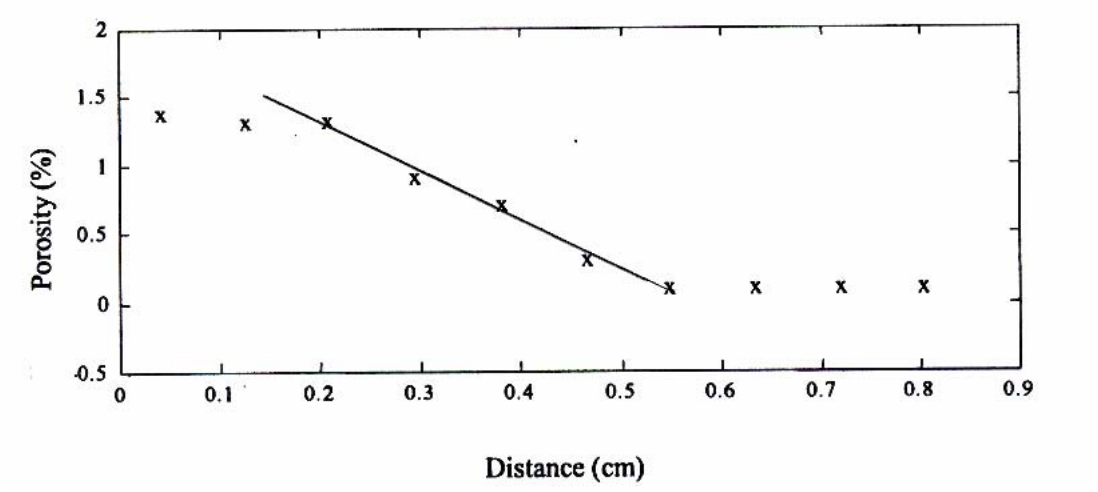

Figure 4-4. *Measured porosity, from Byegård et al. (2001). Solid line gives the slope shown in Figure 4-3.*

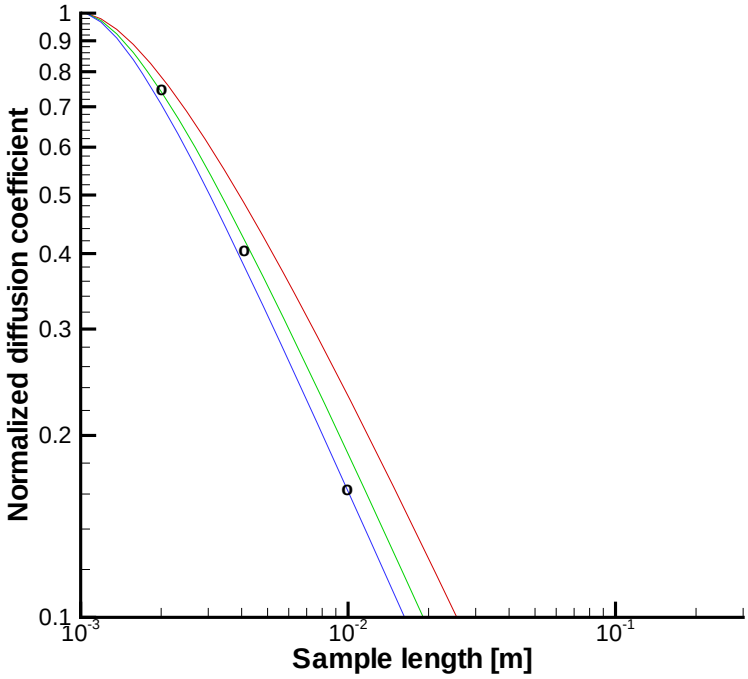

Figure 4-5. *Normalised diffusion coefficient* $\left(D_e / D_w\right)$ *versus sample lengths. Points give estimates from Archie's law. Solid lines simulations with* $\psi = -1.5$ *(blue), -1.0 (green) and -0.5 (red).*

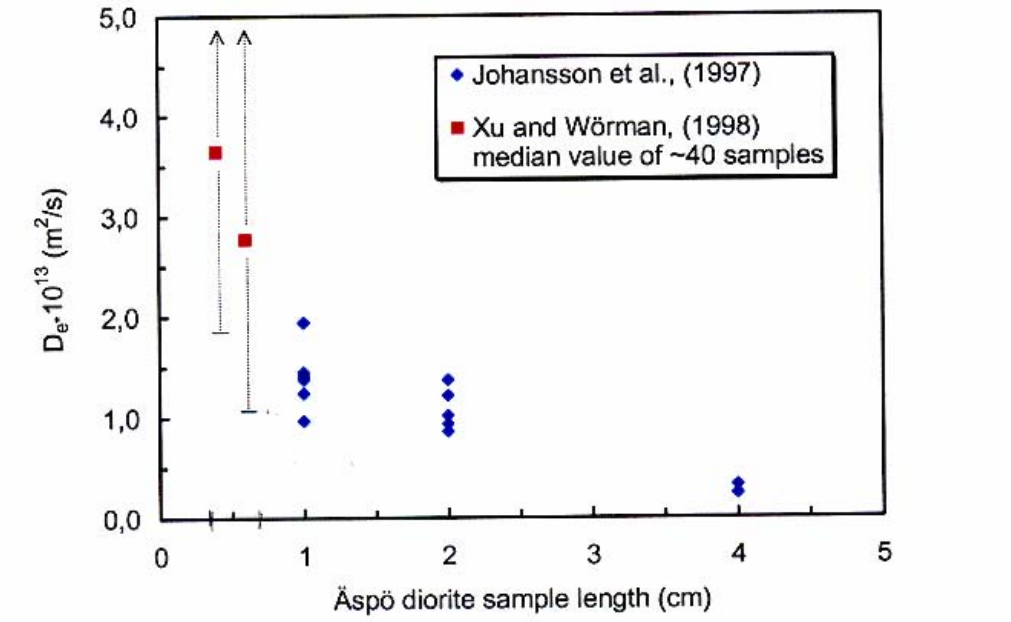

Figure 4-6. *Effective diffusion coefficient versus sample length, from Byegård et al. (2001).*

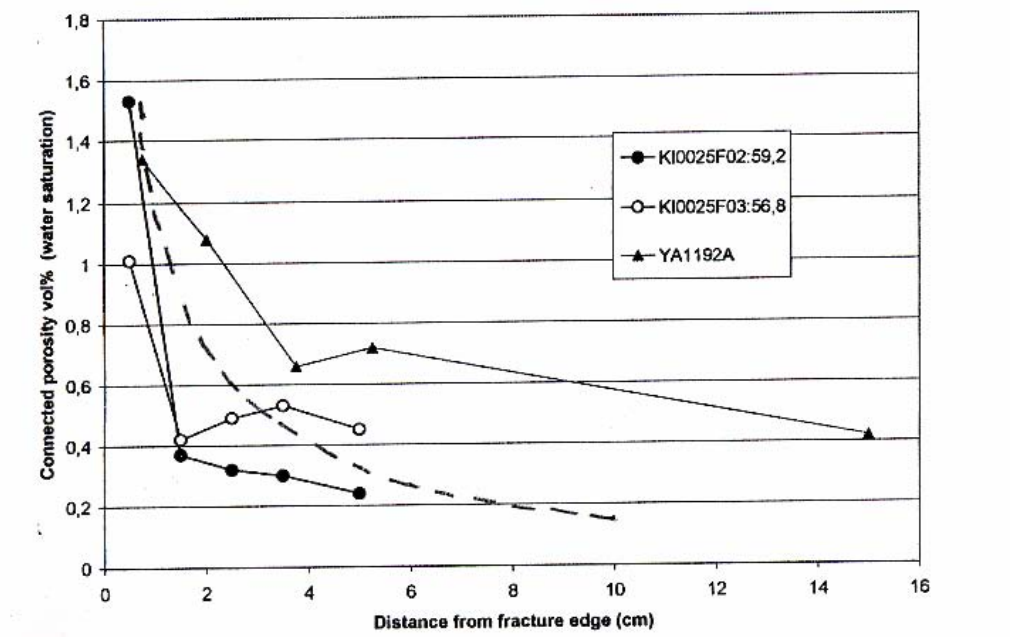

Figure 4-7. *Observed porosity distributions at Äspö. Broken line from present work. Basic figure from Winberg et al., 2003*

4.4 Geological structure type and Complexity factor

Next we consider the two constants in Equation (3-2). It is partly a conceptual question as one may have different views on whether "flow in a sparsely fractured granite is in parallel channels or predominantly in a single channel". The present writer favours the latter alternative and we should then put C_{CF} to a small value in order to reduce the influence of parallel flow channels on retention.

It is however possible to base the values of C_{GST} and C_{CF} on data. As shown above, we can estimate a porosity distribution in a direction perpendicular to the flow channel, once β_c has been determined. We will hence try some values on the constants and calculate β_c for all cells and see the implication for the porosity distributions. Three fractures and their cell representations will be focused on, see Table 4-3. Structures 20 and 22 have already been introduced and number 45 is a background fracture with *GST* = 2 and *CF* = 1. It is important to study the cell values in cells which are not crossed by other fractures as this would make a clear interpretation impossible.

Starting with $C_{GST} = C_{CF} = 0.0$ we see that the maximum porosity in the matrix reaches a value of about 0.13. The β_c-values depend on the aperture of the structures and we will here only focus on how β_c changes with C_{GST} and C_{CF}. For $C_{GST} = 0.3$ and $C_{CF} = 0.1$, we see that structure 20 will increase its immobile volumes, while 22 and 45 will be reduced. For $C_{GST} = 0.5$ and $C_{CF} = 0.2$ this tendency is increased, as expected.

In Figure 4-8 the porosity distribution for the three structures and the three constant sets are shown. It is not possible to choose a "best" set of constants as detailed measurements are not available. A rough comparison with the data presented in Table 2-1 is anyway possible, see Figure 4-9. The distributions for structures 20 and 45 are also shown in the figure and a certain agreement can be seen.

However, the main achievement of the study is probably the established relation between the *GST* and *CF* and the effects on a parameter that can be interpreted, i.e. porosity. In the following we will use $C_{CF} = 0.3$ and $C_{CF} = 0.1$, which indicates that a fracture classified as *GST* = 1 and *CF* = 3 will have 50 % higher maximum porosity, as compared to a fracture with *GST* = 2 and *CF* = 1.

Table 4-3. Three investigated structures. Cell values for different sets of C_{GST} and C_{CF}. $\beta_c = vol_{im} / vol_m$ and $\theta_{\max}$ maximum porosity.

			C_{GST}, C_{CF}					
			0.0, 0.0		0.3, 0.1		0.5, 0.2	
Structure	*GST*	*CF*	β_c	$\theta_{\max}$	β_c	$\theta_{\max}$	β_c	$\theta_{\max}$
20	1	3	9.9	0.128	12.4	0.160	14.2	0.183
22	2	2	25.0	0.126	22.2	0.112	20.7	0.105
45	2	1	11.3	0.128	9.1	0.103	7.8	0.088

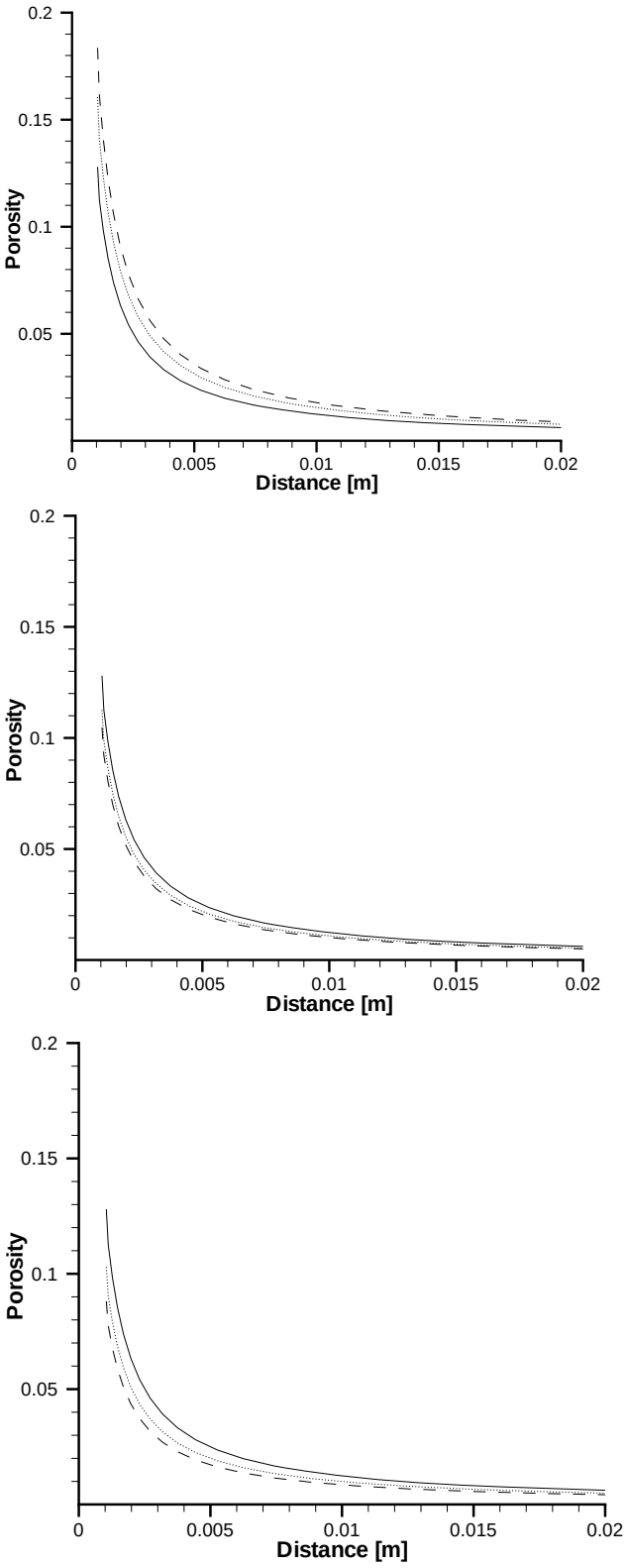

Figure 4-8. *Matrix porosity distribution in structures 20 (top), 22 (middle) and 45 (bottom).*

——— $C_{GST} = 0.0,\ C_{CF} = 0.0$

- - - - - - - $C_{GST} = 0.3,\ C_{CF} = 0.1$

– – – – – $C_{GST} = 0.5,\ C_{CF} = 0.2$

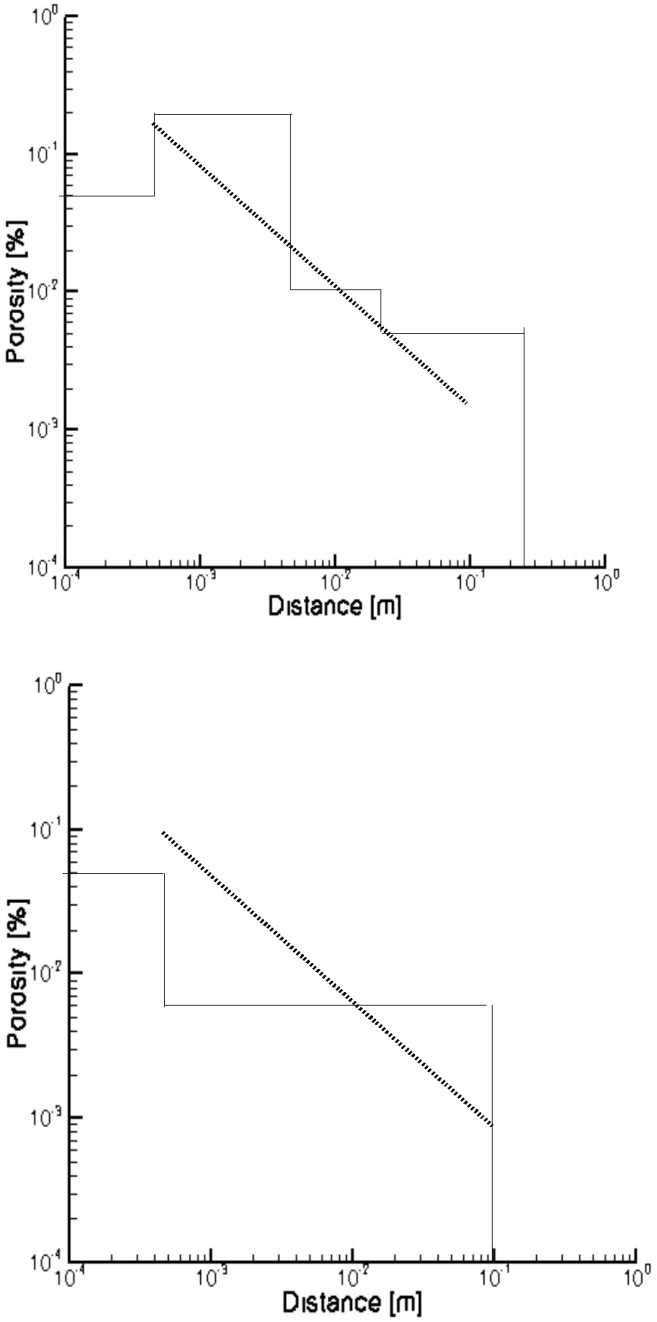

Figure 4-9. *Porosity distribution for geological type 1 (top) and type 2 based on Table 2-1. Calculated distributions (------) for structures 20 (top) and 45, using* $C_{GST} = 0.3$ and $C_{CF} = 0.1$.

4.5 Concluding remarks

In this section the FRAME parameters, as well as GST and CF, have been analysed in some detail. It has been shown that the parameters can be related to measurable quantities like porosity and dispersion (α_L). However, it needs to be said that FRAME rests on some novel concepts and the analysis presented is for this reason tentative.

5 Task 6D

5.1 Modelling strategy

In the Task 6C report a detailed account of the fracture network and the properties of all structures (transmissivity, thickness, aperture, heterogeneity, etc) can be found. Here we will focus on the structures that are expected to be important for the tracer test considered in Task 6D.

In Figure 5-1 the deterministic fractures and the injection and pumping boreholes are shown. Tracers are injected in structure 23 and the main flow path is expected to go through fractures 22 and 20 and then reach the pumped borehole going through structure 21. However, as can be seen in the figure there is also a possible flow path that goes through structure 13.

In Figure 5-2 all fractures that may influence the tracer experiment are shown. New pathways are now possible; in particular the path through the fracture labelled “B” (for background) should be noted, as this path will prove to be important.

As a background to the transport simulations, the flow paths from the injection point to the pumped borehole section have been calculated. In Figure 5-3 the flow paths are shown for two fracture networks. If only deterministic and synthetic fractures are included the flow path is through fractures 22 and 20. If all fractures are considered a significant part of the flow goes through the earlier mentioned background fracture; marked “B” in Figure 5-2. As the background fractures are randomly placed in space, we can already at this stage conclude that the prediction of breakthrough curves (BTC) is not well founded, i.e. if predicted curves should be compared with the measured curves.

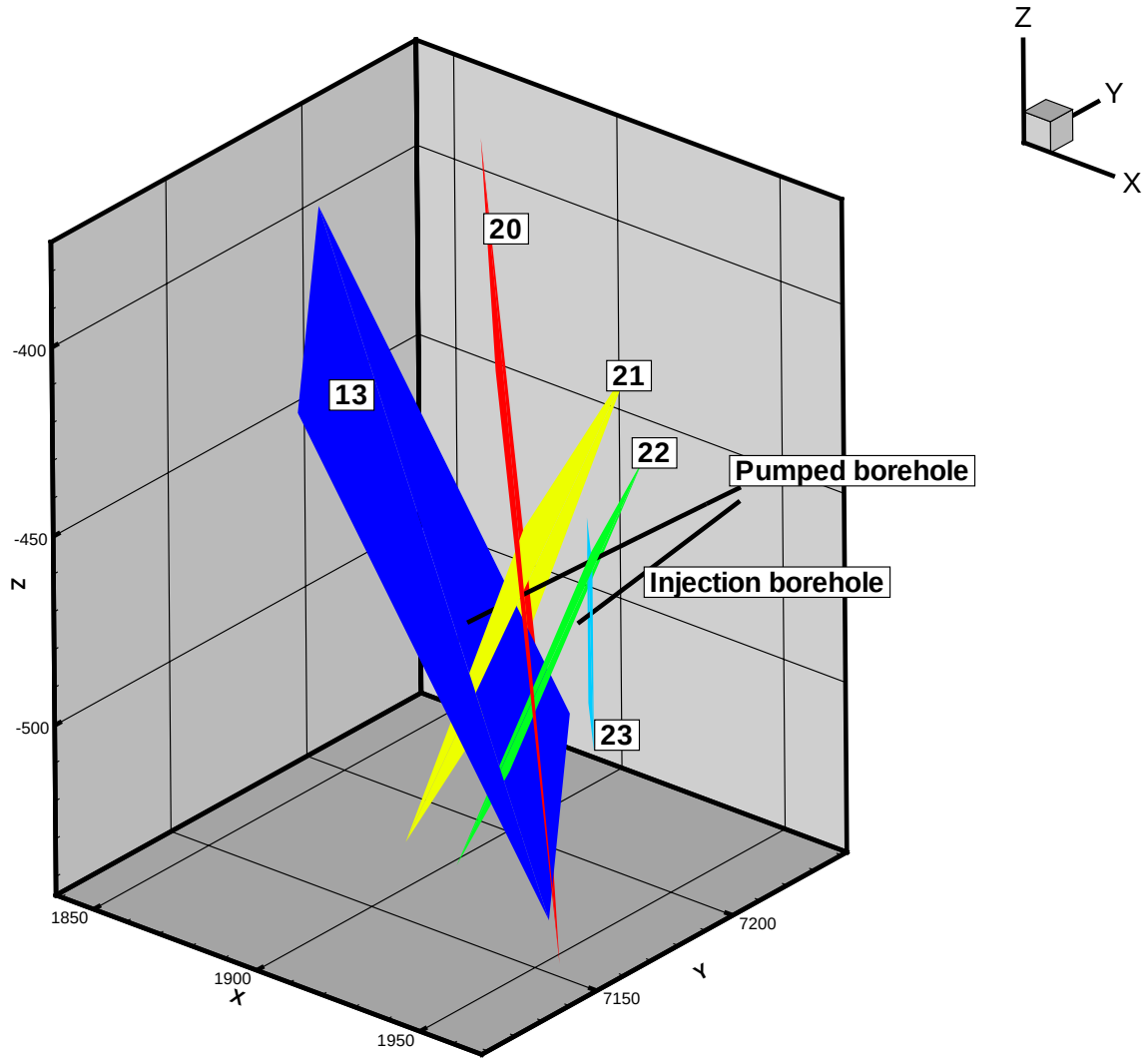

Figure 5-1. *Deterministic structures 13, 20, 21, 22 and 23. Boreholes used for injection and pumping are also shown.*

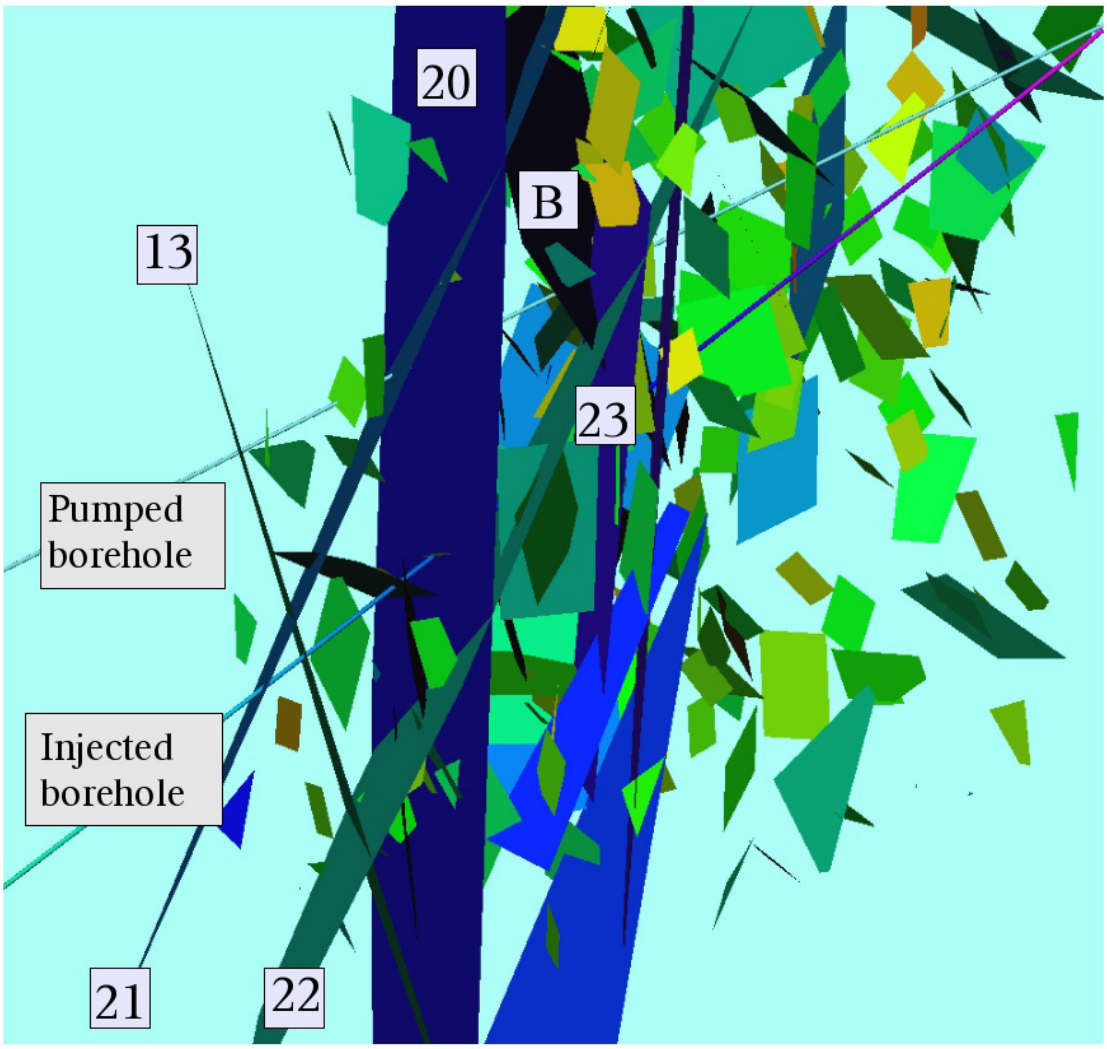

Figure 5-2. *All fractures that may influence the tracer experiment.*

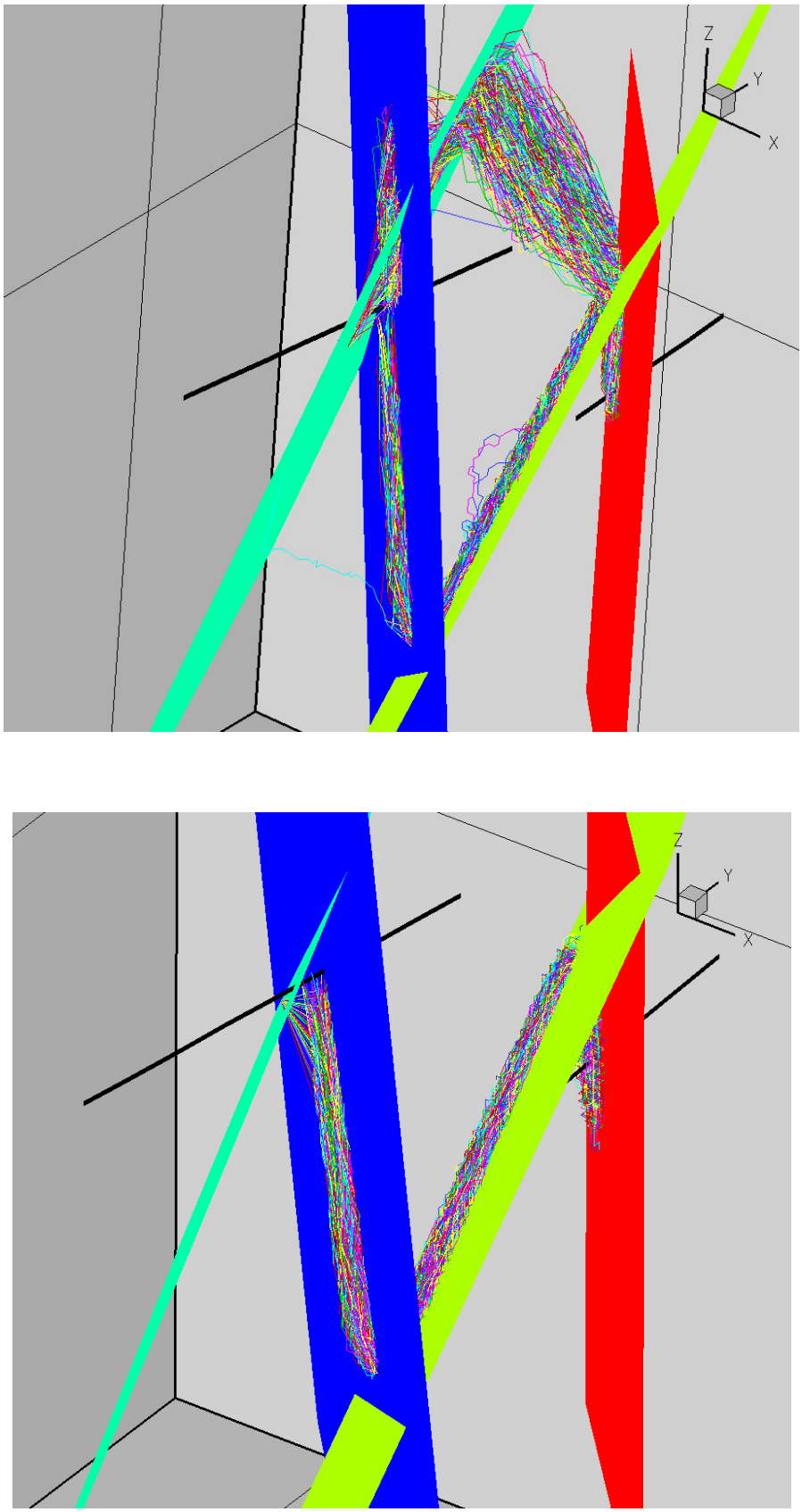

Figure 5-3. *Flow paths in the network with (top) and without background fractures.*

5.2 Modelling calibration

Our ultimate goal is to simulate a tracer experiment and it is hence natural to focus on BTC:s. The situation is however complex and in order to understand how different factors affect the BTC a step by step procedure is adopted. The first case considered is therefore a situation with no immobile zones.

In Figure 5-4, BTC:s for a conservative tracer, injected as a Dirac pulse, are shown. The two BTC:s represents fracture networks with or without background fractures. The single peak BTC represent the case without background fractures and the double peak in the BTC is hence due to the background fracture discussed in Section 5-1. There is however one more thing to learn from this case; the second peak in the BTC with two peaks is due to the flow path through the deterministic structures. With no background fractures this flow path will give a peak in the BTC after 30 hours, while the peak will be delayed to 45 hours with the background fractures included. To prove this statement we look at the trajectories after 35 hours, see Figure 5-5. It is clear that particles travelling through structure 22 have not reached the pumped borehole at this time and can obviously then not contribute to the BTC.

Next we introduce the immobile volumes into the analysis; the tracer is however still a conservative tracer and the injection curve is a Dirac pulse. The volume of the immobile zones will be distributed according to expression (3-2). However in a first case we will assume that $C_{GST} = C_{CF} = 0.0$ (vol_{im} is thus $\sim$ *FWS)* and explicitly modify *FWS* for structures 20 and 22; this to see the influence on the BTC more clearly. In Figure 5-6 the BTC:s for three cases are shown; $vol_{im} \sim FWS$, vol_{im} doubled for structure 20 and vol_{im} doubled for structure 22. We can hence regard the case $vol_{im} \sim FWS$ as a reference and then study the effect when the retention is increased in structures 20 and 22 (by doubling vol_{im}). As can be seen in Figure 5-6, the BTC is not affected by the increased retention in structure 20 The explanation is that the transport velocity in 20 is so high (it is a radially converging flow field) that there is little time for the diffusive mass exchange with the immobile zones. Increasing the retention in structure 22 will however have a significant effect. As discussed above, it is the second peak that represents this flow path and, as can be seen, this peak is delayed and reduced, while the first peak is only slightly affected. The results can hence be explained and understood.

The two BTC:s shown in Figure 5-7 represent $vol_{im} \sim FWS$ and vol_{im} according to expression (3-2). The differences are quite small but still possible to explain:

- The differences are small because structure 20 is not important for retention and the change to structure 22 is small (see Table 4-3). We can not say for certain how the background fracture that gives the first peak changes its retention, but it has *GST* = 2 and *CF* =2 and will hence be reduced. Note that the background fracture in Table 4-3 is not the one that gives the first peak. However, the retention reduction should be similar.

- The first arrival is faster and the peak is higher for vol_{im} according to expression (3-2). This is expected if the background fracture retention is decreased.

- The second peak is somewhat higher with expression (3-2) which is due to the decreased retention in structure 22.

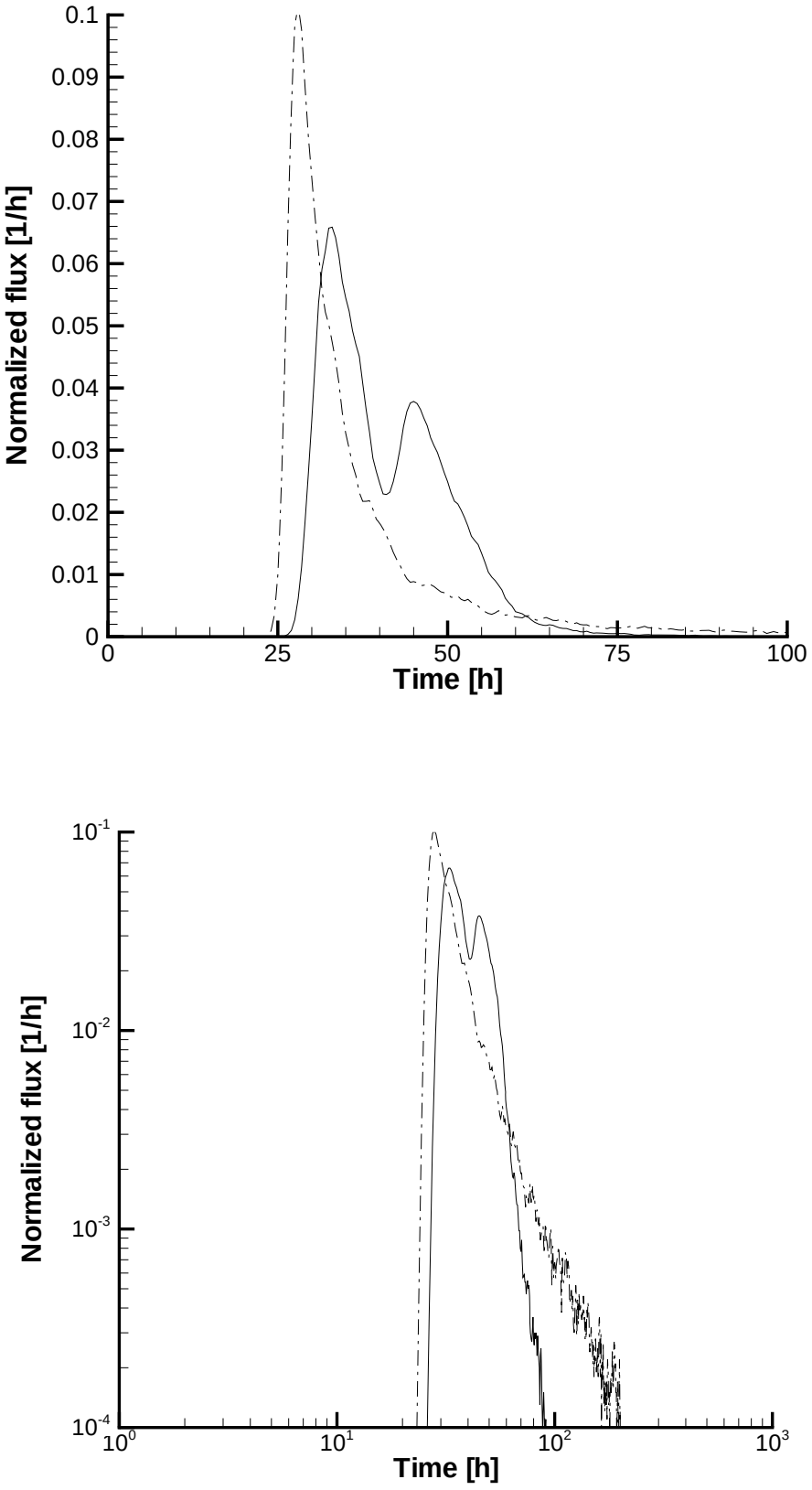

Figure 5-4. *BTC:s for a fracture network with (——) and without (– · –) background fractures. Linear scales (top) and log-log scales.*

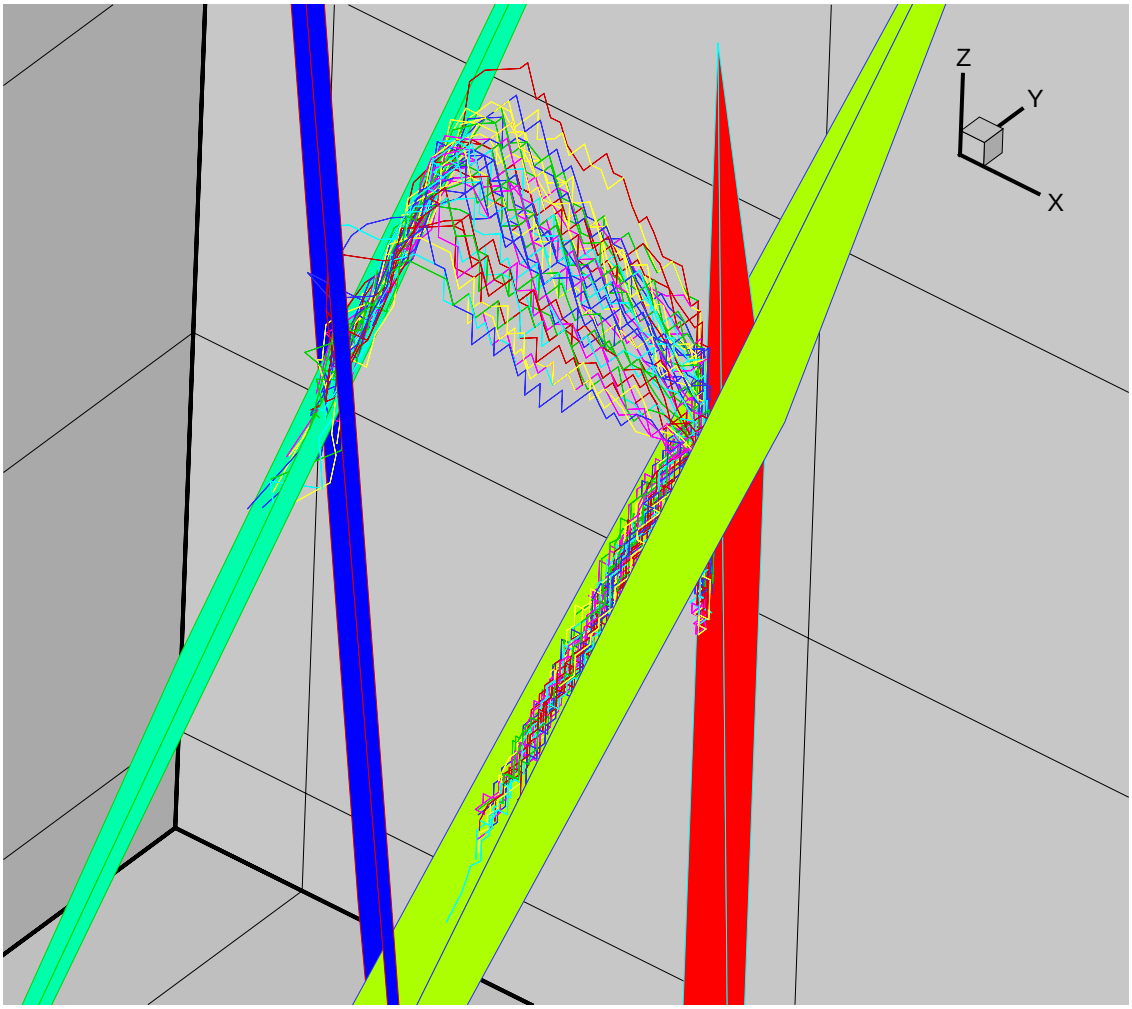

Figure 5-5. *Trajectories at 35 hours after injection. Fracture network with background fractures.*

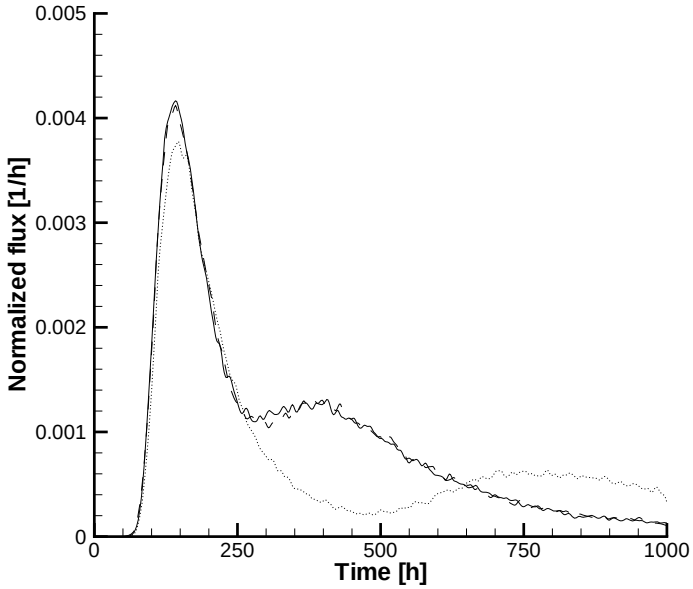

Figure 5-6. *BTC:s for three cases*

——— vol_{im} ~ *FWS*
- - - - - - - doubled retention for structure 20
..... doubled retention for structure 22

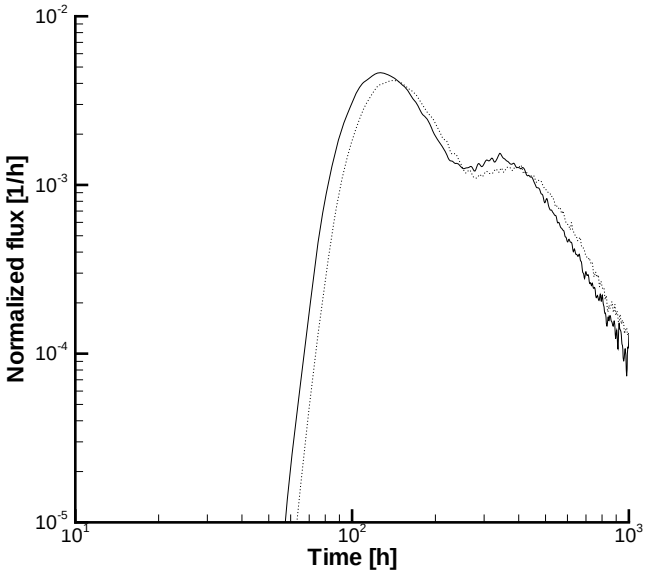

Figure 5-7. *BTC:s for two cases.* vol_{im} *distributed according to expression (3-2).*

——— $C_{GST} = 0.3,\ C_{CF} = 0.1$
..... $C_{GST} = C_{CF} = 0.0$

So far we have assumed that structures and fractures have uniform properties within the fracture plane. The Task 6C report does however provide information about in plane heterogeneity, in particular with respect to transmissivity. DarcyTools can generate heterogeneous fracture properties with specified standard deviations, correlation lengths and anisotropy. These features will be briefly tested in this section.

In the first case considered, heterogeneous transmissivity and aperture fields for structures 20, 22 and B (see Figure 5-2) are generated. We do not generate heterogeneous fields for structures 23 (injection point) or 21 (pumping point) as local effects around these points may make the interpretation more difficult. Based on the Task 6C report, we specify a $\log_{10}$ *St.Dev.* of transmissivity equal to 0.6 for the three considered structures. It then follows (from a relation between aperture and transmissivity) that the $\log_{10}$ *St.Dev.* for aperture should be 0.36. The correlation length is specified to 4.0 metres. In Figure 5-8 the BTC for this case is shown together with the BTC for homogeneous conditions. The following effects can be identified:

- The first arrival time is shorter for the heterogeneous case. This can be expected as we create fast channels.
- The peak value is higher. Same explanation as above may apply as fast channels allow less interaction with the matrix.
- The second peak is delayed and reduced. There is no obvious explanation to this effect. One possibility is that the flow channels that should connect structures 20 and 22 are disconnected at the fracture intersection as the random fields in the two fractures are generated independently.

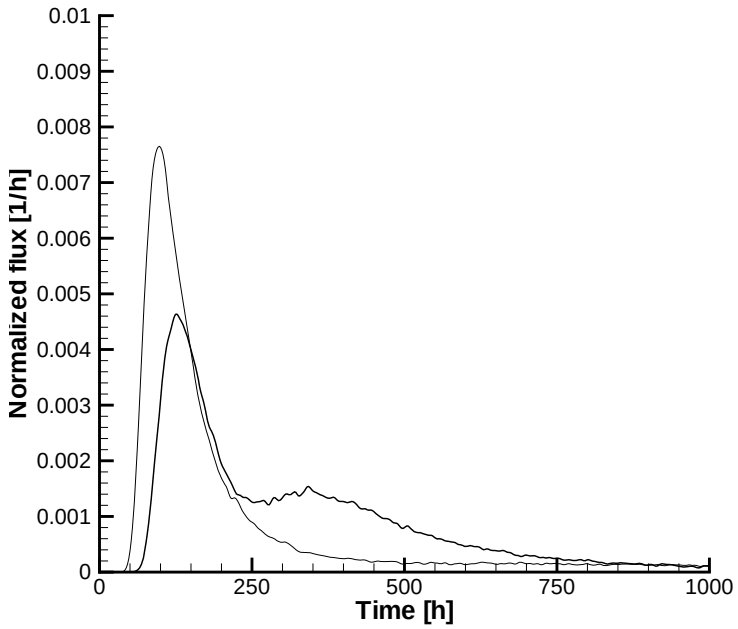

Figure 5-8. *BTC:s for homogeneous (——) and heterogeneous (·····) in plane conditions with respect to transmissivity and aperture.*

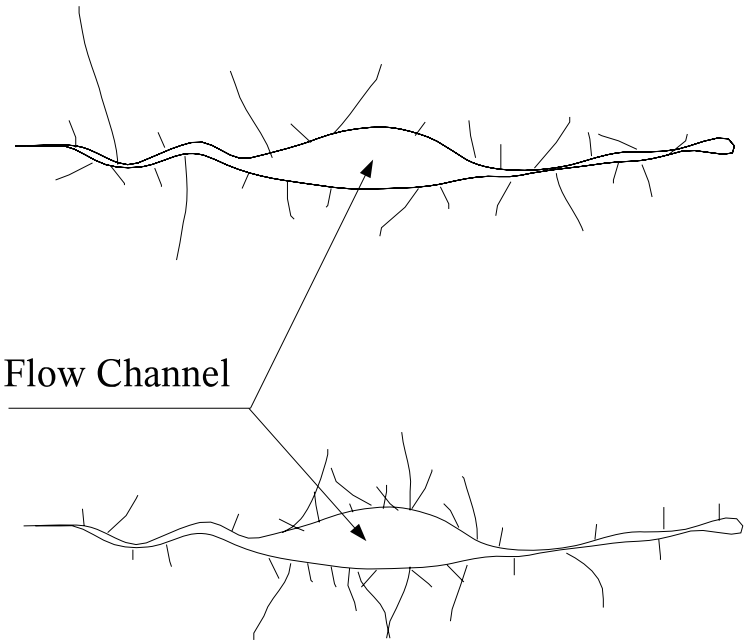

Figure 5-9. *Immobile volumes homogeneously distributed (top) or concentrated to flow channels.*

Next we consider how immobile volumes should be distributed in the fracture plane. The conceptual question is whether immobile volumes should be concentrated to flow channels or not. In Figure 5-9 two situations are illustrated; one with homogeneously distributed immobile zones and one with immobile zones concentrated to flow channels. In DarcyTools we can specify the heterogeneous case based on the same random number distribution as used for transmissivity and aperture and we can also specify the standard deviation independently for the immobile volume distribution. In Figure 5-10 the homogeneous case and two heterogeneous cases are illustrated. The following can be noted:

- The heterogeneous cases give a lower peak value. This is expected as the peak represents the "main flow channels" and we have now more immobile volumes connected to these.

- Increasing the *St.Dev.* further does not give a further decrease of the peak value (not shown in the figure). The explanation to this effect is probably that all immobile volumes are in context with the main flow channels and further concentration does not give any effect.

Some further tests revealed that the peak value is very sensitive to the *St.Dev.* for transmissivity and aperture. Decreasing the *St.Dev.* for transmissivity by 2 % and increasing the *St.Dev.* for aperture by 2 % reduces the peak in Figure 5-8 from 0.0078 to 0.005. Further tests should be carried out to establish if this effect is realistic.

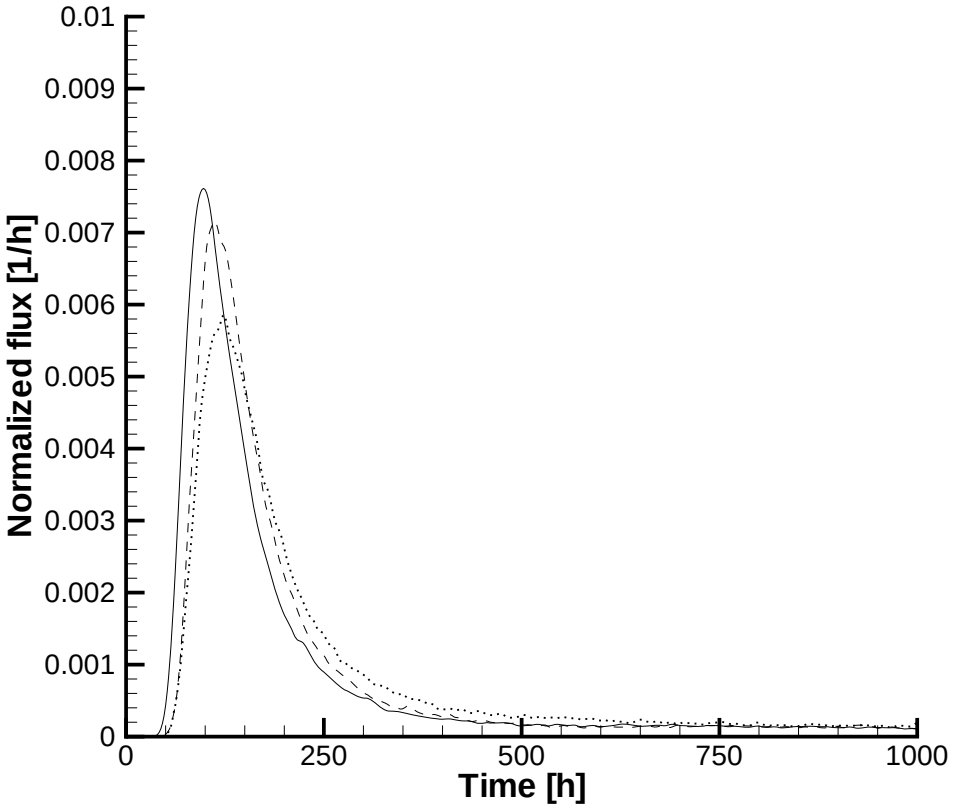

Figure 5-10. *BTC:s for three values of the* $\log_{10}$ *St.Dev. of the distribution parameter (expression, 3-2).*

0.0 ——
0.1 - - - -
0.2 .....

5.3 Modelling Results

It is now time to address the tracer experiment. A range of tracers, sorbing and non-sorbing, was injected in structure 23 (see Figure 5-1) and BTC:s were recorded in structure 21. The simulations require quite a lot of input data and these are first summarised; first data related to the fracture network and the pump test are given, then the tracer property data.

The model developed in this report does introduce a number of new concepts and assumptions but, on the other hand, also utilize available information. Retention is attributed to exchange with immobile volumes and the model focuses on how these should be distributed. The main points and associated data are:

- The basic idea is to distribute the immobile volumes in proportion to the flow wetted surface, *FWS*. The *FWS* is first specified to $2\ m^2/m^2$. The domain integrated immobile volume is then scaled with a global mean $\beta_G\ (= vol_{im}/vol_m)$, which is considered to be an input parameter. This is called the "standard" procedure in DarcyTools.

- Next we consider the "Geological Structure Type" (*GST*) and "Complexity Factor" (*CF*). vol_{im} is now redistributed with respect to a weighting factor which reads: $\left(1+C_{GST}\left(2-GST\right)\right)\times\left(1+C_{CF}\left(CF-1\right)\right)$ where C_{GST} and C_{CF} are unknown constants. Here we will use $C_{GST}=0.3$ and $C_{CF}=0.1$. Note that this is a redistribution of vol_{im} in between structures and fractures, which all have been assigned a *GST* and *CF* value.
- Finally we redistribute vol_{im} within a fracture plane. Here we will assume that the immobile volumes are concentrated around flow channels and we hence use the same random field for transmissivity, aperture and vol_{im} to generate the heterogeneity. The correlation length is set to 4 metres and the field is isotropic. The $\log_{10}$ *St.Dev.* for transmissivity, aperture and vol_{im}-distribution will be set to 0.6, 0.36 and 0.2 respectively. Only structures 20, 22 and B will be given heterogeneous conditions.

This specification basically determines the ratio $vol_{im}/vol_m\left(=\beta_c\right)$ for a cell. Other FRAME parameters are "standard values" and are summarised as:

- k is fixed to 2.0.
- β_G is equal to 10.0 for a non sorbing tracer, $\overline{\beta}_n$, and equal to $\overline{\beta}_n R_{im}/R_m$ for sorbing tracers.

  Note: $\beta_G=\dfrac{R_{im}V_{im}}{R_mV_m}=\dfrac{R_{im}}{R_m}\overline{\beta}_n$, where V_{im} and V_m are the global volumes of the immobile and mobile zones, respectively.
- $\alpha_{\min}=10^{-10}$ for HTO and equal to $\dfrac{D_w}{R_{im}D_{w,HTO}}\times10^{-10}$ for other tracers.
- $\alpha_{\max}$ is based on an average between $D_w/l_{\min}^2$ and $D_w/\left(l_{\min}^2R_{im}\right)$, see Task 6A, 6B report (Svensson and Follin, 2003).
- $l_{\min}$ is put to 10^{-3} (comparable to a typical aperture).

Tracer data are summarized in Table 5-1. It has not been the objective of this project to analyze or validate these parameters; instead the conclusions from Task 6A and 6B have formed the basis for the values adopted. The arguments are:

- I-129. Conservative tracer. Only D_w needed as input.
- Ca-47. According to Table 2-4 in the Task 6C report, this tracer has the same properties as Strontium, used in Task 6A. Use the Strontium data input found in Task 6A.
- Cs-137. Close to Cobolt, used in Task 6A. Use these data.
- Ra-226. According to the Task 6C report, data for this tracer are obtained by multiplying K_a and K_d values for Ba^{2+} by a factor of 10. It is then found that values roughly 10 % smaller than Cs-137 should be used.

The K_d -values given in Table 2-4 in the Task 6C report are generally higher than the values adopted. Some preliminary tests also indicate that the values give too much retention. However, as mentioned it has not been the objective of this study to find suitable K_d -values; instead it was decided that the Task 6A results should be built upon.

Breakthrough curves for a Dirac pulse are shown in Figure 5-11 and recovery times for 5, 50 and 95% of the injected mass can be found in Table 5-2.

Simulations using measured injection curves were found to be very similar to the curves obtained from the Dirac pulse and the Dirac pulse results were therefore also used for BTC:s expressed as Bq/kg versus time. The results are shown in Figure 5-12 and Table 5-3.

During the tracer experiment the steady state heads in the injected and pumped borehole sections were -69 m and -500 m, respectively according to the simulation model. The head in the pumped cell is of course depending on the cell size used (0.5 x 0.5 x 0.5 m in the present model) as a larger cell would give less drawdown.

Table 5-1. Tracer property data.

Tracer	D_w $\left(x10^{-9}\right)$ **[m²/s]**	K_a **[m]**	K_d **[m³/kg]**	R_m	R_{im}
I-129	2.00	0	0	1	1
Ca-47	0.79	8×10^{-6}	4.7×10^{-6}	1.02	4.2
Cs-137	0.50	8×10^{-3}	8×10^{-4}	17	542
Ra-226	0.89	7×10^{-3}	7×10^{-4}	15	473
Tc-99	0.5	0.2	0.2	401	1.35×10^{5}
Am-241	0.6	0.5	0.5	1001	3.38×10^{5}
$R_m = 1+\frac{2K_a}{10^{-3}},\ R_{im} = 1+\frac{2700K_d}{0.004}$					

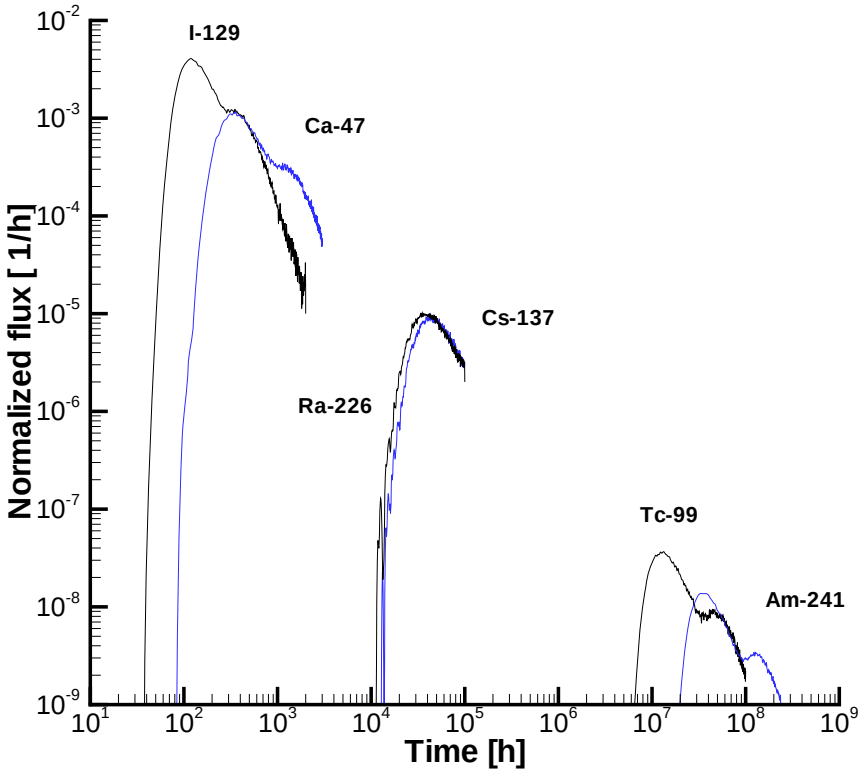

Figure 5-11. *BTC:s for a Dirac pulse.*

Table5-2. Breakthrough times (in hours) for recovery (in %). Dirac pulse.

Tracer	$t_{5\%}$	$t_{50\%}$	$t_{95\%}$	**Maximum release [1/h]**
I-129	94	270	1280	4×10^{-3}
Ca-47	258	900	4700	10^{-3}
Cs-137	3.3×10^{4}	1.2×10^{5}	6.1×10^{5}	9×10^{-6}
Ra-226	2.9×10^{4}	1.0×10^{5}	5.5×10^{5}	10^{-5}
Tc-99	10^{7}	3.1×10^{7}	1.5×10^{8}	4×10^{-8}
Am-241	2.8×10^{7}	8.2×10^{7}	3.8×10^{8}	1.5×10^{-8}

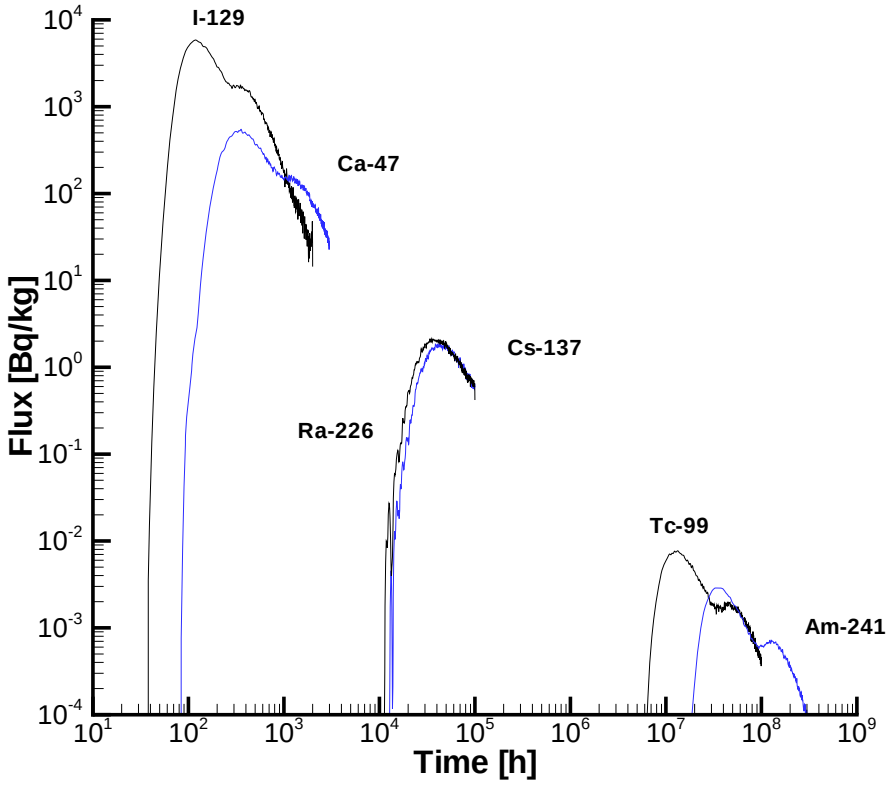

Figure 5-12. *BTC:s for measured injection curves.*

Table 5-3. Breakthrough times (in hours) for recovery (in %). Measured injection curves.

Tracer	$t_{5\%}$	$t_{50\%}$	$t_{95\%}$	**Maximum release** Bq/kg	**Assumed injected activity** $[Bq]\times 10^7$
I-129	94	270	1280	5.8×10^3	17.1
Ca-47	258	900	4700	4.7×10^2	5.64
Cs-137	3.3×10^4	1.2×10^5	6.1×10^5	1.8	2.35
Ra-226	2.9×10^4	1.0×10^5	5.5×10^5	2.1	2.5
Tc-99	10^7	3.1×10^7	1.5×10^8	8.4×10^{-3}	2.5
Am-241	2.8×10^7	8.2×10^7	3.8×10^8	3.2×10^{-3}	2.5

6 Task 6E

6.1 Modelling strategy

Task 6E is intended to be similar to Task 6D, but for PA time scales. This is achieved by specifying a head gradient of 1 m from the east to the west boundary of the domain. In the Task 6C report a detailed account of the fracture network and the properties of all structures (transmissivity, thickness, aperture, heterogeneity, etc) can be found. Here we will focus on the structures that are expected to be important for the tracer test considered in Task 6E.

In Figure 6-1 the deterministic and synthetic fractures and the injection point are shown. Tracers are injected in structure 23 and the main flow path is expected to start through fractures 22 and 20 and then go through several fractures before reaching the western boundary.

In Figures 6-2 and 6-3 all fractures that may influence the tracer experiment are shown. New pathways are now possible; in particular the background fracture connecting fractures 21 and 22 should be noted, as this path seems to provide a shortcut.

6.2 Modelling calibration

No calibration was performed as it is argued that the model should be as similar as possible to the one used in Task 6D.

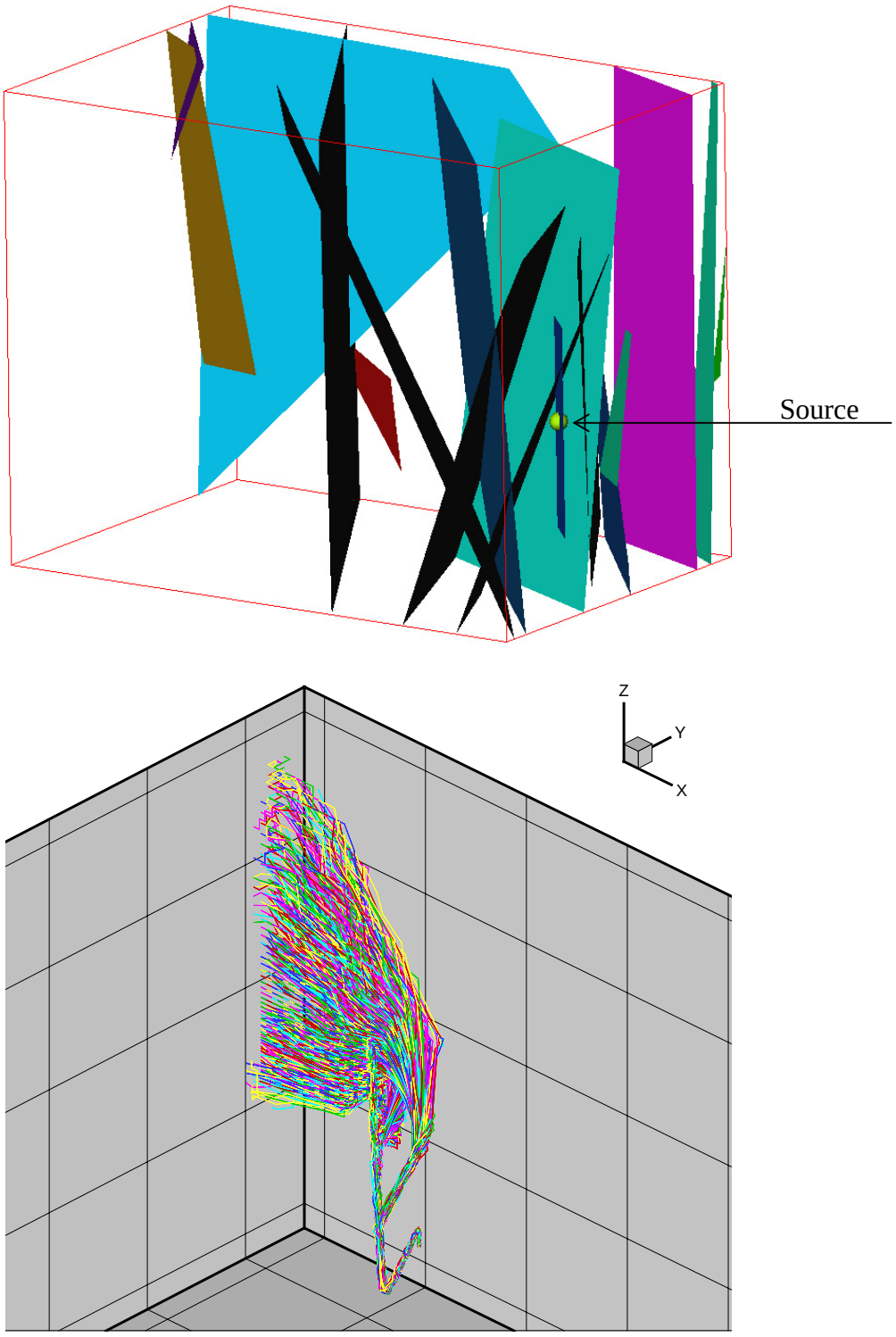

Figure 6-1. *Fracture network based on deterministic and synthetic structures (top) and the corresponding flow paths. Fractures shown in a bounding box (top) with coordinates:*

x: 1 800 → 1 935 m
y: 7 165 → 7 255 m
z: -520 → -410 m

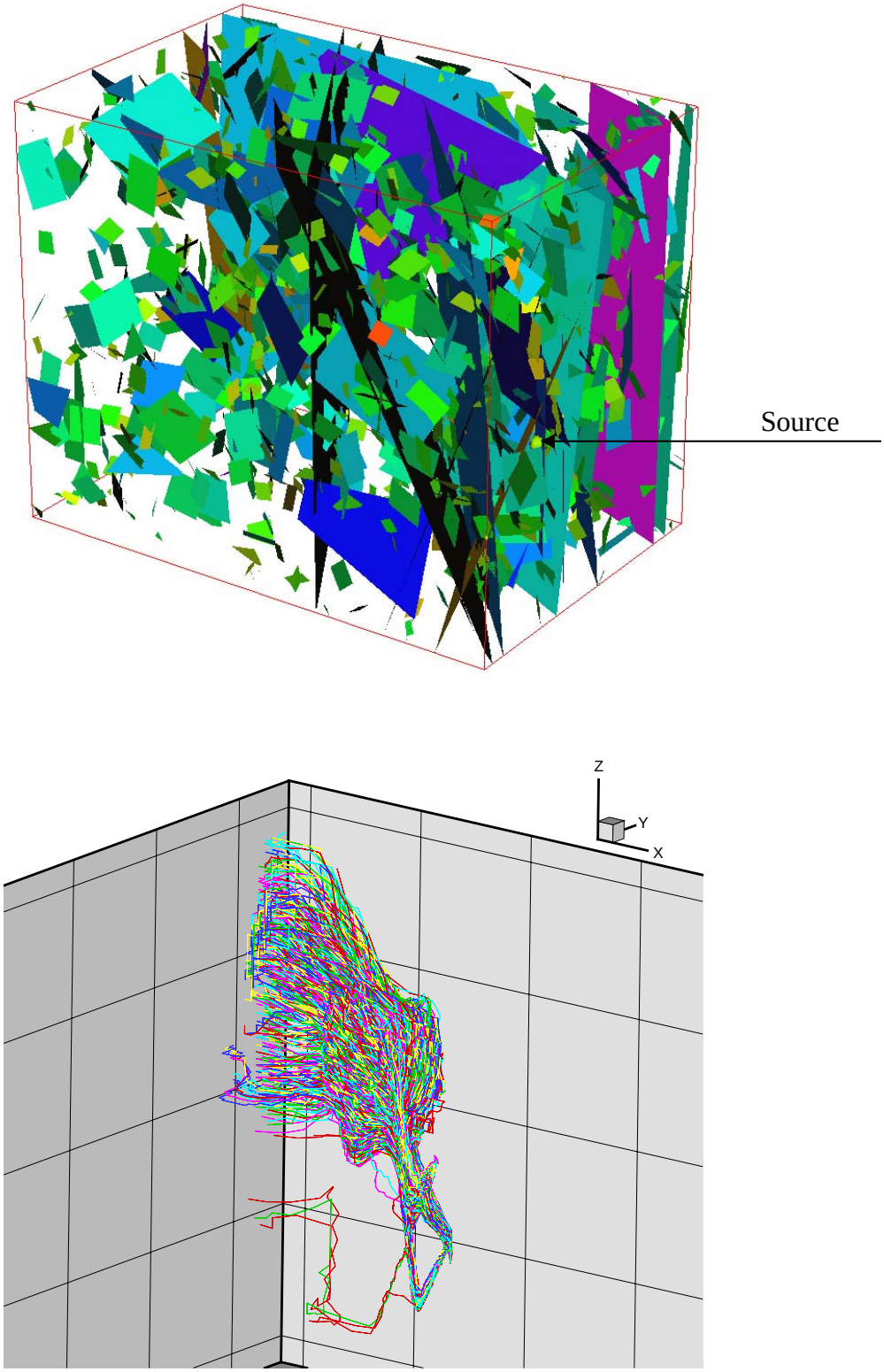

Figure 6-2. *Fracture network based on all fractures (top) and the corresponding flow paths. Bounding box coordinates: see Figure 1.*

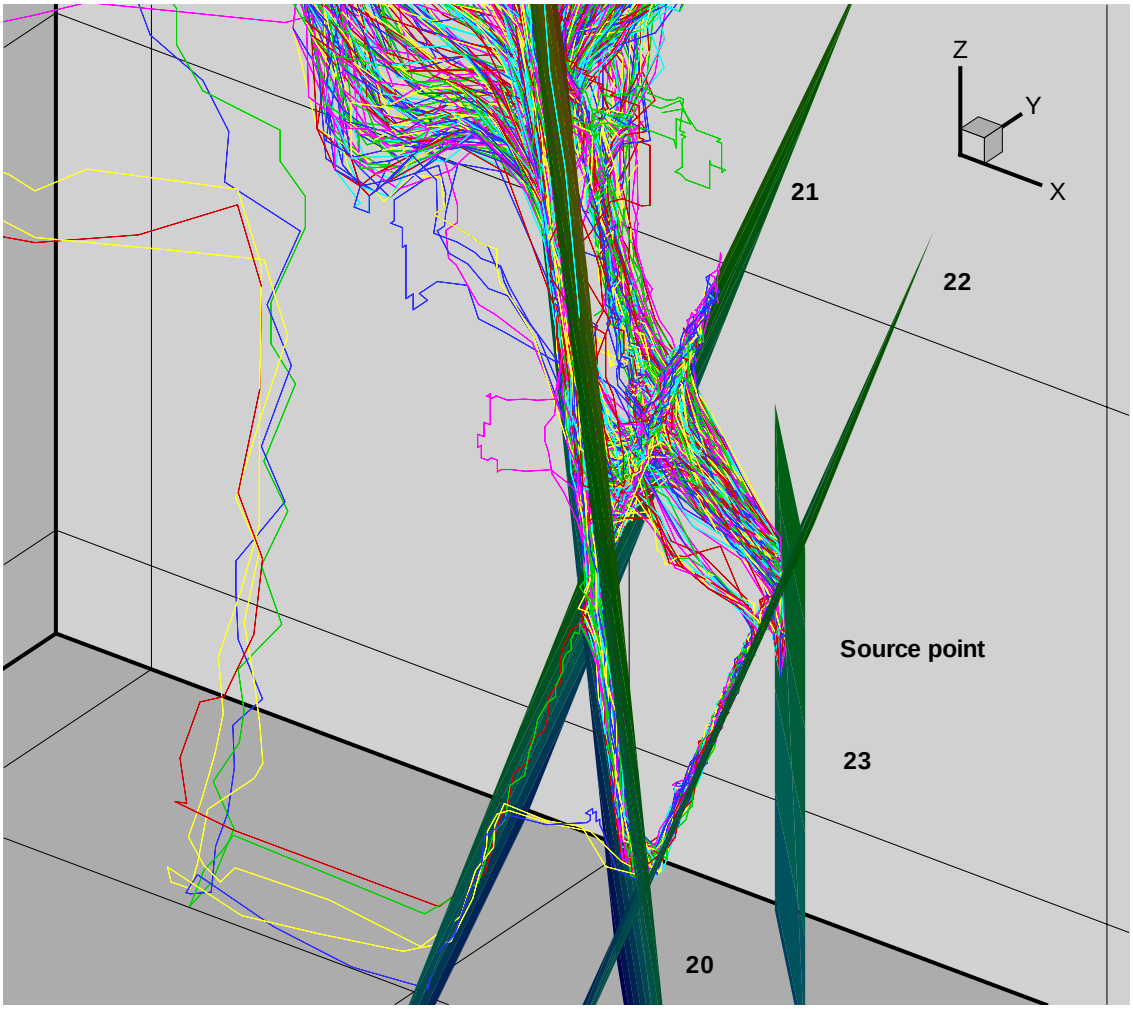

Figure 6-3. *A close-up view. Some deterministic zones and flow paths for a network that includes all zones and fractures.*

6.3 Results

It is now time to address the tracer experiment. A range of tracers, sorbing and non-sorbing, are injected in structure 23 (see Figure 6-1) and BTC:s were recorded in vertical planes at different downstream locations.

Breakthrough curves for a Dirac pulse are shown in Figures 6-4, 6-5 and 6-6 and recovery times for 5, 50 and 95% of the injected mass can be found in Tables 6-1, 6-2 and 6-3. The three sets of results give the BTC:s at three distances (10m, 50m and domain boundary) from the source. As can be expected, the maximum release rates are higher closer to the source.

Breakthrough curves for an extended pulse are shown in Figures 6-7, 6-8 and 6-9 and recovery times for 5, 50 and 95% of the injected mass can be found in Tables 6-4, 6-5 and 6-6. The extended pulse is specified as a continuous release during 1000 years. The three sets of results give the BTC:s at three distances (10m, 50m and domain boundary) from the source. As can be expected, the maximum release rates are higher closer to the source. It was found that the BTC:s for Tc-99 and Am-241 are very similar to the ones for a Dirac pulse, and these were hence used also for the extended pulse.

Finally the development of the F-factor versus time is discussed, see Figure 6-10. There seems to be two main flow paths, one with an advective time of about 2 years and the other with 5 years. It is further interesting to note the different slopes for the slower flow path; these probably indicate a further split of the flow path into fractures with different a_w-values. Figure 6-11 gives the water residence time distribution, which confirms that the first pulse arrives after roughly two years.

The F-factor is defined as $F = a_w t$, where a_w is the flow wetted surface per unit mobile volume and *t* time. The subgrid model FRAME puts $\beta_c \sim (Vol_{im} / Vol_m)$ in focus but the two parameters, i.e. a_w and β_c, are in fact linearly related (see Section 4-2). It is hence of interest to study the β_c values for the given fracture network. In Figure 6-12 the relation β_c-porosity is shown. As we can expect that larger zones and fractures generate the higher cell porosity values, we can conclude that these have β_c values in the range $1 \rightarrow 10$; for the given network the corresponding a_w-values are obtained by multiplying with 1.4×10^3. One may also conclude that a flow path through small fractures (lower cell porosities) will result in higher a_w-values and hence a larger F-factor.

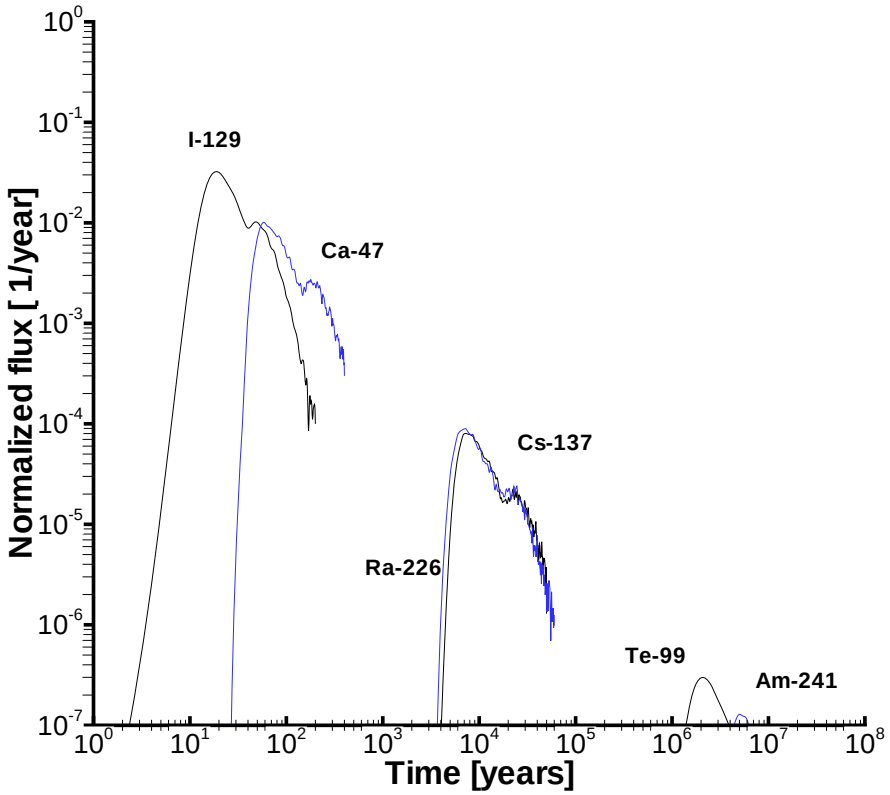

Figure 6-4. *BTC:s at the Western boundary for a Dirac pulse.*

Table 6-1. Breakthrough times (in years) for recovery (in %). Dirac pulse.

Tracer	$t_{5\%}$	$t_{50\%}$	$t_{95\%}$	**Maximum release [1/year]**
I-129	15	33	107	3×10^{-2}
Ca-47	51	116	409	10^{-2}
Cs-137	6.4×10^{3}	1.4×10^{4}	5×10^{4}	7×10^{-5}
Ra-226	5.8×10^{3}	1.3×10^{4}	4.4×10^{4}	8×10^{-5}
Tc-99	1.7×10^{6}	3.7×10^{6}	1.3×10^{7}	3×10^{-7}
Am-241	4.4×10^{6}	9.2×10^{6}	3.1×10^{7}	1×10^{-7}

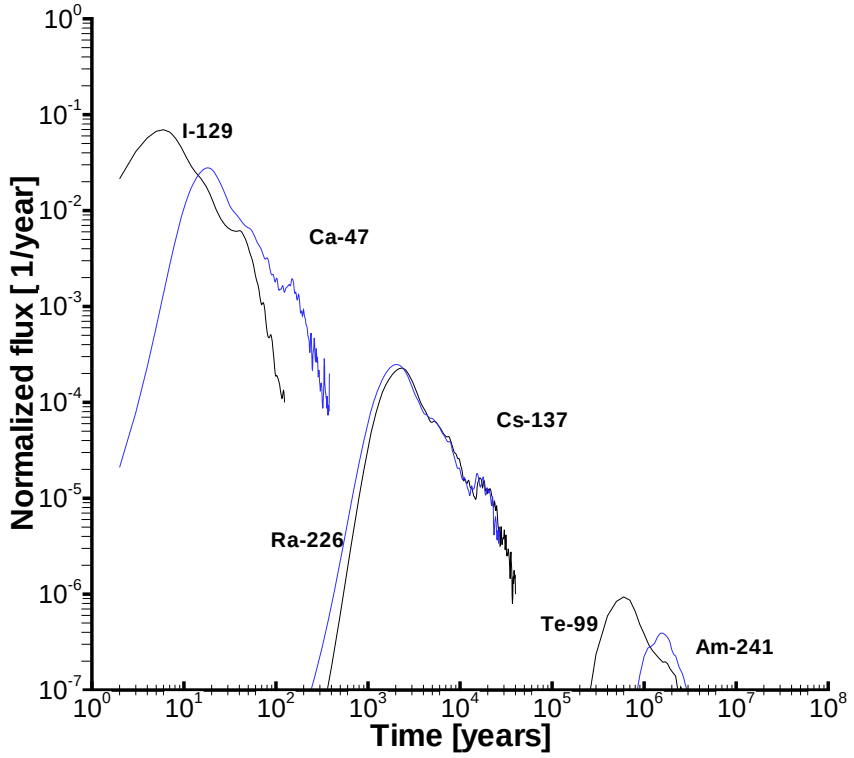

Figure 6-5. *BTC:s at a vertical plane 10 metres from source, for a Dirac pulse.*

Table 6-2. Breakthrough times (in years) for recovery (in %). Dirac pulse.

Tracer	$t_{5\%}$	$t_{50\%}$	$t_{95\%}$	**Maximum release [1/year]**
I-129	4	10	55	7×10^{-2}
Ca-47	12	35	212	3×10^{-2}
Cs-137	1.5×10^{3}	4.4×10^{3}	2.6×10^{4}	2×10^{-4}
Ra-226	1.4×10^{3}	4.0×10^{3}	2.3×10^{4}	2×10^{-4}
Tc-99	4×10^{5}	1.0×10^{6}	6.0×10^{6}	9×10^{-7}
Am-241	1.1×10^{6}	2.7×10^{6}	1.5×10^{7}	4×10^{-7}

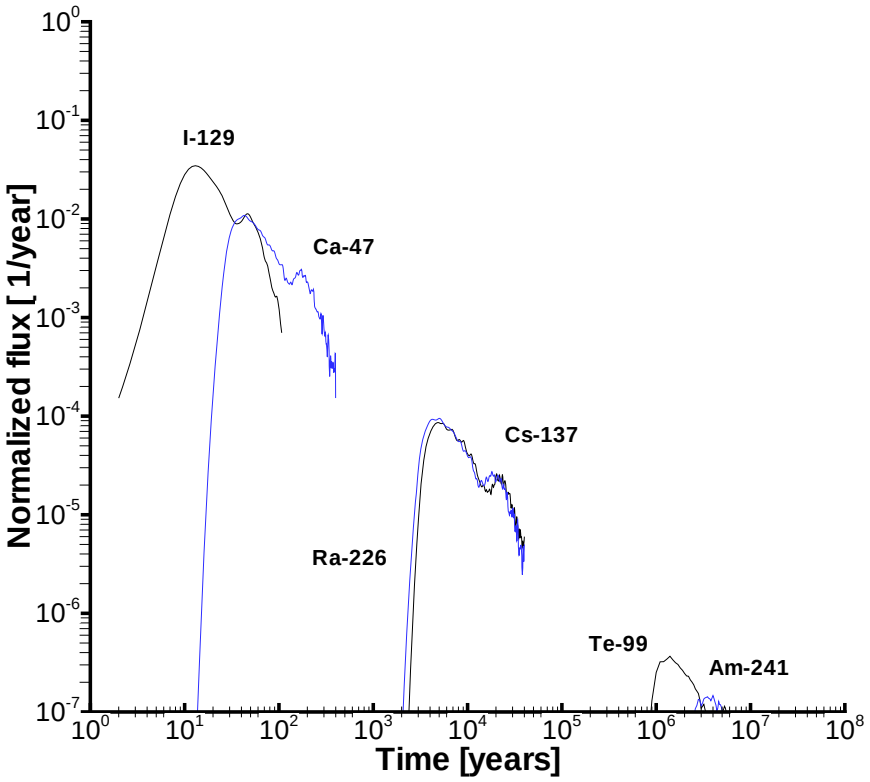

Figure 6-6. *BTC:s at a vertical plane 50 metres from source, for a Dirac pulse.*

Table 6-3. Breakthrough times (in years) for recovery (in %). Dirac pulse.

Tracer	$t_{5\%}$	$t_{50\%}$	$t_{95\%}$	**Maximum release [1/year]**
I-129	10	26	88	3×10^{-2}
Ca-47	33	93	333	1×10^{-2}
Cs-137	4.2×10^{3}	1.2×10^{4}	4.1×10^{4}	1×10^{-4}
Ra-226	3.8×10^{3}	1.1×10^{4}	3.7×10^{4}	1×10^{-4}
Tc-99	1.1×10^{6}	2.8×10^{6}	8.9×10^{6}	3×10^{-7}
Am-241	2.8×10^{6}	7.1×10^{6}	2.3×10^{6}	1×10^{-7}

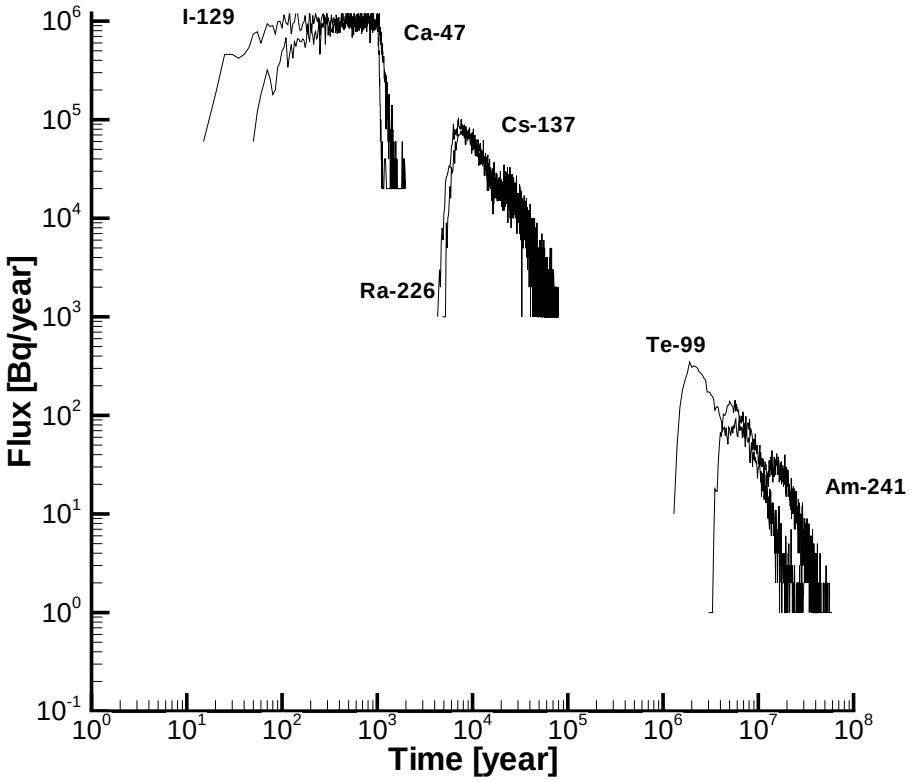

Figure 6-7. *BTC:s at the Western boundary for an extended pulse.*

Table 6-4. Breakthrough times (in years) for recovery (in %). Extended pulse.

Tracer	$t_{5\%}$	$t_{50\%}$	$t_{95\%}$	**Maximum release [Bq/year]**
I-129	80	545	995	10^6
Ca-47	165	660	1160	10^6
Cs-137	9×10^3	1.5×10^4	5.2×10^4	7×10^4
Ra-226	6.2×10^3	1.4×10^4	4.7×10^4	8×10^4
Tc-99	1.7×10^6	3.7×10^6	1.3×10^7	3×10^2
Am-241	4.4×10^6	9.2×10^6	3.1×10^7	1×10^2

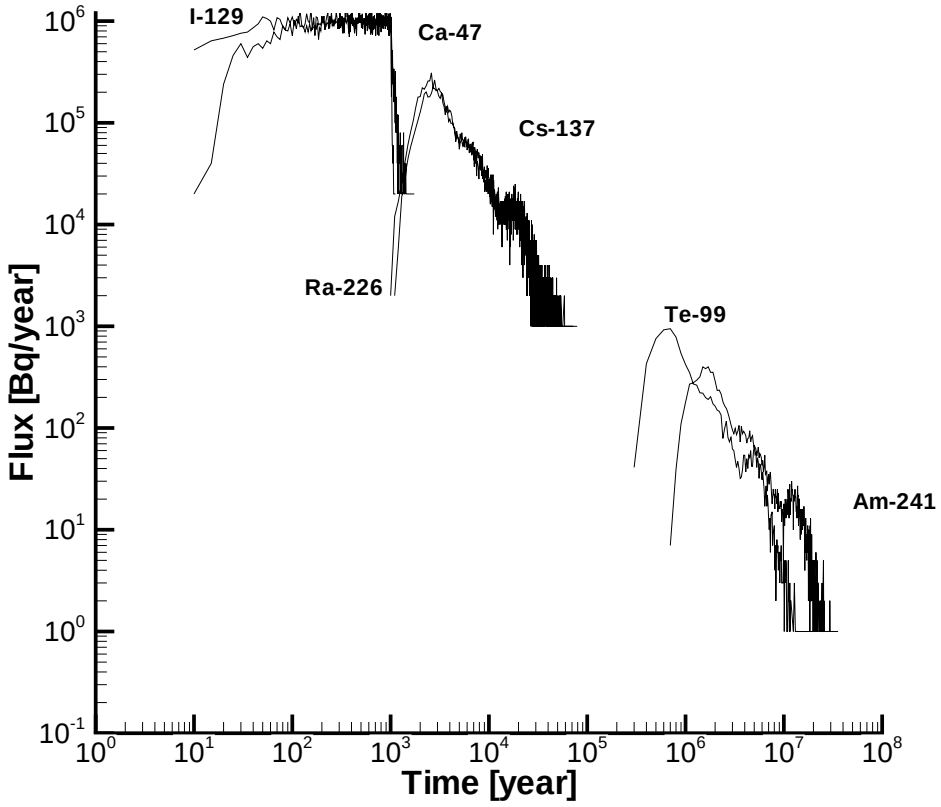

Figure 6-8. *BTC:s at a vertical plane 10 metres from source, for an extended pulse.*

Table 6-5. Breakthrough times (in years) for recovery (in %). Extended pulse.

Tracer	$t_{5\%}$	$t_{50\%}$	$t_{95\%}$	**Maximum release [Bq/year]**
I-129	65	515	965	10^6
Ca-47	95	560	1010	10^6
Cs-137	2.0×10^3	5.0×10^3	2.7×10^4	2×10^5
Ra-226	1.8×10^3	4.3×10^3	2.3×10^4	2×10^5
Tc-99	4×10^5	1.0×10^6	6.0×10^6	9×10^2
Am-241	1.1×10^6	2.7×10^6	1.5×10^7	4×10^2

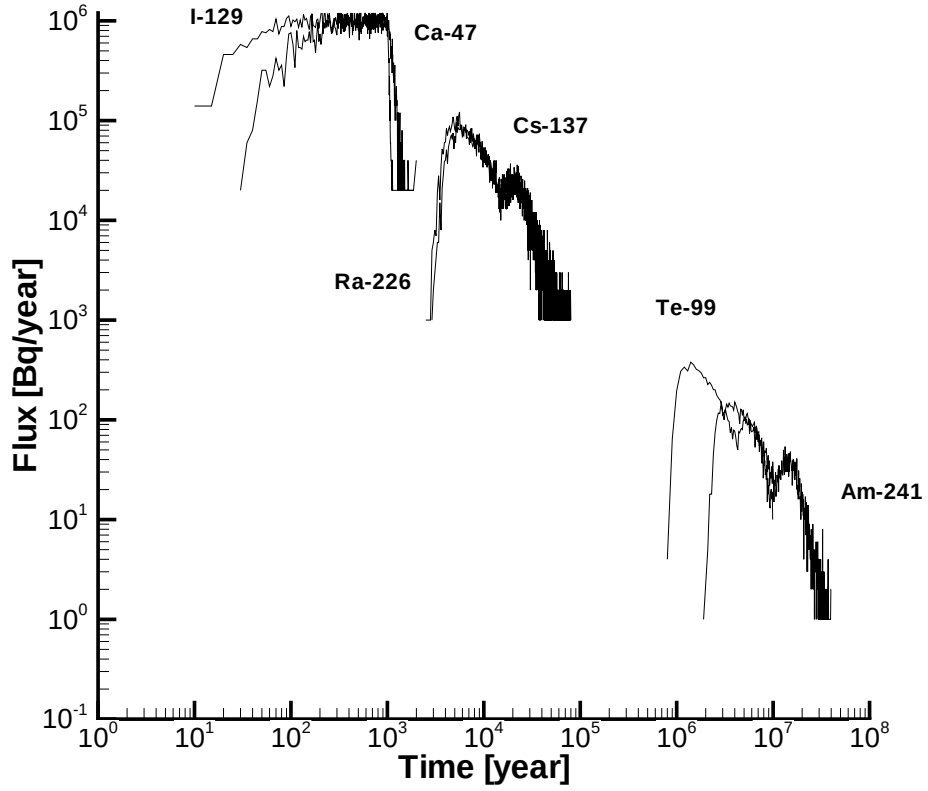

Figure 6-9. *BTC:s at a vertical plane 50 metres from source, for an extended pulse.*

Table 6-6. Breakthrough times (in years) for recovery (in %). Extended pulse.

Tracer	$t_{5\%}$	$t_{50\%}$	$t_{95\%}$	**Maximum release [Bq/year]**
I-129	85	535	985	10^6
Ca-47	145	630	1115	10^6
Cs-137	4.6×10^3	1.2×10^4	4.2×10^4	1×10^5
Ra-226	4.2×10^3	1.1×10^4	3.7×10^4	1×10^5
Tc-99	1.1×10^6	2.8×10^6	8.9×10^6	3×10^2
Am-241	2.8×10^6	7.1×10^6	2.3×10^6	1×10^2

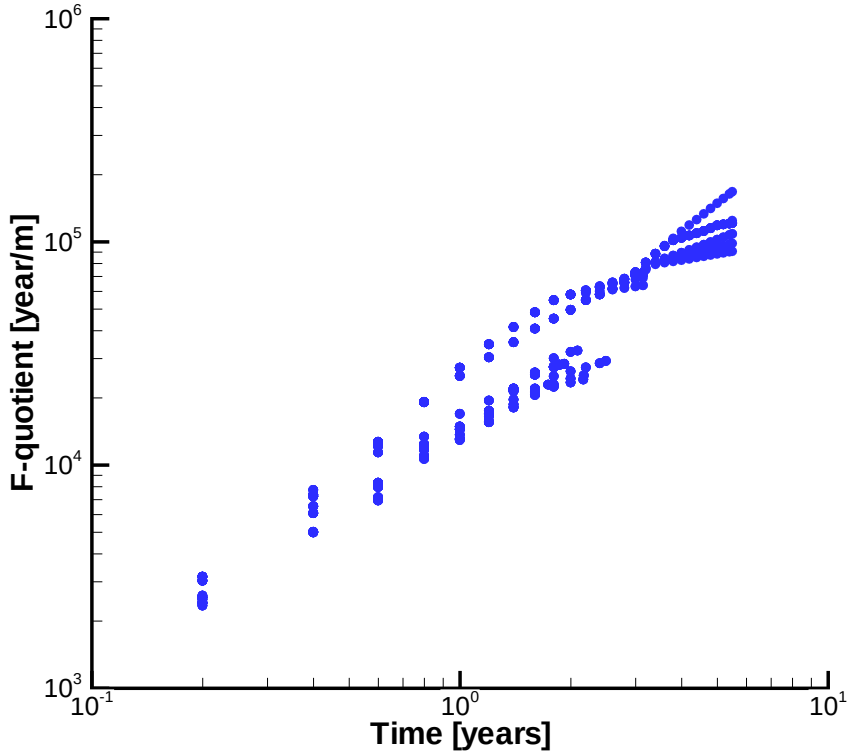

Figure 6-10. *The F-factor versus time.*

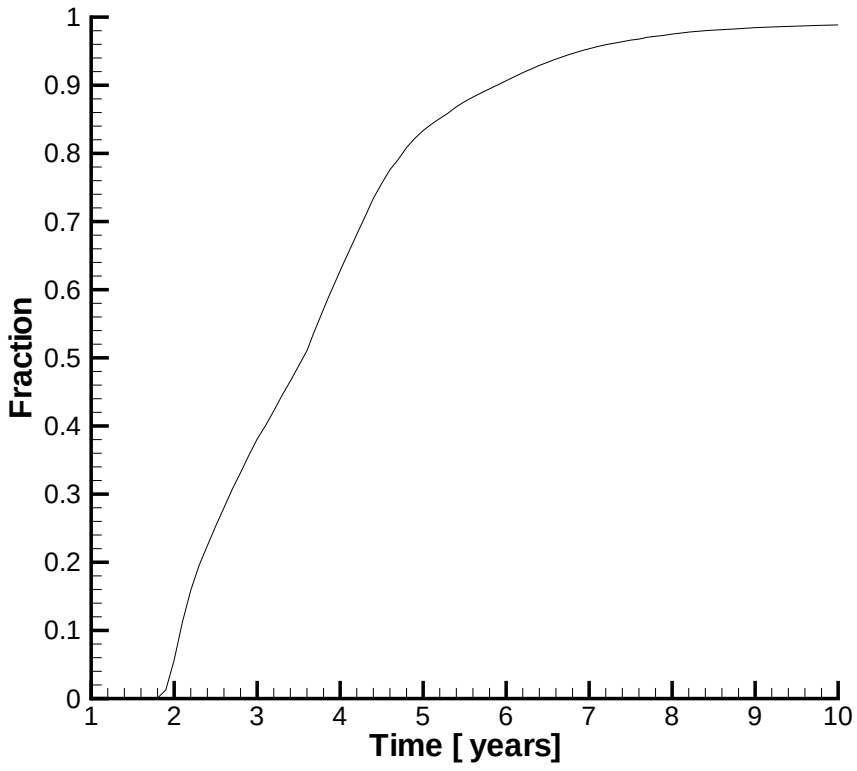

Figure 6-11. *Cumulative water residence time distribution.*

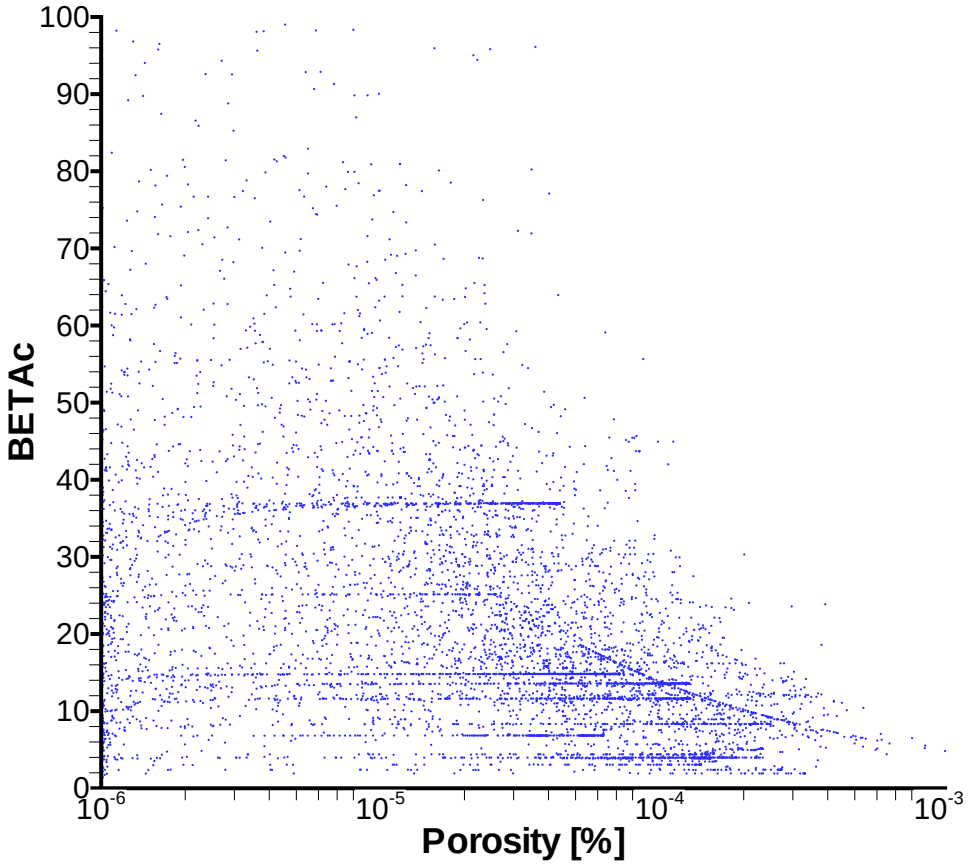

Figure 6-12. *The β_c-porosity relation.*

7 Task 6F

7.1 Modelling strategy

Task 6F is specified in Elert and Selroos (2004). Basically, a 20 metres long section of a fracture is considered. The fracture can be of Geologic Structure Type (GST) 1 or 2. Three head boundary conditions and three tracers are to be tested.

In the present study the problem is considered to be one dimensional and the three head boundary conditions are then implemented as three specified water velocities (U_w). Tracer properties are taken from earlier Task 6 studies.

A way to implement GST and Complexity Factor (CF) was suggested in Section 3-4. It was argued that both GST and CF could be represented by a modification of how much immobile volume should be attributed to a specific feature; the following was suggested:

$$Vol_{im} \sim FWS \times \left(1 + C_{GST}\left(2 - GST\right)\right) \times \left(1 + C_{CF}\left(CF - 1\right)\right) \qquad (7\text{-}1)$$

where C_{GST} and C_{CF} are constants. Expression (7-1) should be considered as tentative and the constants as largely unknown; it is however suggested that "GST and CF could change the fracture wall porosity by 50%". From the previous sections it was found that β_c should be in the range $1 \rightarrow 5$ for a water carrying fracture.

From this discussion, it is suggested that the two GST:s to be analyzed can be represented by $\beta_c = 2.0$ (GST = 2) and $\beta_c = 3.0$ (GST =1). Obviously, these values are no more than qualified guesses, based on the information compiled in the previous sections.

7.2 Modelling calibration

As a background to the results of Task 6F, a sensitivity case is first discussed, see Figure 7-1. Three BTC:s, for $\beta_c = 1$, 3 and 5, are shown. The length of the channel was 20 metres and the water velocity was set to 6.34×10^{-7} m/s, giving an advective transport time of 1 year.

It is found that the variation in β_c gives a significant effect on the BTC.

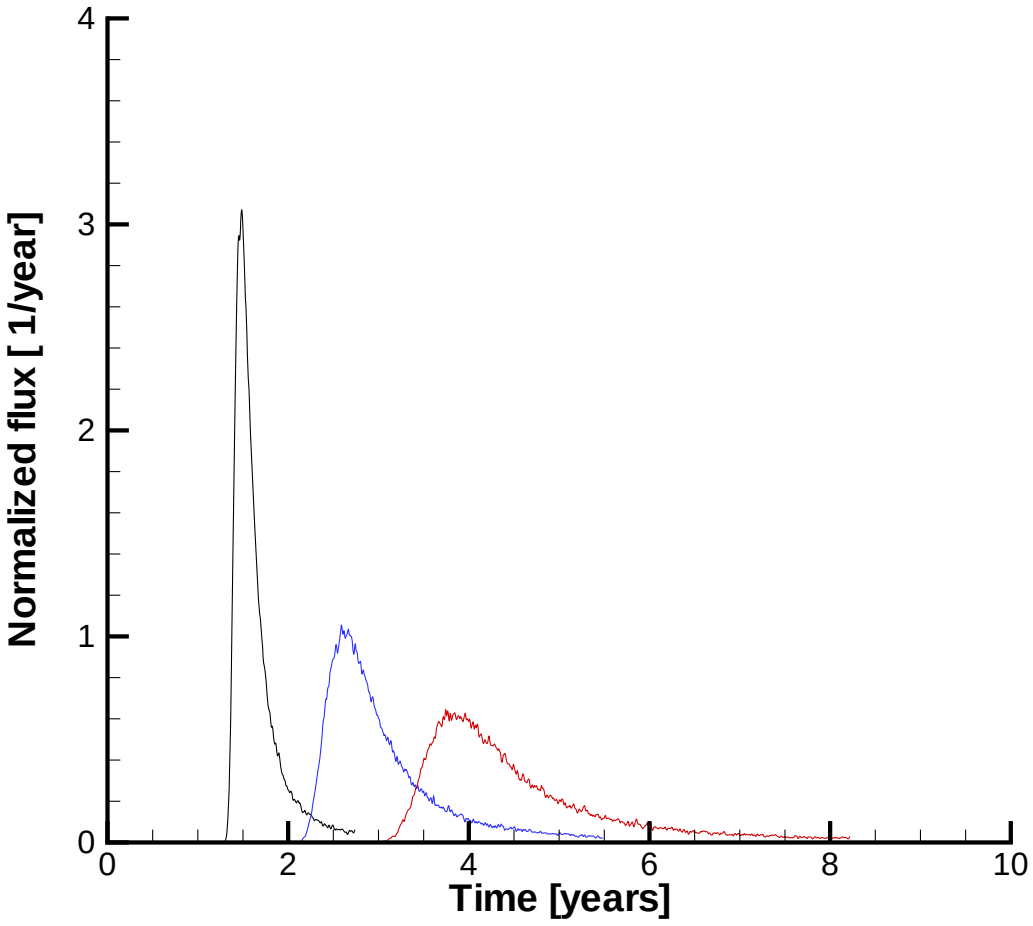

Figure 7-1. *BTC:s for three* β_c - values.

- *Black line,* $\beta_c = 1$
- *Blue line,* $\beta_c = 3$
- *Red line,* $\beta_c = 5$

7.3 Results

The tracer properties are taken from earlier Task 6 studies (Svensson and Follin, 2003) and summarized in Table 7-1. Also based on earlier work, the related FRAME parameters can be specified, see Table 7-2. In this table we see that β_c is set to 2.0 for I-129 (conservative) and GST = 2 and to 3.0 for the GST = 1. For other tracers R_{im} and R_m will also influence β_c.

Elert and Selroos (2004), specify six cases, see Table 7-3, and their notation will be followed. As we have three tracers altogether 18 simulations are to be reported.

The requested results are given by Table 7-4 and Figures 7-2, 7-3 and 7-4. From the figures it is seen that GST = 1 will delay and reduce the peak in the BTC:s somewhat (as compared to GST = 2), which is the expected effect.

Table 7-1. Tracer property data.

Tracer	D_w $\left(x10^{-9}\right)$ **[m²/s]**	K_a **[m]**	K_d **[m³/kg]**	R_m	R_{im}
I-129	2.00	0	0	1	1
Cs-137	0.50	8×10^{-3}	8×10^{-4}	17	542
Am-241	0.6	0.5	0.5	1001	3.38×10^{5}
$R_m = 1+\frac{2K_a}{10^{-3}}$, $R_{im} = 1+\frac{2700K_d}{0.004}$					

Table 7-2. FRAME parameters.

Tracer	$\alpha_{\min}$	$\alpha_{\max}$	β_c, GST=1	β_c, GST=2
I-129	0.95×10^{-10}	2.0×10^{-3}	3	2
Cs-137	4.4×10^{-14}	5.0×10^{-6}	96	64
Am-241	8.9×10^{-17}	1.0×10^{-7}	1014	676
$\beta_c = \beta_c^0 \times R_{im} / R_m$, where β_c^0 is the value for a conservative tracer				

Table 7-3 Six cases, defined by Elert and Selroos (2004).

Groundwater travel time	**Feature 1S Geological Type 1**	**Feature 4S Geological Type 2**
0.1 yr	Case A1	Case A2
1 yr	Case B1	Case B2
10 yr	Case C1	Case C2

Table 7-4. Summary of simulation results.

Case	Tracer	$t_{5\%}$	$t_{50\%}$	$t_{95\%}$	Maximum release [1/year]
A1	I-129	0.20	0.25	0.61	10
	Cs-137	52	77	255	0.03
	Am-241	4.0E4	5.4E4	1.5E5	4.0E-5
A2	I-129	0.16	0.19	0.44	12
	Cs-137	33	50	171	0.04
	Am-241	2.5E4	3.4E4	8.5E4	6.0E-5
B1	I-129	2.4	2.9	5.7	1.0
	Cs-137	720	960	2250	2.0E-3
	Am-241	5.1E5	6.4E5	1.2E6	4.0E-6
B2	I-129	1.9	2.2	4.2	1.5
	Cs-137	460	630	1710	3.0E-3
	Am-241	3.3E5	4.2E5	8.5E5	6.0E-6
C1	I-129	27.9	32.8	55.2	0.1
	Cs-137	9.2E3	1.2E4	2.3E4	2.0E-4
	Am-241	6.2E6	7.4E6	1.2E7	4.0E-7
C2	I-129	21.5	24.8	42.0	0.15
	Cs-137	6.0E3	7.6E3	1.6E4	3.0E-4
	Am-241	4.0E6	4.9E6	8.2E6	6.0E-7

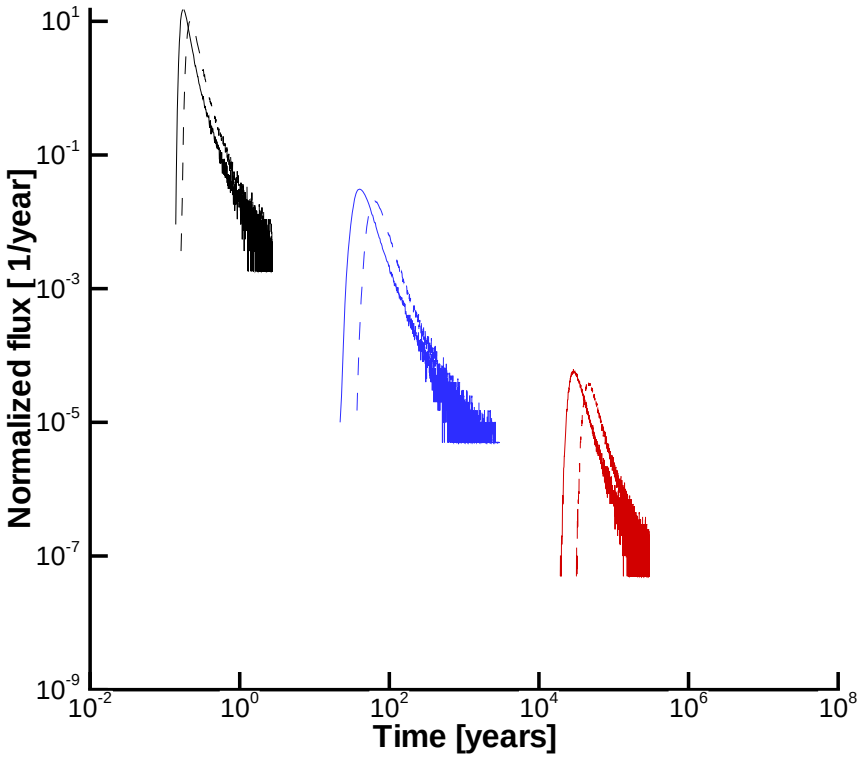

Figure 7-2. *BTC:s for I-129 (black), Cs-137 (blue) and Am-241 (red). Solid lines represent GST =2 and broken lines GST =1. Advective travel time: 0.1 year.*

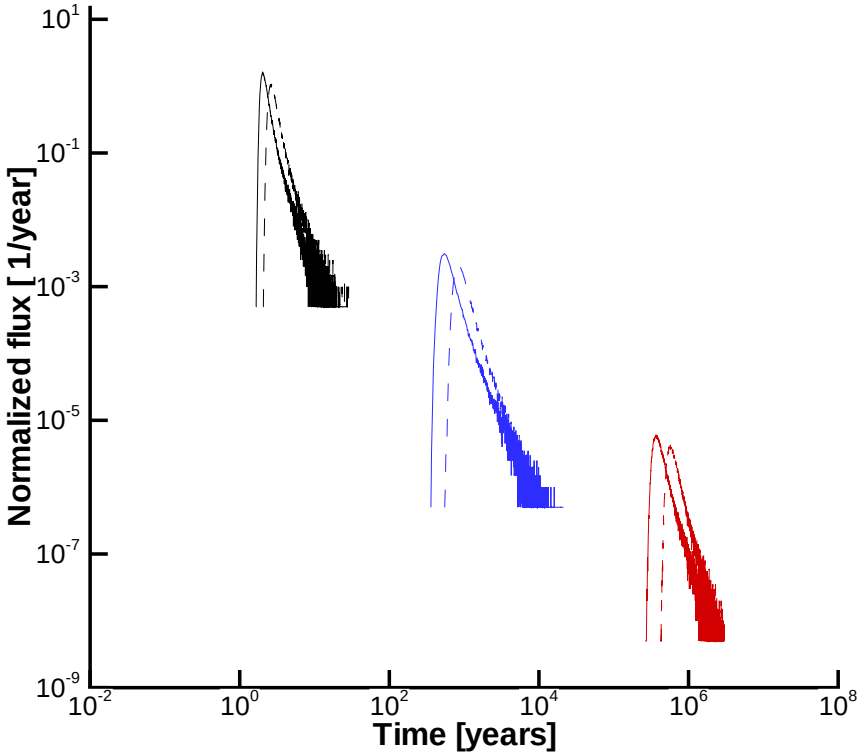

Figure 7-3. *BTC:s for I-129 (black), Cs-137 (blue) and Am-241 (red). Solid lines represent GST =2 and broken lines GST =1. Advective travel time: 1.0 year.*

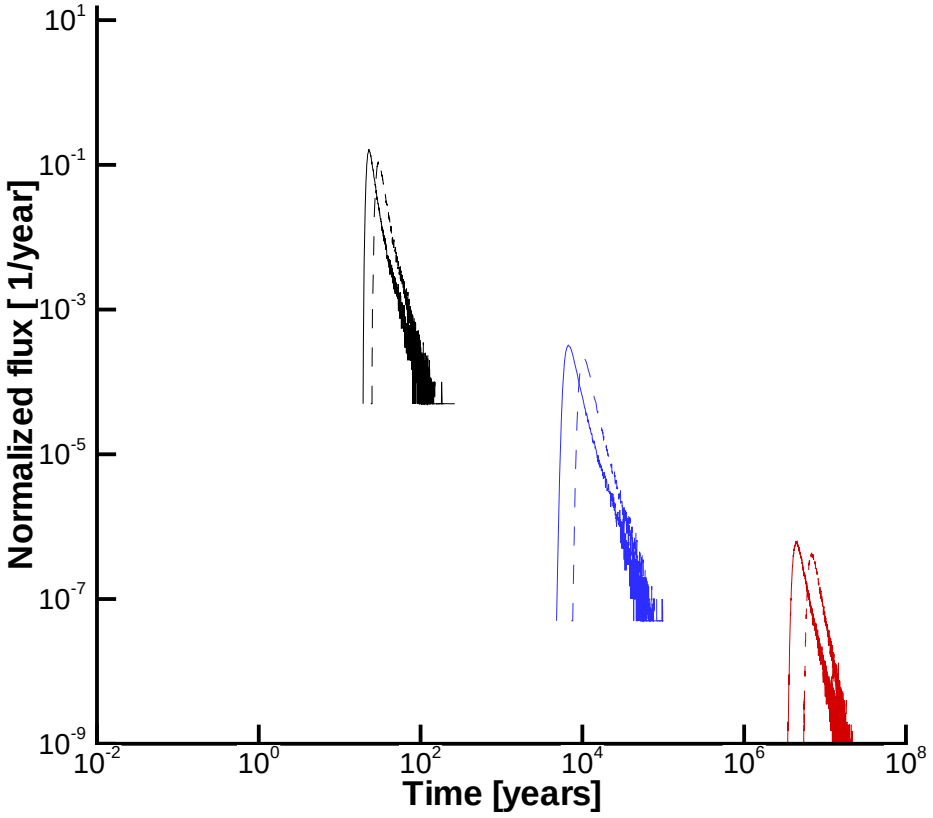

Figure 7-4. *BTC:s for I-129 (black), Cs-137 (blue) and Am-241 (red). Solid lines represent GST =2 and broken lines GST =1. Advective travel time: 10.0 years.*

8 Task 6F2
Some suggestions on the generation of fracture networks

8.1 Background

It goes without saying that the fracture network and its properties are important for flow and transport in a fractured rock; no fractures, no flow and no transport times. It is equally obvious that the characteristics of the network largely determine the flow distribution and transport times.

In Figure 8-1 a rock block with a fracture network is illustrated, together with some key elements of the specification of a network. The present report will discuss an approach to this specification, with special reference to the requirements of numerical simulation models.

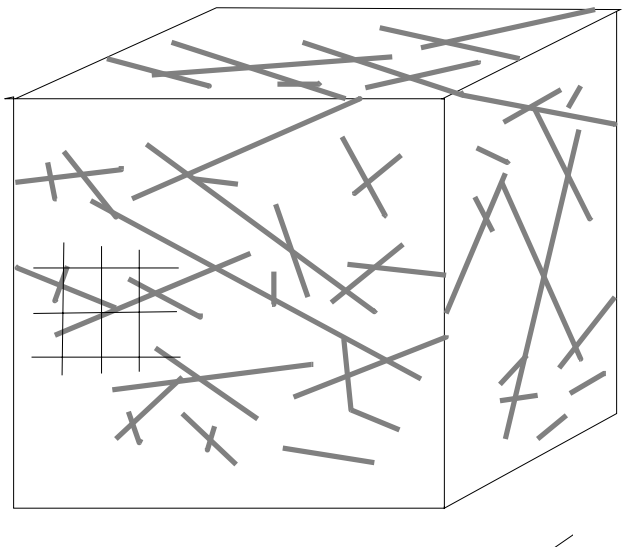

Figure 8-1. *Illustration of a rock block with a fracture network.*

The fracture network can be specified by:

- A power-law for length-distribution
- A fractal dimension for spatial distribution
- An intensity for total number of fractures
- Properties of each fracture/zone (aperture, transmissivity, storativity, etc)

8.2 Objective

For a given conceptual model, discuss and suggest a methodology for constraining the generation of a fracture network, including its properties.

8.3 Scope

It is expected that the methodology will depend on the basic conceptual model adopted. In this report the basic concepts of the code DarcyTools will define the starting point. For a full discussion of these the reader is referred to Svensson et al. (2006); here some of the concepts relevant for the present task are listed:

- The fracture length distribution is described by a power law

$$n = \frac{\alpha}{a-1}\left(l_{\min}^{-a+1} - l_{\max}^{-a+1}\right) \qquad (8\text{-}1)$$

where n is the number of fracture centres per unit volume, α a constant, a the power-law exponent and $l_{\min}$, $l_{\max}$ the length interval considered.

- SOS (Separation Of Scales). The numerical resolution defines a separation, above which fractures are resolved explicitly. Below this scale the network is parameterized by a subgrid model called FRAME.
- The spatial distribution is assumed to be Poissonian.
- Isolated fractures or groups of fractures are removed; only the connected network is hence considered.

8.4 The problem considered

A rather detailed account of the input parameters and the performance measures is given by Table 8-1. As mentioned above, the table is tailored for one particular code and may also be specific for one particular site.

Let us have a look on the input specification.

- Deterministic zones are expected to be known and hence form the backbone for the smaller, stochastically generated, fractures.
- The stochastic network requires a lot of parameters for its specification. Some of these are defined by Equation (8-1) above. The transmissivity and aperture models are other important parts.
- The sub grid network is parameterized by the model FRAME, which has its own set of input parameters.

The performance measures are the result of the chosen input specification. It is of course advantageous if these can be directly compared with measured data but sometimes only “expert judgement” can be applied. In Table 8-1 a division into three groups is made, depending on the kind of simulation that is required for the performance measure. In the first, “Geometry”, some measures that only require a fracture network generation are compiled. As an example, when the network with properties is generated it is easy to calculate the kinematic porosity of the computational domain. The second group “Flow” requires flow simulations and the third group “Transport” requires various kinds of transport simulations.

We now have the necessary background to formulate the key question of this report “How do we specify the input parameters with the objective of fulfilling as many performance measures as possible?”. Some readers may immediately respond by stating that “It depends on what you want to simulate” or “All performance measures are not of equal importance”. However, if we adopt the view that the input parameters should be valid for a range of simulations (tunnel effects, breakthrough curves, long time scenarios) and agree with available measurements and expert judgments, the question is relevant. It is the author’s view that various projects often sub-optimize the input specification; the kinematic porosity is tuned to fit a single transport experiment. The same effect could perhaps be achieved by changing the intensity of the network or the transmissivity model.

One approach that may seem logical is indicated by the number in brackets, after some of the performance measures. If a drawdown experiment is available (pumped borehole or tunnel) it seems logical to tune the model to this experiment as we then get the right relation between flow and drawdown, i.e. the mean hydraulic conductivity. The next step would then be to distribute this mean conductivity on a certain number of fractures and the HPF (high permeability features) statistics could be used for this purpose. This is thus step [2]. The third step would be to consider the porosity values and we would have a model ready for transport simulations. However, a more careful analysis shows that we will be faced with the same problem again; several input parameters can be tuned to fit the performance measures.

The above discussion shows that Table 8-1 is useful to illustrate the number of input parameters and performance measures at hand, but it does not provide a strategy for chosing, or constraining, input parameters.

8.5 Suggested methodology

The approach to be suggested rests on two principles.

- “One thing at the time”. The example given above illustrates that many performance measures can be fulfilled by tuning of different input parameters. It is crucial to eliminate interdependencies as far as possible.

- “Formulate priorities”. Based on physical arguments, focus must be on the relevant scales and parameters. Examples: “When power-law parameters are evaluated, anisotropies in the distributions may need to be neglected”. “When a transmissivity model is specified large scale features should be in focus as most of the water is carried by the large features”.

Figure 8-2 illustrates the methodology. The figure can also be interpreted as a work plan as one should start from left and carry out the tasks indicated in the boxes. Some further comments:

- The first box concerns the power-law parameters (see also Equation 8-1). Often these are evaluated from pumped boreholes, by various techniques. In the author's view there are two drawbacks with this approach; the analysis is mixed with the formulation of a transmissivity model and, secondly, it focuses on the small scale features. The present approach thus separates the determination of power-law parameters from the transmissivity model and further focuses on large scale features.

Table 8-1. An overview of the fracture network generation task. Input data and semi-empirical relations result in a network that can be judged by a number of Performance Measures.

Case: Äspö			
Input	**Performance Measures**		
Deterministic zones - Coordinates - Properties (T, n, s, CF, GST,..) Stochastic network - Intensity - Power-law exponent - $l_{\min}$, $l_{\max}$ - $T-l$ - e_T-T - Thickness-l - Fisher-orientation - FWS - CF and GST - Storativity Subgrid network - β_G (total immobile vol.) - $\alpha_{\min}$, $\alpha_{\max}$, k	GEOMETRY	Measured data	1. HPF-frequency [2] 2. P_{32}, P_{10}, etc. 3. Fractal dimension
		Expert judgement	1. Porosities n_{kin}, $n_{connected}$ [3] 2. a_w -statistics 3. Scale of critical connectivity
	FLOW	Measured data	1. Drawdown data (tunnel, LPT2, etc.). [1] 2. Inflow distribution to tunnel, time dependent.
		Expert judgement	1. Block-conductivities for different scales. 2. Number of flow channels/m^2.
	TRANSPORT	Measured data	1. $\alpha_L / L = 0.05 \rightarrow 0.10$ 2. Water types (Glacial, etc.). 3. Salinity data 4. Tracer experiments, BTC:s.
		Expert judgment	1. F-factor. $F-t$ 2. Trajectory visualisation. 3. Water Residence time.

- Once the geometry, i.e. the power-law parameters, of the network is specified the transmissivity model is considered. The focus should be on length scales from the deterministic features down to, say, 5-10% of this length as most of the water will be carried by these fractures.

- The next step is indicated by a circle, witch means a simulation with an evaluation against field data. A steady state drawdown experiment should be simulated. Steady state conditions are preferred to avoid storativity effects. If possible, gravitational effects (due to salinity or temperature) should play a minor role in the pressure responses.

- The diamond shaped box in the bottom of the figure provides a way back in the workplan. If the steady state drawdown simulation is not acceptable, the earlier steps need to be revisited.

After the steady state drawdown simulation one may like to consider an unsteady drawdown case, in order to specifically evaluate the storativity parameter. This step is not shown in the work plan, instead parameters relevant for transport simulations are considered.

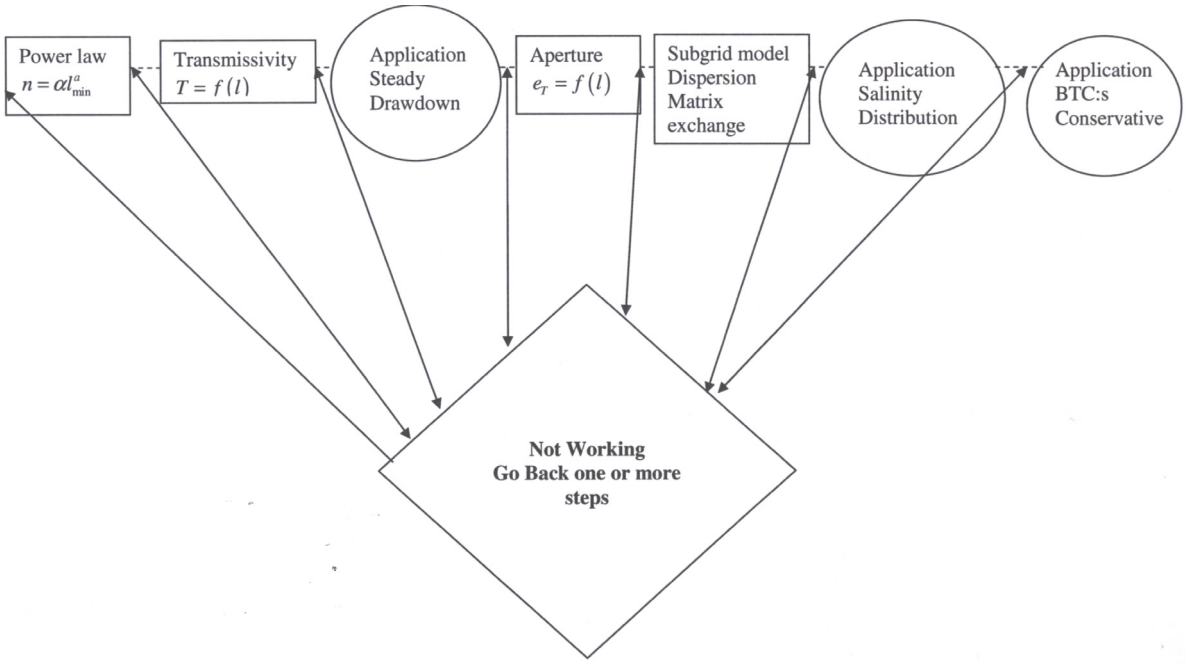

Figure 8-2. *Approach & Workplan. Considered as a work plan, one should work from left to right in the diagram.*

Hopefully these comments are sufficient to convey the suggested methodology. The following chapters will outline an application of the approach.

8.6 The power law parameters

According to the methodology chosen we should evaluate the power-law parameters without employing transmissivity data and we should further focus on the most important length scales.

The method selected is based on the number of known fractures larger than a certain $l_{\min}$. From Equation 8-1.

$$n = \frac{\alpha}{a-1}\left(l_{\min}^{-a+1} - l_{\max}^{-a+1}\right) \approx \frac{\alpha l_{\min}^{-a+1}}{a-1}$$

If $N = n \times V$, where N is number of known fractures and V is the volume, we get:

$$\alpha = n(a-1)l_{\min}^{a-1} = \frac{N}{V}(a-1)l_{\min}^{a-1} \qquad (8\text{-}2)$$

which is the expression we will use to get relations between α and a.

In Table 8-2 four cases, giving relations between a and α, are summarized. These relations are illustrated in Figure 8-3. We note that Equation 8-2 implies a trend; increasing α will increase a. However the information compiled only results in a relation between a and α; we need to constrain the relation in some way. A brief review of the literature shows that the intensity α is fairly unknown, while the power-law exponent a has been studied extensively:

- La Pointe et al. (1999) found $a = 3.6$ (in our notation) based on an extensive survey. This is the value adopted for the earlier Äspö-models.
- Darcel (2003) found values of 3.8 – 4.0 after reviewing data from Äspö/Simpevarp.
- The present Site Investigation (Follin et al., 2004) points to a value of 3.6 $(k_{3D} = 2.6)$.
- Sahimi (1995) summarizes a lot of data and finds that $a = 3.4 - 3.7$.

Table 8-2. Compilation of data for specification of $\alpha - a$ relations.

Case	V	$l_{\min}$	N	Comments, Reference
Lineaments Reg. scale	8 x 3 x 2 = 48 km^3	1000	75	Number of structures in a subvolume of the regional model. Follin et al. (2006).
Det. Zones Äspö	1 km^3	300	20	Named zones at Äspö
True Block Scale volume	200^3 m^3	50	30	Identified and synthetic structures, Task 6C-report.
Äspö tunnel	7 x 7 x 2400 m^3	5	113	Number of structures that cross the whole tunnel section. Tunnel coordinates: 600→3000 m

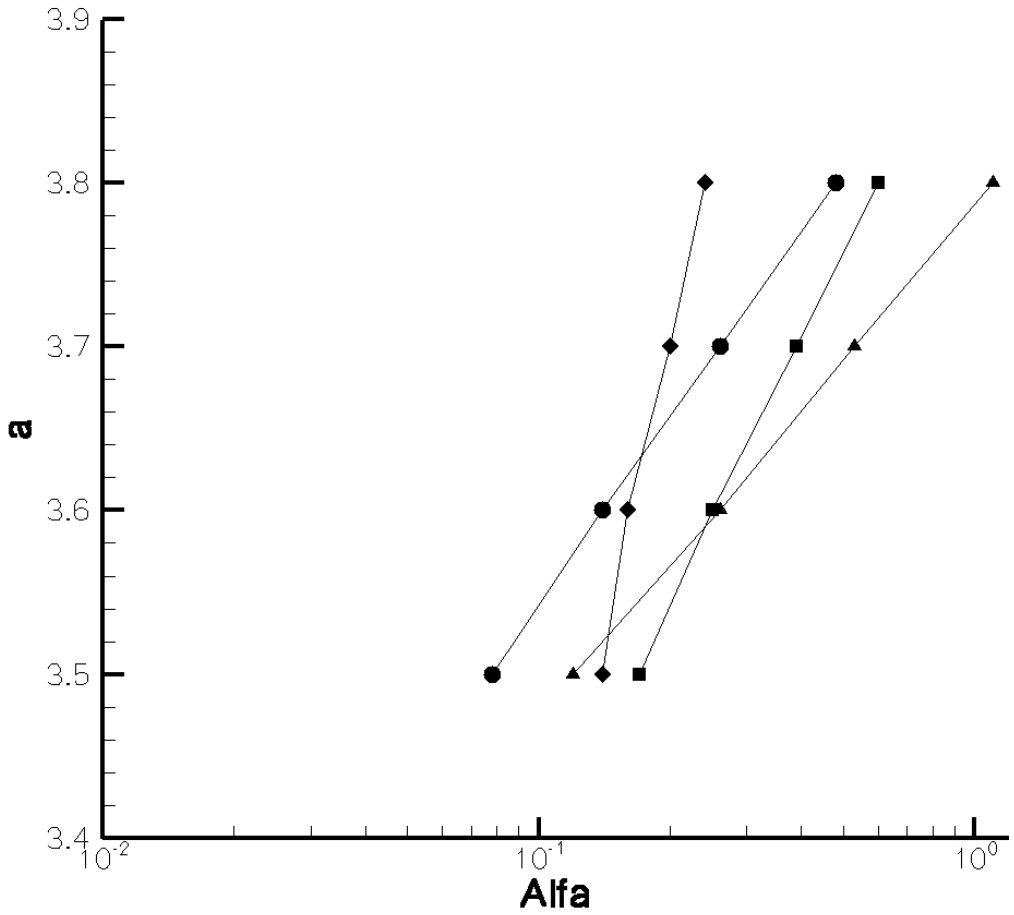

Figure 8-3. *The a-α relation for four cases:*

Lineaments on a regional scale

Deformation zones at Äspö

Structures in the TRUE Block volume

Structures that cross the Äspö tunnel

From this list we conclude that *a* should be in the range 3.5 – 3.7 and we can recommend a quite narrow combination of values.

This may all seem quite convincing, but it should be regarded as illustrations of a methodology. It is however possible to eliminate most of the gross simplifications made above by actually generating the fracture networks. For the Äspö Tunnel case we should thus generate a network for the Äspö site and count the number of complete crossings with the tunnel. If one then specifies an α -value and find the *a*-value that results in the correct number of crossings we have found one α -*a* pair. By repeating this procedure for a new α another pair, and eventually a line, is obtained. For the lineaments one could compare the total fracture length in a given horizontal plane and this way get a α -*a* correlation.

It should also be noted that the power-law is very sensitive to the parameters. A test was made for the TRUE Block Scale volume (200 x 200 x 200 m^3) with a $l_{min} = 2$ m. Two sets of α -*a* values, (0.1, 3.6) and (0.5, 3.8), were used. The first set resulted in 25 000 fractures larger than 2 metres, while the corresponding value for the second pair was 300 000.

This test shows that we may need additional criteria to constrain the network. It is presently not clear how these should be formulated, but maybe the two diagrams shown in Figure 8-4 can suggest a way. The top one simply shows the number of fractures per m^3 as a function of l_{min} .The dots mark the values for the four cases presented in Table 4-1, while the straight line is fitted by eye. The two pair of values used in our test case would both be correct for the "True Block Scale point" (l_{min} = 50 m), but would have different slopes. The bottom diagram in Figure 8-4 gives the number of connected cells (i.e. at least one of the cell walls is crossed by a fracture) as a function of cell size. This diagram is interesting as the bounding values are known; for very large cell sizes (perhaps $\Delta > 10^3$) we know that all cells are connected and percolating and for very small cells (perhaps $\Delta < 10^{-4}$) the percent should be equal to the porosity as we can then regard the cells as points. The interesting part is $0.1 < \Delta < 100$ m. At the lower limit one could use P_{10} values to estimate the % connected cells (cell size is then equal to the borehole diameter). If the connected P_{10} -value is 0.2 this means that on the average the spacing between connected 0.078 m cells is 5 metres. This gives a connected % of 1.5. Similarly we may subdivide all 5m tunnel cells into connected and not connected 5 metres cells and get another "field data point" in the diagram. The line should represent the result from the numerical simulation. Coming back to the True Block Scale simulation with $l_{min} = 2$ metres and cell size 2 metres, we may note that the $(\alpha,\ a)$ pair (0.1, 3.6) resulted in 28% connected cells, while the figure was 92% for (0.5, 3.8). Once again we find that the diagram (if anchored with experimental data) could discriminate between the two cases.

It is now time for some concluding remarks about power-law parameters and these will be given with the methodology aspect in mind.

- A method to estimate the power-law parameters, without considering transmissivity data, has been discussed and illustrated.
- The method attempts to determine the optimal parameters for the length interval (5 → 1 000 metres) that is believed to be of most importance in flow simulations.
- Additional diagrams that could further constrain the parameter ranges have been suggested. These diagrams should include field data information.

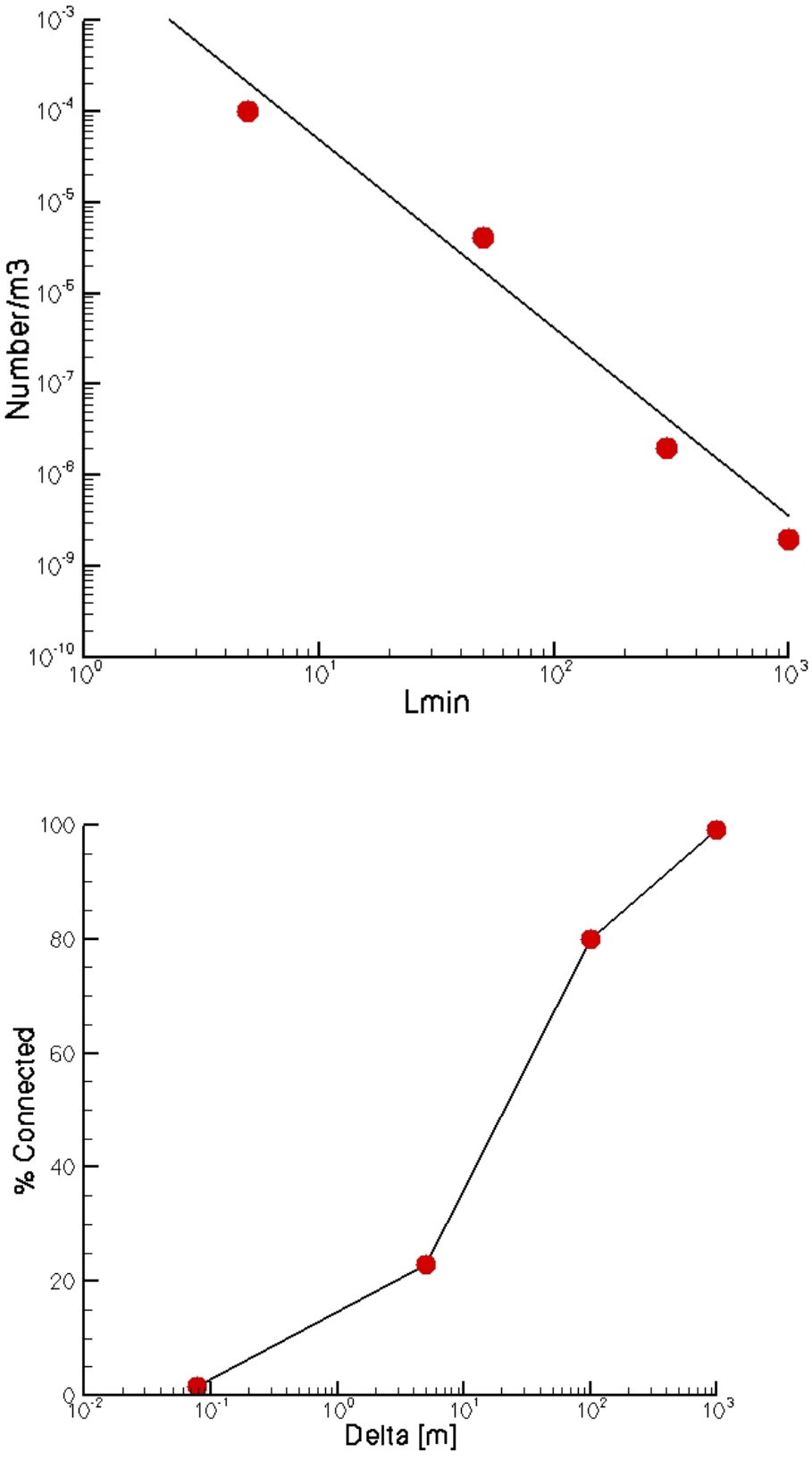

Figure 8-4. *Number of fractures per m^3 as a function of l_{min} (top) and % connected cells as a function of cell size Δ. The dots in the top diagram are based on values given in Table 8-2, while the dots in the bottom figure are not based on data.*

8.7 Transmissivity model

Next the transmissivity model will be discussed. The discussions and illustrations will not be as detailed as for the power-law parameters, but will hopefully serve the purpose as being "a second example of the methodology". For this reason the focus will be on strategy rather than on field data.

So let us first define our starting point with reference to Figure 8-2 and the general outline in Section 8-5.

- We should now consider the geometry of the network as known. If we can not formulate a working transmissivity model with the given geometry, we need to go back to the power-law parameters.
- The focus should be on the large *T*-values as fractures with large *T*-values carry most of the flow.
- From our chosen conceptual model we accept that $T = f(l)$, where l is the length scale of the fracture/zone.
- When a *T*-*l* relation is established, one should try to avoid influences from processes "to the right of the *T*-*l* box in Figure 8-2". Transient experiments may for example include a storativity effect and gravitational effects may influence a measured flow rate.

The following list of sub-tasks is suggested as a means to arrive at a working *T*-*l* relation.

- Compile *T*-*l* data and represent these data in a diagram. Such a compilation has recently been carried out by Vidstrand (2006) and his diagram is shown in Figure 8-5. The *T*-*l* relations suggested in this diagram will be our "base case".
- High Permeability Feature (HPF) statistics is available for the Äspö Site. This information is derived from borehole data and give answers to questions like "How often does one encounter a *T*-value of 10^{-5}, 10^{-6} or 10^{-7} m^2/s along a borehole at Äspö?" Once we have generated a network for Äspö and assigned *T*-values to all fractures and zones, it is straight forward to place boreholes in the numerical model and evaluate the HPF statistics. In the author's view this evaluation of a *T*-*l* relation is extremely valuable as we focus on the high transmissivities.
- Block conductivities. As a numerical model is structured in blocks, or cells, it is of interest to study block conductivities as function of a block size. Note that this evaluation is related to the number of connected cells, discussed earlier, as a disconnected cell is a cell with zero conductivity. An example of a block conductivity diagram is given by Figure 8-6. Both the trend and spread versus Δ is of interest to compare with field data.

It is believed that a well founded *T*-*l* relation will result if these subtasks are carried out.

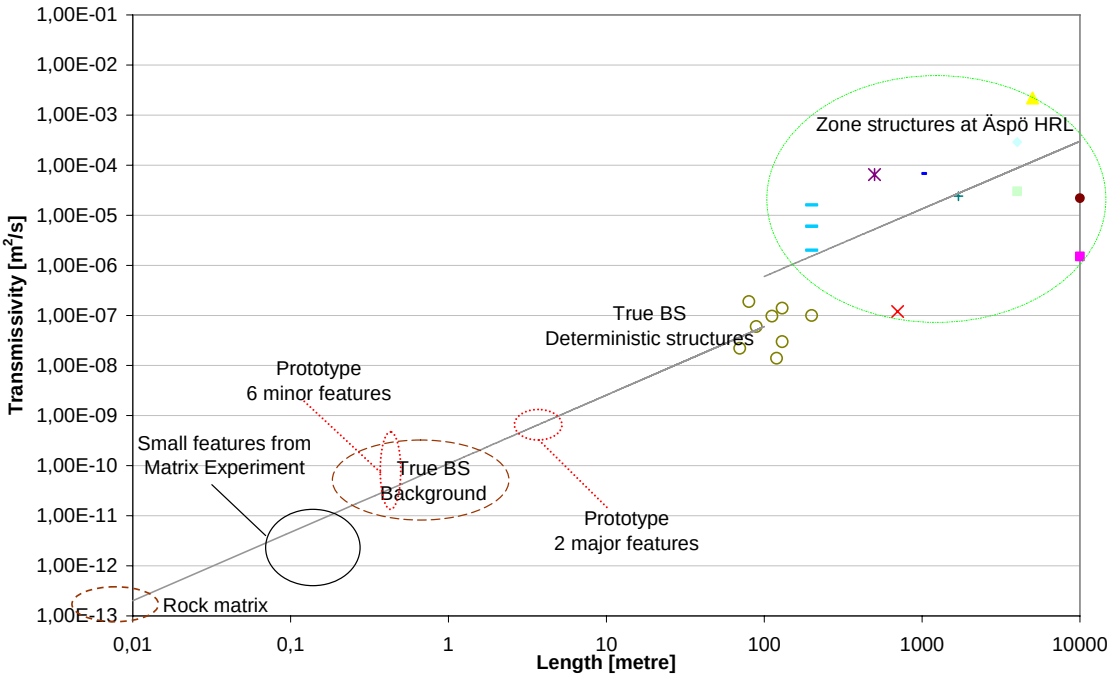

Figure 8-5. *Proposed relationship between transmissivity and length for Äspö HRL features. From Vidstrand (2006).*

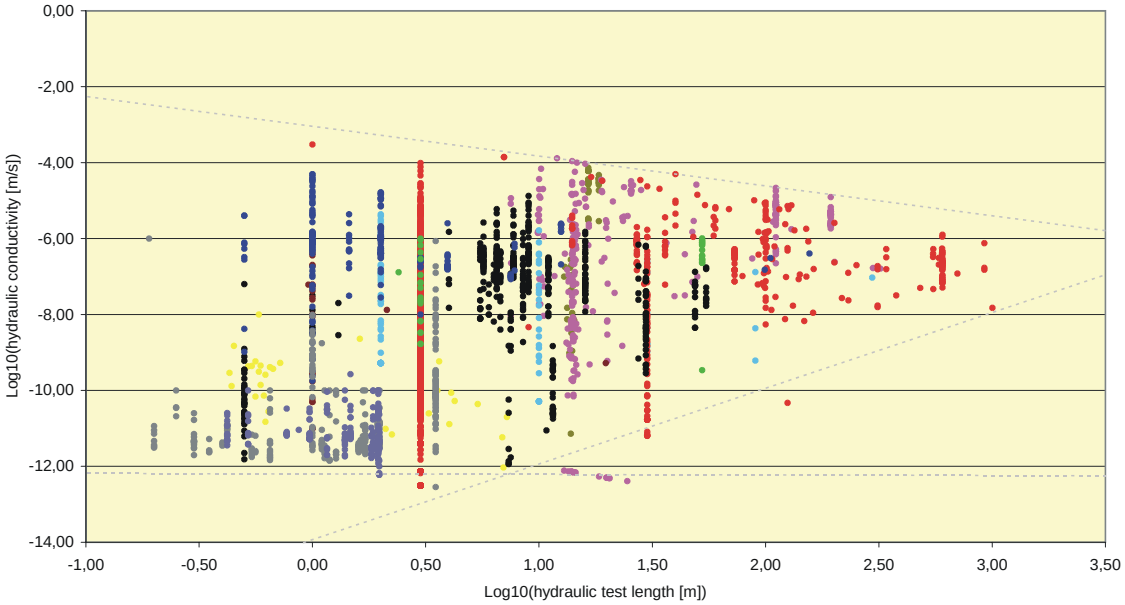

Figure 8-6. *Distribution of hydraulic conductivity values from the Äspö Hard Rock Laboratory with test scale. The figure contains data from 3310 unique hydraulic tests. Data from different experiments are visualized with different colours. From Bockgård et al. (2006).*

8.8 Flow simulations

It should be noted that the tasks suggested in Sections 8.4 and 8.5 do not involve any flow simulations. However, we are now at the first round circle in our work plan (Figure 8-2) and it is time for "Steady State Drawdown Simulations". These simulations could include the drawdown due to a tunnel or a pumped borehole. It is also the right time to consider the inflow distribution to a single pumped borehole.

We will not speculate about these simulations, but simply state that the loop discussed, i.e. power-law parameters → *T-l* relation, drawdown simulations, should be fully explored before the next part, which aims at transport simulations, is considered.

8.9 Discussion and conclusions

The problem addressed in Task 6F2 is a major one, and the ideas put forward in this work should be regarded as suggestions and contributions to a continued discussion. It is however striking how uncertain the specification of the fracture network is and how sensitive the result is to the parameters chosen. In this work it was for example shown that the number of fractures larger than 2 metres in the TRUE Block Scale volume was 25 000 for one set of power-law parameters and 300 000 for another set; both sets can be supported by field data!

The study presented has several limitations and the most serious one is perhaps that the information gathered and analysed in the SKB Site-Investigation has not been considered. The only reason for this is lack of time.

Conclusions from the study should focus on the approach suggested:

- A new methodology to constrain the parameter values used in fracture network generation has been suggested.
- The methodology emphasizes that it is essential to determine "one parameter group at the time" and to "focus on the relevant scale". For example, the power-law parameters should be determined without the use of transmissivity data.

9 Discussion and conclusions

9.1 Discussion of results

One objective of this report is to evaluate FRAME and it's parameters. We will use the discussion section to summarise the main features of FRAME and then discuss some details concerning the parameters.

Main features of FRAME

- For a conservative tracer we only need to specify four parameters ($\alpha_{\min}$ and $\alpha_{\max}$ which specify the range of immobile volumes, *k* which gives the late time slope of the BTC and β_G which is the global ratio of immobile to mobile volumes), which all have a clear physical interpretation.
- FRAME handles both storage in the matrix and longitudinal dispersion (giving long-tailed distributions). Hence, there is no need to specify a longitudinal dispersion coefficient.
- Both long and short time scales can be handled without changing the four parameters. In this report the shortest t_{50} considered is 7.8 hours (field experiments), and the longest millions of years.
- Both particle tracking methods and advection diffusion equations, like the salinity equation, can employ FRAME in the present version of DarcyTools.
- The β_c-values are directly linked to the properties of the fracture network. As we have established the β_c-a_w link, it is clear that FRAME relates directly to the F-factor concept, which may prove important.

Details about parameters

- $\alpha_{\max}$ is in this study set to 10^{-3}, which can be interpreted as "a molecular diffusion coefficient of 10^{-9} m^2/s and a length scale of 10^{-3}m" as $\alpha_{\max} \approx D_{mol}/l^2$. This value is thus associated with fast exchange on small length scales, for example diffusion into a stagnant pool that is in contact with the mobile water. With this interpretation we expect $\alpha_{\max}$ to be of this magnitude.
- $\alpha_{\min}$ is associated with diffusion deep into fractures connected with the mobile water. The diffusion coefficient is then reduced; if an estimate of the length scale is to be done we may use 10^{-11} m^2/s, which gives a length of ≈ 0.3m for the $\alpha_{\min} = 10^{-10}\ \left(s^{-1}\right)$. Changing $\alpha_{\min}$ will of course affect β_G (and hence β_c). The value used in this study, 10^{-10}, is thus linked to the β-values found suitable. It is however analytically determined, see the DarcyTools manuals (Svensson et al., 2006), how a change in $\alpha_{\min}$ affects β_G. So, if in a long time simulation one expects that $\alpha_{\min}$ ought to be reduced one can calculate a new β_G that does not change the volumes of the faster boxes. This technique was used in the parametric study of FRAME; $\alpha_{\min}$ was reduced to 10^{-12} which resulted in an increase of β_G with 28.6%.

- The late time slope of the BTC, *k*, was put to 2.0 in this study. In a classical double-porosity model, with infinite matrix of uniform properties, $k = 1.5$ and for a multi-rate model we know that $k > 1.5$. Earlier work has indicated that $k = 2.0$ fits experimental data on BTC:s in the TRUE Block Scale experiments; a value of $2.1 \rightarrow 2.2$ has also been suggested in the literature (Haggerty et al., 2000). It is also possible to relate *k* to the properties of the matrix, see Section 4-3. This approach to determine *k* also gives a $k \approx 2.0$.
- Finally, β_G and β_c have been discussed in this report. It seems that $\beta_G \approx 10$ will give a fracture network with the right dispersion characteristics. It has been found that β_c will then be in the range $1 \rightarrow 5$ for the largest fractures/zones in the network. The link to a_w ought to be further explored.

In the author's view, the FRAME parameters are far from "tuning knobs"; in fact, the values adopted seems to be quite well established, having real world simulations in mind. From a more theoretical point of view, it is of course of interest to derive closed form solutions for the delay and dispersion of a tracer cloud.

9.2 Main conclusions

As pointed out already in Chapter 3, the development of DarcyTools started at the time when Task 6 was initiated. The work performed in Task 6 has therefore to a large extent been an evaluation of the methods and concepts in DarcyTools. For this reason the main conclusions will be concerned with how DarcyTools has performed in Task 6.

- The present conceptual view of a conductive structure (see Figure 2-2) is that a range (in terms of length and time scales) of immobile water volumes is in contact with the mobile water. The subgrid model FRAME is based on the multi-rate diffusion model, which is designed to handle such cases. We may hence conclude that the basic concept in FRAME is well suited for the present task.

- During the course of the work, the FRAME parameters have been evaluated and a set of parameters has been established. It should be noted that FRAME departs from traditional models in several ways (long-tailed breakthrough-curves, no dispersion coefficients, mass-centre does not move with the water velocity). These features have contributed to the prediction of realistic breakthrough-curves.

- The fact that FRAME is fully integrated in a 3D flow code has simplified simulations in the fracture network tasks. The split-up of a tracer cloud at fracture intersections and inclusion of heterogeneity in a fracture plane are hence accounted for.

These experiences from the application of DarcyTools/FRAME in Task 6, lead to the conclusion that FRAME is well suited to handle tracer transport along single flow channels or in complex fracture networks. Also the different time scales considered in Task 6 can be handled without problem, as the multirate model accommodates such effects by definition.

9.3 Lessons learned and implications for Task 6 objectives

The lessons learned are well summarized by what has been described in Sections 9.1 and 9.2. One thing that can be added concerns further development of FRAME. In Task 6 it has been discussed if very reactive tracers require more advanced chemical description ("reactive transport modelling"). If this is the case one may find that FRAME can not easily be developed in such a direction.

Concerning implications for the Task 6 objectives, we may first repeat these objectives:

Äspö Task Force Task 6 consists of a set of numerical experiments that use a common set of hydrostructural models to test performance assessment codes and site characterisation codes. The comparison of the results of these simulations serves several objectives (Benabderrahmane et al., 2000):

1. *Assessment of simplifications used in PA models.*
2. *Determination of how the experimental tracer and flow experiments can constrain the range of parameters used in PA models.*
3. *Support of the design of site characterisation programs to assure that the results have optimal value for performance assessment calculations.*
4. *Better understanding of site-specific flow and transport behaviour at different scales using site characterisation models.*

The following remarks can be made about the implications for the objectives:

- Only one code has been used and no simplifications have been made, when *PA* time scale problems have been addressed. Perhaps one can see a trend that the same models can be applied to both *SC* and *PA* time scales.
- The question whether tracer experiments can constrain the parameters in *PA*-models, has been discussed within the project. The general opinion seems to be that they can not. The present writer does not want to oppose this conclusion but simply add the following view: if one thinks of the immobile volumes as layers at various distances from the flowing water, it is easy to motivate why short term experiments do not give any information about *PA*-scales; the deeper layers are not affected and there is hence no way to learn about their characteristics. However, if we think of the immobile volumes as a connected fracture network an alternative view is possible. If one assumes that the fracture network follows the same power-law from the largest scales (~ 1 km) down to the mm scale, then we also know something about the immobile volumes that are active on the *PA* time scales (presumably within length scales from 0.1 → 10 metres). A field experiment that samples the network at the mm to cm scale is then of value for the *PA* scale, as we determine the characteristics of a power law that is continuous. The subgrid model FRAME is built on this view.
- Contributions to the last objective listed have been achieved by the modelling exercises carried out. The introduction of "Geological Structure Type" and "Complexity Factor" in transport modelling is a major step forward.

10 References

Benabderrahmane, H., Dershowitz, W.S., Selroos, J-O., Uchida, M. and Winberg, A. 2000. Task 6 proposal –Performance Assessment Modelling Using Site Characterisation Data (PASC). Unpublished proposal to the Äspö Task Force, November 2000.

Bockgård, N., Vidstrand, P., Svensson, U. and Sjöland, A. 2006. Hydrological Research at the Äspö Hard Rock Laboratory, Sweden. IHLRWM 2006, Las Vegas, NV.

Byegård, J., Skålberg, M., Widestrand, H. and Tullborg, E-L. 2001. Effects of Heterogeneous Porosity on Retention – Results from the TRUE Laboratory Experiments. Geotrap V, Oskarshamn.

Cvetkovic, V., Painter, S., Outters N. and Selroos J.O. 2004. Stochastic simulation of radionuclide migration in discretely fractured rock near the Äspö Hard Rock Laboratory. Water Resources Research, Vol. 40, W02404.

Darcel C. 2003. Äspö Hard Rock Laboratory. TRUE Block scale continuation project. Assessment of the feasibility of tracer tests with injection in "background fractures" using a model based on a power law fracture length distribution. Swedish Nuclear Fuel and Waste Management Company (SKB), IPR-03-41.

Dershowitz, W., Winberg, A., Hermansson, J., Byegård, J., Tullborg, E-L., Andersson, P. and Mazurek, M. 2003. Äspö Hard Rock Laboratory. Äspö Task Force on modelling of groundwater flow and transport of solutes. Task 6C. A semi-synthetic model of block scale conductive structures at the Äspö HRL. SKB International Progress Report, IPR-03-13.

Elert, M. and Selroos, J-O. 2004. Task 6E Modelling task specification. Unpublished note.

Elert, M. and Selroos, J-O. 2004. Task 6F sensitivity analysis. Modelling task specification. Simplified "Test Bench" transport calculations. Version 2.0. Unpublished note.

Follin, S., Stigsson, M., Berglund, S. Svensson, U., 2004. Variable-density groundwater flow simulations and particle tracking –Numerical modelling using DarcyTools, Preliminary site description Simpevarp subarea – version 1.2, SKB R-04-65, Svensk Kärnbränslehantering AB.

Follin, S., Stigsson, M., Svensson, U., 2006. Hydrological DFN modelling using structural and hydraulic data from KLX04. Preliminary site description Laxemar subarea – version 1.2. SKB R-06-24, Svensk Kärnbränslehantering AB.

Haggerty, R., Gorelick, S. M. 1995. Multiple-rate mass transfer for modelling diffusion and surface reactions in media with pore-scale heterogeneity. Water Resources Research, Vol. 31, No. 10, Pages 2383-2400.

Haggerty, R., McKenna, S.A., Meigs L.C. 2000. On the late-time behavior of tracer test breakthrough curves. Water Resources Research, Vol. 36, No. 12, Pages 3467-3479.

Harlow F. H. and Welch J.E., 1965. Numerical Calculation of Time-Dependent Viscous Incompressible Flow of Fluid with Free Surface. Phys. Fluids, vol. 8, p. 2182.

Neretnieks I., 1993. Solute transport in fractured rock -applications to radionuclide waste repositories. In "Flow and Contaminant Transport in Fractured Rock", 39-127. Academic Press, Inc.

Patankar S.V., 1980. Numerical heat transfer and fluid flow. Hemisphere Publishing Corporation, McGraw-Hill Book Company.

Sahimi M., 1995. Flow and transport in porous media and fractured rock. VCH Verlagsgesellschaft mbH, Weinheim.

Svensson, U. and Follin, S. 2003. Simulation of tracer transport, considering both experimental and natural, long, time scales. Äspö Task Force; Task 6A, 6B and 6B2. SKB International Progress Report, IPR-04-42.

Svensson, U., Kuylenstierna, H-O., Ferry, M. 2006. DarcyTools –Concepts, method, equations and demo simulations.

Vidstrand, P. 2006. Work in progress.

Winberg, A., Andersson, P., Byegård, J., Poteri, A., Cvetkovic, V., Dershowitz, W., Doe, T., Hermansson, J., Gómez-Hernandez, J., Hautojärvi, A., Billaux, D., Tullborg, E-L., Holton, D., Meier, P. and Medina, A. 2003. Final Report of the TRUE Block Scale project. 4. Synthesis of flow, transport and retention in the block scale. SKB Technical Report, TR-02-16.

Appendix A

Frame – a parametric study

There is no analytical solution that gives the dispersion and delay of a tracer for the multirate diffusion model. However, it is of interest to have this information from a practical point of view. In this section a parametric study will be performed with the ambition to find empirical relations that give the information sought. Some features of the study:

- The water velocity, U_w, is specified for a long (1000 m) one-dimensional channel. The reason for the extremely long channel is that we want to capture the long tail of the profile.
- Study a range of U_w $\left(10^{-7} \rightarrow 10^{-4} \text{ m/s}\right)$ and β_c $\left(1 \rightarrow 10\right)$ values.
- Calculate the dispersion coefficient, D_L, in space by the definition of D_L:

$$D_L = \frac{1}{2}\frac{d\sigma_L^2}{dt} \tag{A-1}$$

D_L is estimated by calculating σ_L^2 for two positions of the tracer cloud.

- The number of the particles used in the simulations ranged from 10^4 to 10^5.

Simulation results are presented in Table A-1. An inspection of D_L and U_m (the velocity of the mass centre) suggested that the following empirical relations summarize the results quite well.

$$U_m = \frac{U_w}{1 + C_u \beta_c} \tag{A-2}$$

$$D_L = \frac{C_D U_w^{3/2} L}{1 + \beta_c} \tag{A-3}$$

where C_u and C_D are constants. From the simulations, see Table A-1, we find that $C_u \approx 0.7$ and $C_D \approx 10$. It should be emphasized that these relations do not have any theoretical justification; the only objective is to summarize the simulations. As an example of the empirical nature of the relations we may note that D_L does not go to zero when $\beta \rightarrow 0$ and we may also note that the relation is not dimensionally correct.

In Table A-1 also α_L / L is given. This ratio was calculated from:

$$D_L = \frac{\alpha_L}{L} U_m L \tag{A-4}$$

where one should note that U_m is used as the scaling velocity. It is believed that this velocity is the most relevant if comparisons with field data are to be performed, as this (or perhaps T_{50}/L) is the velocity of the tracer cloud that is actually observed.

In spite of what has been said, it is argued that relations A-2 and A-3 are useful from a practical point of view, which will be demonstrated in the following sections.

Relations (A-2) and (A-3) were derived solely from a parametric study of β_c, assuming $k = 2.0$, $\alpha_{\min} = 10^{-10}$ and $\alpha_{\max} = 10^{-3}$. We will now check whether the relations are consistent with the earlier discussed TRUE Block Scale experiments. It is important to note that we use the word "consistent" and not "verification"; the reason is that the β_c and U_w values obtained in the calibration process are to be used in the relations (A-2) and (A-3). Hence, the comparisons to be shown do not verify FRAME in any sense, but are still of some interest.

The results are given by Table A-2 and Figures A-1, A-2 and A-3. Starting with the velocity of the tracer cloud, we can estimate this from the field data as L/T_{50}. This velocity is called U_{50} in the following. From relation (A-2) we can also calculate the corresponding velocities for the mass-centre of the cloud, called U_m. A comparison between U_{50} and U_m is given in Figure A-1. A clear correlation is found, although the U_m-values are always smaller than U_{50}. This is in fact to be expected as U_m should be smaller than U_{50} for a long-tailed profile.

Next we study the dispersion coefficients, see Figure A-2 and Table A-2. For the field data we calculate D_L as $\alpha_L U_{50}$, while we use relation (A-3) as an estimate of the simulated dispersion. A graphical comparison is found in Figure A-2; as can be seen a fair agreement is found.

Regarding α_L / L, one can see in Table A-2 that the average measured value is 0.07. For the simulation, we combine relations (A-2) and (A-3), which yields:

$$D_L = \frac{10\ U_m^{3/2} L \left(1 + 0.7\beta_c\right)^{3/2}}{1 + \beta_c} \tag{A-5}$$

and as $D_L = \alpha_L U_m$ we get:

$$\frac{\alpha_L}{L} = \frac{10\ U_m^{1/2} \left(1 + 0.7\beta_c\right)^{3/2}}{1 + \beta_c} \tag{A-6}$$

which indicates that α_L / L is dependent on both U_m and β. However, one should remember that all relations discussed are based on a parametric model study and are so far not verified. Relation (A-6) is shown in Figure A-3 where also the field data are shown (hence both U_m and U_{50} on the horizontal axis). It is seen that relation (A-6) gives somewhat higher α_L / L, as compared to the field data.

The general conclusion from the analysis presented is that the relations from the parametric study are consistent with the TRUE Block Scale experimental data.

Table A-1. FRAME, a parametric study.

U_w $(\mathrm{m/s})$	β_c $(-)$	$\frac{U_m}{U_w}$ $(-)$	D_L $(\mathrm{m^2/s})$	C_u $(-)$	C_D $(\mathrm{s^{1/2}/m^{1/2}})$	$\frac{\alpha_L}{L}$ $(-)$
10^{-4}	1	0.59	1.51×10^{-3}	0.71	5.2	0.044
	3	0.37	1.27×10^{-3}	0.57	9.2	0.062
	5	0.23	1.00×10^{-3}	0.67	8.8	0.078
	7	0.19	1.73×10^{-3}	0.61	10.3	0.075
	10	0.12	1.51×10^{-3}	0.71	11.3	0.083
10^{-5}	1	0.59	1.20×10^{-4}	0.69	11.6	0.031
	3	0.32	1.70×10^{-4}	0.71	18.3	0.045
	5	0.25	0.59×10^{-4}	0.62	20.0	0.043
	7	0.16	0.46×10^{-4}	0.75	19.2	0.047
	10	0.12	0.21×10^{-4}	0.76	12.3	0.030
10^{-6}	1	0.56	5.02×10^{-6}	0.79	13.8	0.012
	3	0.30	1.74×10^{-6}	0.80	12.1	0.011
	5	0.20	0.88×10^{-6}	0.80	8.8	0.0073
	7	0.15	0.50×10^{-6}	0.80	7.6	0.0051
	10	0.11	0.34×10^{-6}	0.80	7.1	0.0058
10^{-7}	1	0.56	4.56×10^{-8}	0.78	3.9	0.0011
	3	0.28	2.24×10^{-8}	0.80	3.5	0.00095
	5	0.20	0.98×10^{-8}	0.81	2.8	0.00069
	7	0.15	0.61×10^{-8}	0.80	2.3	0.00058
	10	0.11	0.34×10^{-8}	0.80	2.0	0.00052
Averages				≈ 0.7	≈ 10.0	

Table A-2. Consistency between measured and simulated characteristics of the TRUE Block Scale Experiments.

Test	Measurements						Simulations				
	Path L (m)	α_L (m)	T_{50} (h)	$\frac{\alpha_L}{L}$ $(-)$	$U_{50}\times10^4$ $(=L/T_{50})$ $(\mathrm{m/s})$	$D_L\times10^4$ $(=\alpha_L U_{50})$ $(\mathrm{m/s})$	$U_w\times10^4$ $(\mathrm{m/s})$	β_c	$\frac{\alpha_L}{L}$ $(-)$	$U_m\times10^4$ $(\mathrm{m/s})$ (m/s)	$D_L\times10^4$ $(\mathrm{m^2/s})$
C1	17.9	1.5	20	0.084	2.49	3.73	3.8	2.5	0.15	1.38	3.79
C2	68.6	5.9	260	0.086	0.73	4.3	1.9	4.4	0.10	0.47	3.32
C3	32.5	2.0	820	0.062	0.11	0.22	0.28	3.6	0.04	0.08	0.11
A5e	35.0	2.8	153.6	0.080	0.63	1.77	1.4	3.5	0.09	0.41	1.29
A5a	38.4	2.3	81.8	0.060	1.30	2.99	2.2	2.3	0.12	0.84	3.80
A5c	12.9	1.0	7.8	0.078	4.59	4.59	5.9	2.1	0.19	2.39	5.96
A4b	52.7	2.0	163.5	0.038	0.90	1.79	1.4	1.7	0.09	0.64	3.23
B2a	52.7	4.1	460.7	0.078	0.32	1.30	0.85	4.2	0.07	0.22	0.79
B2b	32.5	2.0	472.9	0.062	0.19	0.38	0.42	3.1	0.05	0.13	0.22
Averages:				0.07	1.25	2.34		3.0	0.10	0.73	2.50

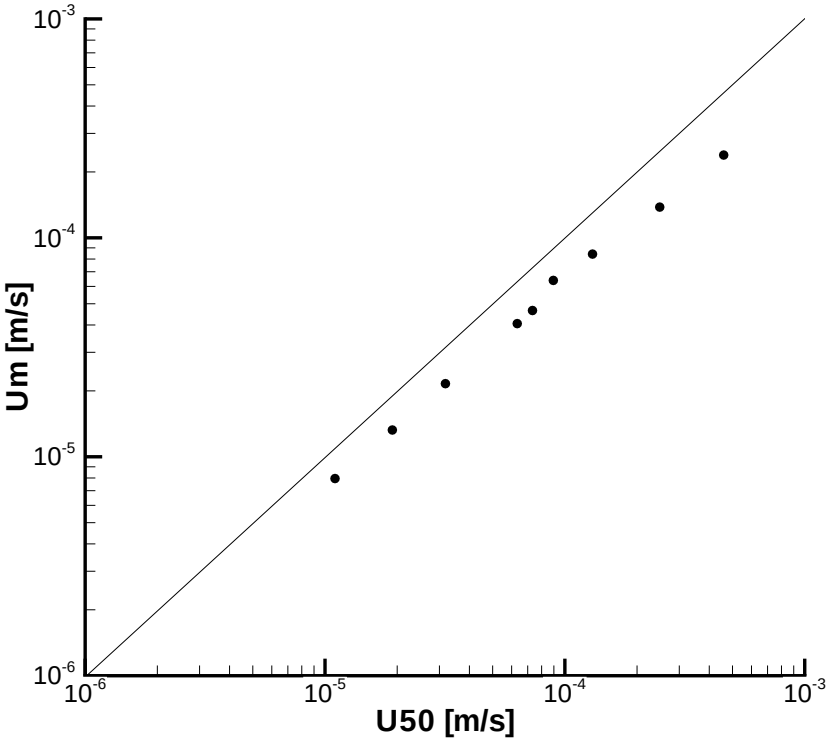

Figure A-1. *The TRUE Block Scale experiments. Relation between* U_{50} *and* U_m.

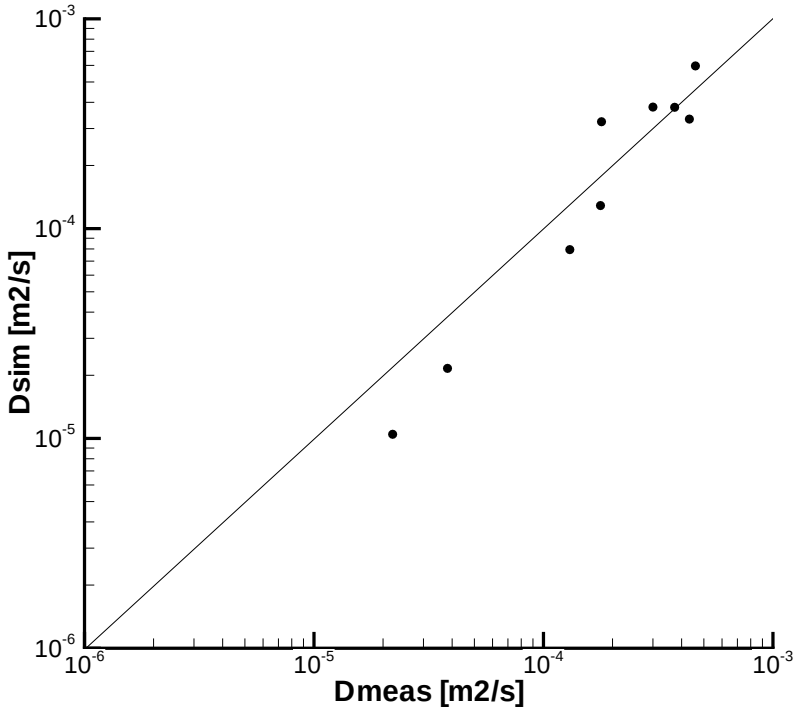

Figure A-2. *The TRUE Block Scale experiments. Relation between measured* $\left(D_{meas}\right)$ *and simulated* $\left(D_{sim}\right)$ *dispersion coefficients.*

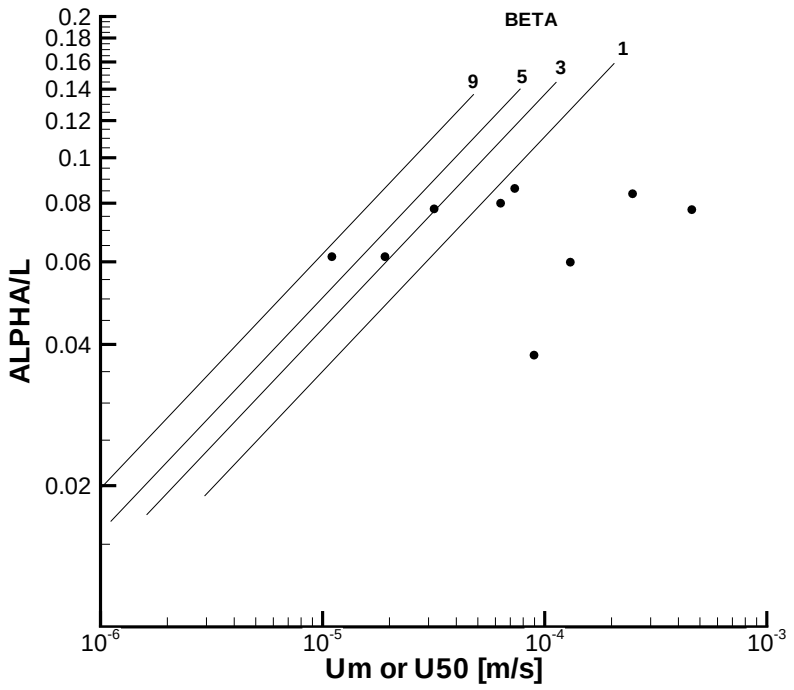

Figure A-3. *The TRUE Block Scale experiments. Relation between* α_L / L, β_c *and* U_m *by FRAME (lines) and* α_L / L *and* U_{50} *from experiments (dots).*